



**HAL**  
open science

# Herschel-Quincke filters for passive vibration mitigation

Stepan Avetisov

► **To cite this version:**

Stepan Avetisov. Herschel-Quincke filters for passive vibration mitigation. Acoustics [physics.class-ph]. Le Mans Université, 2024. English. NNT : 2024LEMA1018 . tel-04786557

**HAL Id: tel-04786557**

**<https://theses.hal.science/tel-04786557v1>**

Submitted on 16 Nov 2024

**HAL** is a multi-disciplinary open access archive for the deposit and dissemination of scientific research documents, whether they are published or not. The documents may come from teaching and research institutions in France or abroad, or from public or private research centers.

L'archive ouverte pluridisciplinaire **HAL**, est destinée au dépôt et à la diffusion de documents scientifiques de niveau recherche, publiés ou non, émanant des établissements d'enseignement et de recherche français ou étrangers, des laboratoires publics ou privés.

# THESE DE DOCTORAT

DE  
LE MANS UNIVERSITE

SOUS LE SCEAU DE  
LA COMUE ANGERS – LE MANS

ECOLE DOCTORALE N° 602  
*Sciences de l'Ingénierie et des Systèmes*  
Spécialité : Acoustique

Par

**Stepan Avetisov**

**«Herschel-Quincke filters for passive vibration mitigation»**

Soutenance envisagée le 24 septembre 2024 sous réserve de l'autorisation des rapporteurs  
Unité de recherche : UMR CNRS 6613, Laboratoire d'Acoustique de l'Université du Mans (LAUM)  
Thèse N°: 2024LEMA1018

## Rapporteurs avant soutenance :

Roberto Arruda  
Elke Deckers

Professeur, University of Campinas, Brazil  
Professeur, KU Leuven, Belgium

## Composition du Jury :

Examineurs : Emmanuel Perrey-Debain

Professeur, Université de Technologie de Compiègne, France

Dir. de thèse : Adrien Pelat  
Co-dir. de thèse : François Gautier  
Sergey Sorokin

Professeur, Le Mans Université, France  
Professeur, Le Mans Université, France  
Professeur, Aalborg University, Denmark

## Invité(s)

Jacky Mardjono

Ingénieur, Safran



# Herschel-Quincke filters for passive vibration mitigation

**Stepan Avetisov**

Acoustics Laboratory of Le Mans University UMR CNRS 6613,  
Institut of Acoustics Graduate School (IA-GS)  
Le Mans, France

This dissertation is submitted for the degree of  
*Doctor of Philosophy*

July 2024



---

## ACKNOWLEDGEMENTS

---

The journey toward the completion of this PhD has been both challenging and deeply rewarding. I would like to take this opportunity to express my sincere gratitude to the many individuals and institutions that have supported me throughout this process.

First and foremost, I extend my deepest thanks to acoustic laboratory at Le Mans University, where this research was carried out. The vibrant academic environment, coupled with the cutting-edge facilities, made this laboratory a perfect place to grow as a researcher. I am grateful to the university for providing the resources and support necessary for my work.

I am especially indebted to my supervisors, Adrien Pelat, François Gautier and Sergey Sorokin, for their invaluable guidance, patience, and encouragement. Their expertise and insights have shaped this project from its inception, and their unwavering support has been a source of motivation throughout the most difficult phases of this research. I feel fortunate to have had the opportunity to work with such dedicated and inspiring mentors.

I would also like to extend my sincere appreciation to the members of my thesis review committee, Roberto Arruda, Elke Deckers, for taking the time to review my work. Their thoughtful feedback has greatly contributed to improving the quality of this thesis, and I am truly grateful for their valuable input.

My heartfelt thanks go to my colleagues and friends, Théo, Ammar, Wala, Kyu, Lilit, Alex, Erwan, Guillaume, Patrick, Audrey, Nadine, Elliott, Chiara, and many others, for their companionship, intellectual discussions, and unwavering support. The shared experiences, challenges, and laughter we enjoyed along the way have been an essential part of this journey. I am truly grateful for the collaborative spirit and camaraderie that made even the toughest days more manageable.

And finally, most importantly, I want to thank my family. To my parents, Artur and Inna, and my brother Grigor and beloved sister Nina—your unconditional love, support, and belief in me provided the energy and motivation that fueled the writing of this thesis. Your emotional and practical support has been fundamental to its completion.

To everyone who has contributed to this achievement, directly or indirectly, I extend my deepest appreciation. Thank you for making this journey possible.

---

## ABSTRACT

---

Vibration and structure borne noise are generally undesirable phenomena for both the reliability and comfort issues. Many approaches to vibration control have been studied over the years, using various geometrical designs, damping materials, or active control strategies. In addition, lightening mechanical structures is a major challenge in terms of energy consumption, particularly for transport applications.

In these combined contexts, the aim of this thesis is to develop new vibration control concepts by adapting the principle of Herschel-Quincke (HQ) filters, traditionally applied to plane acoustic waves in tubes, to the realm of elastic waves in beams and plates. In acoustics, HQ filters exploit the principle of a phase shift between two parallel tubes of varying lengths created from a primary tube, resulting in destructive interference and hence zero transmission at certain frequencies. The attractiveness of HQ filters lies in their capacity to provide multiple transmission loss peaks, presenting a viable alternative to traditional resonance-based approaches.

This study extends this principle to bending waves by partitioning a thin beam into two segments of equal length but different thicknesses. The resulting disparity in bending stiffness induces the requisite phase difference, leading to wave filtering. This approach positions HQ filters as a promising solution for vibration and noise control applications without increasing the mass of the considered structure. First, the HQ principle for structural dynamics is theoretically analysed through wave based models considering non dispersive longitudinal or torsional waves and bending waves in beams. An experimental study also demonstrates the practical interest of this filtering technique. Then, the principle is extended to plates structures, leading to annular filters that may surround a vibration source and so isolate it from the rest of the plate. Third, some more sophisticated designs based on serial, parallel or periodic arrangements of structural HQ devices are proposed and analyzed to assess how they can optimize vibration filtering performance.



---

## RÉSUMÉ

---

Les vibrations et les bruits de structure sont généralement des phénomènes indésirables pour des raisons de fiabilité et de confort. De nombreuses approches du contrôle des vibrations ont été étudiées au fil des ans, en utilisant diverses conceptions géométriques, des matériaux d'amortissement ou des stratégies de contrôle actif. En outre, l'allègement des structures mécaniques est un défi majeur en termes de consommation d'énergie, en particulier pour les applications de transport.

Dans ces contextes combinés, l'objectif de cette thèse est de développer de nouveaux concepts de contrôle des vibrations en adaptant le principe des filtres de Herschel-Quincke (HQ), traditionnellement appliqué aux ondes acoustiques planes dans les tubes, au domaine des ondes élastiques dans les poutres et les plaques. En acoustique, les filtres HQ exploitent le principe de la différence de marche entre deux tubes parallèles de longueurs variables créés à partir d'un tube primaire, ce qui entraîne une interférence destructive et donc une transmission nulle à certaines fréquences.

Cette étude étend ce principe aux ondes de flexion en divisant une poutre mince en deux segments de longueur égale mais d'épaisseur différente. La différence de rigidité de flexion qui en résulte induit la différence de phase requise, ce qui conduit au filtrage des ondes. Cette approche fait des filtres HQ une solution prometteuse pour les applications de contrôle des vibrations et du bruit sans augmenter la masse de la structure considérée. Premièrement, le principe HQ pour la dynamique structurelle est analysé théoriquement à travers des modèles basés sur les ondes considérant les ondes longitudinales ou torsionnelles non dispersives et les ondes de flexion dans les poutres. Une étude expérimentale démontre également l'intérêt pratique de cette technique de filtrage. Ensuite, le principe est étendu aux structures de plaques, ce qui conduit à des filtres annulaires qui peuvent entourer une source de vibration et ainsi l'isoler du reste de la plaque. Enfin, des conceptions plus sophistiquées basées sur des arrangements sériels, parallèles ou périodiques de dispositifs structurels HQ sont proposées et analysées afin d'évaluer comment elles peuvent optimiser les performances de filtrage des vibrations.



---

## TABLE OF CONTENTS

---

<b>1</b>	<b>Context</b>	<b>1</b>
1.1	Vibroacoustic control and filtering . . . . .	1
1.2	Literature Review Herschel-Quincke tubes . . . . .	4
1.2.1	Acoustic tubes . . . . .	4
1.2.2	Strings . . . . .	14
1.2.3	Beams . . . . .	16
1.3	Thesis goals and plan . . . . .	19
<b>2</b>	<b>Herschel-Quincke filter for non-dispersive elastic waves</b>	<b>23</b>
2.1	Wave model for axial waves in rods . . . . .	24
2.2	Analysis of the filtering properties . . . . .	26
2.2.1	Unit incoming wave problem . . . . .	26
2.2.2	Forced problem . . . . .	31
2.2.3	Zero transmission frequency problem and parametric studies	33
2.2.4	The trapped mode case . . . . .	36
2.3	Adaptation to torsional waves . . . . .	38
2.4	Conclusion . . . . .	40
<b>3</b>	<b>HQ filters for flexural waves in beams</b>	<b>43</b>
3.1	Models of the HQ vibration filter for bending waves . . . . .	43
3.1.1	Wave based model with coupled longitudinal and bending motions . . . . .	43
3.1.2	3D Finite Element model of the HQ filter . . . . .	47
3.2	Analysis of the performances of the HQ filter . . . . .	49
3.2.1	Energy flow . . . . .	49
3.2.2	Modal Analysis of an infinite beam with the HQ filter . . . . .	51
3.3	An alternative formulation of the problem and parametric analyses of location of the zero-transmission frequencies . . . . .	53
3.4	Experimental validation . . . . .	57
3.4.1	Setup and signal processing . . . . .	57

3.4.2	Results . . . . .	58
3.5	Classification of 2 parallel branch configurations . . . . .	61
3.6	Conclusion . . . . .	63
<b>4</b>	<b>HQ filters for flexural waves in plates</b>	<b>65</b>
4.1	Model of the HQ vibration filter in a circular plate . . . . .	65
4.2	Analysis of the filtering properties of the HQ plate . . . . .	68
4.3	Zero transmission frequency for different $n$ . . . . .	73
4.4	Forced problem . . . . .	75
4.5	Energy Flux and Insertion Loss analysis . . . . .	78
4.6	Assessment of performance of HQ device outside zero transmission frequencies . . . . .	80
4.7	Application to sandwich panels . . . . .	83
4.7.1	Classification of HQ sandwich architectures . . . . .	83
4.7.2	Analysis of a perforated skin of HQ plate . . . . .	84
4.7.3	Limitation due to the core . . . . .	86
4.8	Conclusion . . . . .	87
<b>5</b>	<b>Sophisticated HQ filters</b>	<b>89</b>
5.1	Multi-branch configurations . . . . .	90
5.1.1	HQ filter with serial arrangement . . . . .	90
5.1.2	HQ filter with parallel arrangement . . . . .	92
5.1.3	HQ filter with mixed arrangement . . . . .	96
5.1.4	Experimental demonstration . . . . .	98
5.2	Periodic chain of HQ insertions for axial waves . . . . .	101
5.2.1	Simple periodic chain configuration of HQ inserts for axial waves and its filtering performance . . . . .	101
5.2.2	Pass and stop bands in an infinite periodic structure . . . . .	102
5.2.3	Eigenfrequencies of a periodicity cell and stop-band boundaries	104
5.3	Conclusion . . . . .	108
<b>6</b>	<b>Conclusions and perspectives</b>	<b>109</b>
6.1	Conclusions . . . . .	109
6.2	Perspectives . . . . .	111
	<b>References</b>	<b>113</b>

**Appendix A** **120**

    A.1 Dynamic matrix simulation . . . . . **120**

    A.2 Analysis of the equivalent characteristic for a perforated plate . . . . **123**

---

## CONTEXT

---

### 1.1 VIBROACOUSTIC CONTROL AND FILTERING

Vibration control is an important part of any noise control program as it often leads to excessive noise, mechanical wear, structural fatigue and possible failure. Effective management of vibration is essential across all industries to maintain operational efficiency and ensure the longevity of equipment and structures. An illustrative example of a canonical noise control problem is depicted in Fig.1.1, [1]. In such

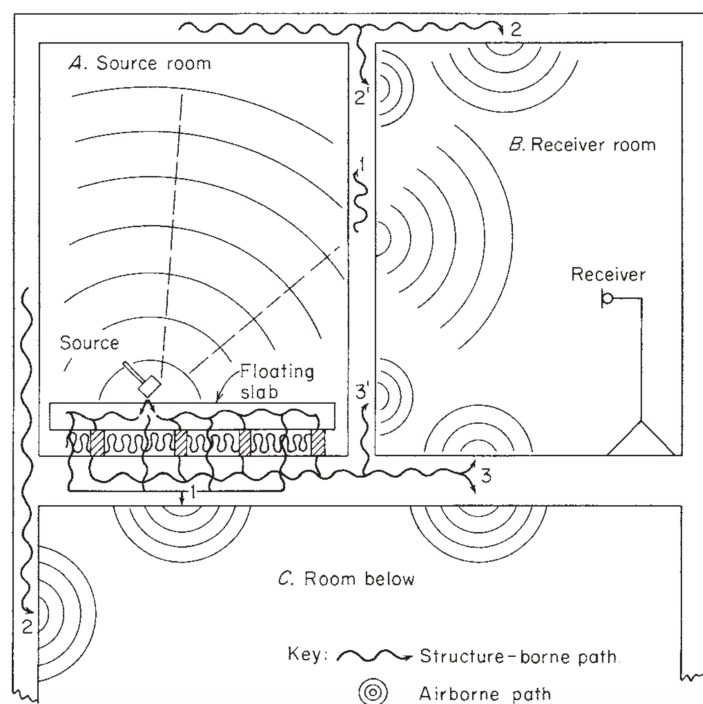


Fig. 1.1 Sound-transmission paths between an impact source in room A and a receiver in room B. Also shown are the paths to room C, below [1].

scenarios, which can include thin-walled partitions in buildings, shipbuilding, railway engineering, and automotive engineering, noise issues can arise from both airborne and structure-borne sources. In a building acoustic context, for example, airborne noise is transmitted 'directly' into the receiver room through solid partitions, while structural noise is characterized by sound energy dissipated in walls and then transmitted through the resilient layer into the building structure. The primary focus in addressing airborne and structure-borne noise issues involves controlling noise by: 1) sound source modification, 2) control of the transmission path and 3) modification of the receiver [1–5].

There are many possible noise control strategies that can be used to reduce the vibration generated in solid structures such as plates, beams, etc. As shown in Fig.1.2, the basic principles comprise the utilization of various absorbers, barriers, dampers and isolators.

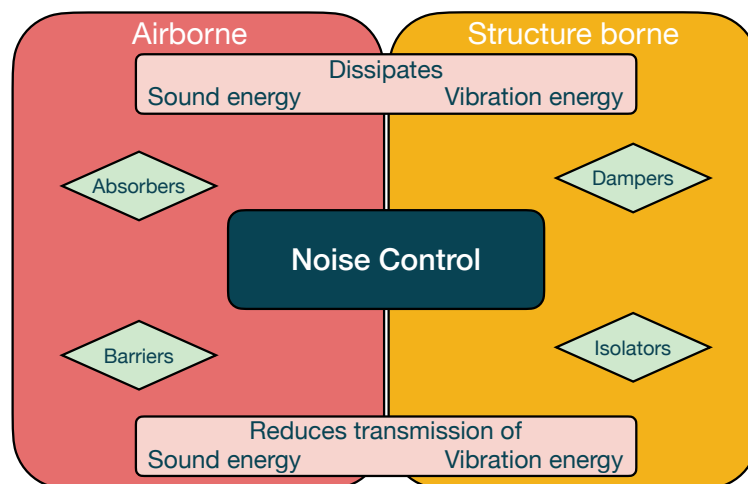


Fig. 1.2 Noise control strategies.

In general, the vibration control methods are based on various passive, active and hybrid control strategies [6, 7]. Active methods utilize control actuators and sensors of various configurations. Among the most common are those that utilize piezoelectric films adhered to a vibrating structure. Hybrid treatments aim to enhance passive damping by integrating various active control mechanisms. This approach compensates for performance degradation due to temperature or

frequency changes. By combining the simplicity of passive damping with the effectiveness of active damping, these methods ensure an optimal combination of their respective advantages [6]. However, both hybrid and active implementations require a significant number of active elements, which can lead to high design costs and recurring maintenance problems. These factors often limit their practical application in industrial settings. The passive control method is simple and robust, and this control method can be easily applied to reduce the structural vibration without resorting to complex active control systems. So the focus of this thesis is on passive vibration mitigation based on the Herschel-Quincke filtering effect.

For many years, passive damping techniques have effectively mitigated vibrations in a diverse array of structures, from basic beams to intricate space assemblies. Examples of these passive damping methods include: a) Free and constrained damping layers, both types of damping are based on the use of viscoelastic material to extract energy from the vibrating structure [6, 8], b) Damping systems with graded properties using a graded impedance interface to reduce energy reflection [9, 10], c) Acoustic Black Holes, lightweight system with a power-law tapered edge and trapping zone that provides absorbing performances [10–12], d) Tuned Vibration Absorbers [13], consists of adding a reactive mass and an resilient element to the structure to be treated. They are typically tuned to interfere with the vibrations of the structure at the perturbation frequency. This results in a change in the frequency response of the primary system and introduces another resonance into the composite system due to the additional degree of freedom provided by the tuned vibration absorbers [10]. e) Damping with Shape Memory Fibers/Alloys [6, 14–16], a shape memory alloy is capable of "remember" its original configuration after deformation when the alloy is heated above its characteristic transition temperature and shape memory alloys belong to the class of smart or intelligent materials. This passive mechanism and damping effect relies on embedding superelastic shape memory fibers in the composite fabric of the vibrating structures to dissipate vibration energy, f) Microstructures of periodic architectures such as lattice structures with unconventional mechanical material properties, can reduce noise by creating band gaps [17–22].

The Herschel-Quincke filter can be presented as one of the passive vibration control methods. The adaptation of Herschel-Quincke filter in this thesis aims to address structure-borne noise by modifying the transmission path through the isolator, i.e., using the concept of destructive interference between two traveling

waves in a thin-walled structures. The filtering effect provided by this device can be applied to attenuate structural vibrations generated by bending waves, which makes it useful in various vibration engineering tasks. The general principles of operation of this device and its effectiveness will be discussed in more detail below.

## 1.2 LITERATURE REVIEW HERSCHEL-QUINCKE TUBES

### 1.2.1 Acoustic tubes

The interest in the Herschel-Quincke (HQ) tube for this work stems from the simplicity of the device design, which is an important practical advantage for producing such a device for application in industry. The basic system is composed of a main pipe and a tube parallel to the latter, called the HQ tube (see Fig.1.3). The HQ tube is of different dimension with respect to the latter; the length of the HQ tube is generally larger. The objective is to create a phase shift between the wave propagating in the main tube  $L_1$  and the wave propagating in the tube in parallel  $L_2$ . This phase shift, due to the difference in length between the paths taken by the two waves, causes destructive interference to appear between them. These interferences cause attenuation of certain frequency bands.

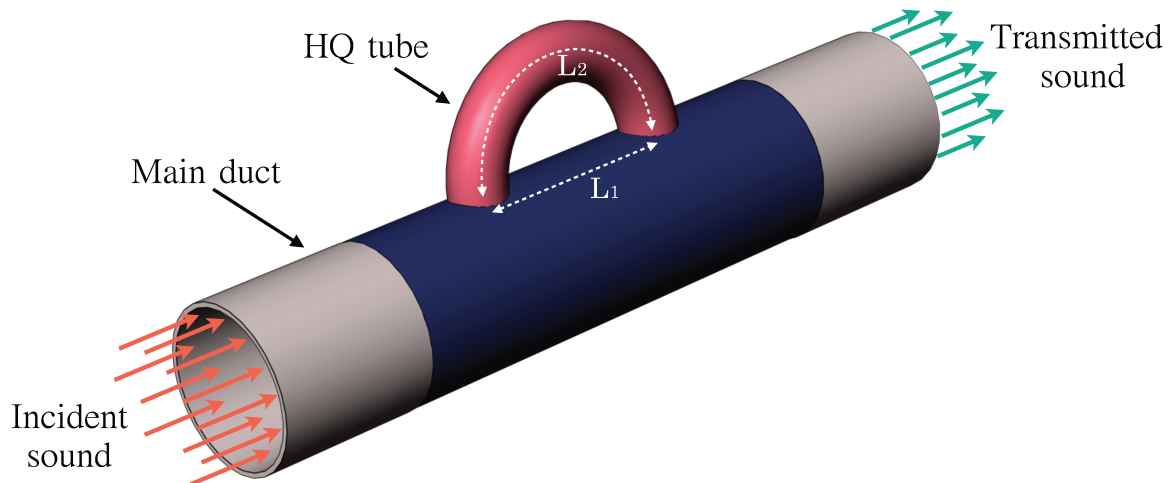


Fig. 1.3 A scheme of Herschel-Quincke tube for plane wave control.

In 1833, J.F.W. Herschel [23] first discussed the idea of investigating the acoustic interference of musical sound and internal reflection using a continual subdivision of the waveguide, as shown in Fig.1.4. This serves as an example of an acoustic

combination, or compound vibrating system, incapable of transmitting a musical sound of a given tone. He predicted that the cancellation of tones would occur when the difference in path length between the recombined signals was  $(2m + 1)(\lambda/2)$ , where  $\lambda$  is the acoustic wavelength and  $m$  is any integer.

Later, in 1866, G.H. Quincke [24] empirically validated the ability of this system to cancel sound, as postulated by J.F.W. Herschel.

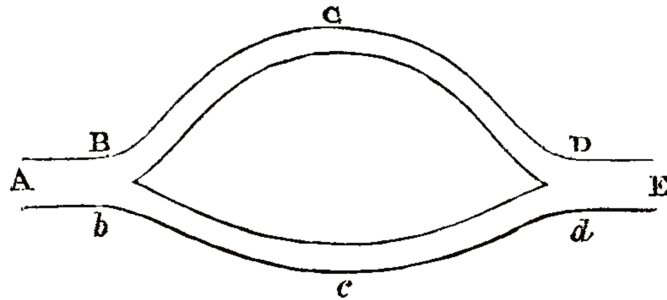


Fig. 1.4 An example of an acoustic combination with pipe A E, which, after proceeding singly a certain length 'A' 'B', at 'B' branches off into two equal and symmetrically disposed pipes 'B' 'C' and 'b' 'c', which reunite again at 'D' 'd', and there again constitute a single pipe 'D' 'E', whose direction shall (like 'A' 'B') bisect the angle between the branches [23].

Then, in the 20th century, G.W. Stewart [25], [26] refined the theory of the HQ concept by comparing theory with experiment (see Fig.1.5) and concluded that waves propagate along two paths in a complex manner that cannot be traced without using equations. Through plane wave analysis, Stewart derived an analytical model describing the ratio of transmitted to incident sound intensity in the system. He verified that the interferences cancel the transmission in the pipe when the phase difference satisfies one of the equations  $\phi_2 - \phi_1 = (2m + 1)\pi$ , as predicted by Herschel [23]. But also when the path length difference is  $\phi_2 + \phi_1 = 2m\pi$ , with limited attenuation at other transitional frequencies. Stewart's description of the attenuation frequencies was limited by the assumption that the cross-sectional areas of the parallel ducts were equal. Although Stewart's research greatly advanced the study of Herschel-Quincke tubes, the model did not account for scenarios involving flowless and plane wave acoustic fields.

Subsequently, A. Selamet et al. [27], [28] extended Stewart's work [25], [26] by deriving an analytical model with the elimination of the restrictions on the duct cross-sectional area. They evaluated the transmission loss characteristics of the Herschel-Quincke tube in terms of a nonlinear one-dimensional finite-difference

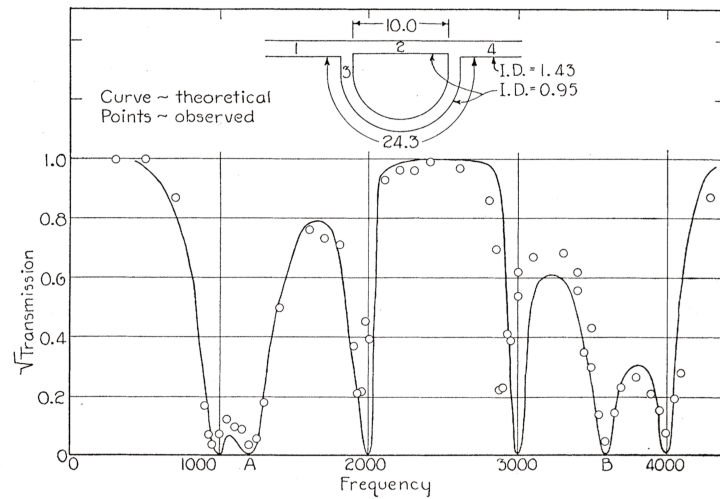


Fig. 1.5 Diagram of Herschel-Quincke tube and the relation between percentage transmission and the square root of the frequency [26].

model. This study showed that the two previously identified sets of noise reduction frequencies are indeed in resonance of the combined parallel duct system. These frequencies were categorised as two types and were found to depend not only on the difference in sound path length, but also on the ratio of the cross-sectional areas of the two branches.

Various authors have extended this basic HQ principle. J.M. Desantes et al.[29] modified HQ system by means of an additional pipe connecting both paths (see Fig.1.6). A.J. Torregrosa [31], [30] considered the HQ system using variable cross-

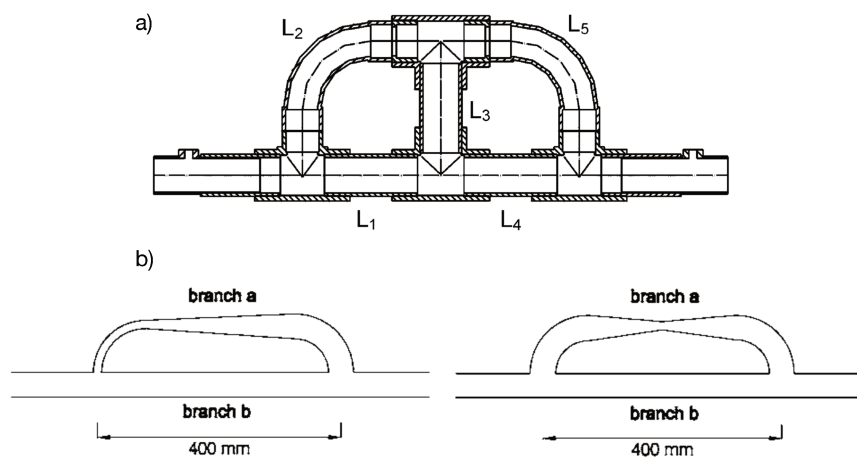


Fig. 1.6 a) A general interferential system with interconnecting branch [29] b) Scheme of Herschel-Quincke duct with non-uniform cross section branches [30].

section ducts in one of the branches or Venturi-shaped branch. Based on this model, conditions for resonant frequencies in several configurations of potential interest were determined and such systems can provide wider attenuation bands than those provided by conventional Herschel-Quincke ducts. The contribution of mean flow was also considered in the linear model by calculating the steady flow in the whole pipe. The results show that the influence of the mean flow results in a quantitative reduction of the attenuation curve and does not change its shape. Then, M. Karlsson [32] proposed a general expression for the transmission loss of an N-duct system with mean flow and two types of conditions giving attenuation maxima. In the work of Z. Zhichi et al. [33] considered a flow duct with a single-bypass and a double-bypass in order to widen the band of attenuation. And the effect of end reflections from the duct outlet was also studied. Indeed, in the presence of end reflections, the frequency dependence of the transmission loss becomes more complex since the transmission loss varies according to different reflection coefficients and the length between the end of Herschel-Quincke tube and the outlet duct. S.N. Panigrahi [34] reviewed the sound attenuation behavior of an acoustic network with many nodes and branches in order to attempt a broad band sound attenuation respectively. The obtained results show the acoustic resonant frequencies of the complex network systems and also show the influence of higher order modes.

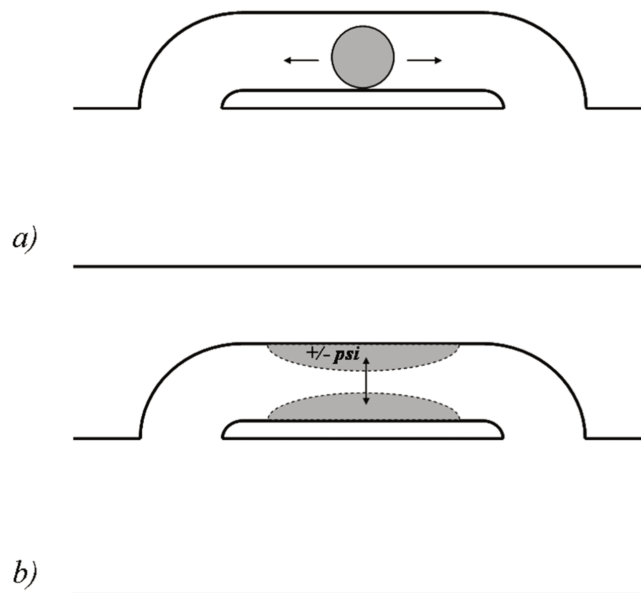


Fig. 1.7 Schematic of adaptive HQ tubes using the (a) ball and (b) diaphragm [35].

In the work of Alonso et al. [35] proposed to modify the cross-section of the HQ branch and improve the narrow band attenuation capabilities to target tonal noise of variable frequency, using adaptive concepts. The adaptive concepts are based on shifting the resonance frequencies of the HQ tube by creating a smooth constriction inside the waveguide. The effect of this constriction is to change the mass and stiffness characteristics of the equivalent dynamic system, resulting in a shift in the natural frequencies of the HQ tube vibrations. The first option is to add a ball device inside a straight Herschel-Quincke tube, as shown in Fig1.7. Rolling the ball is an easy way to vary the HQ branch profile and thus to control the

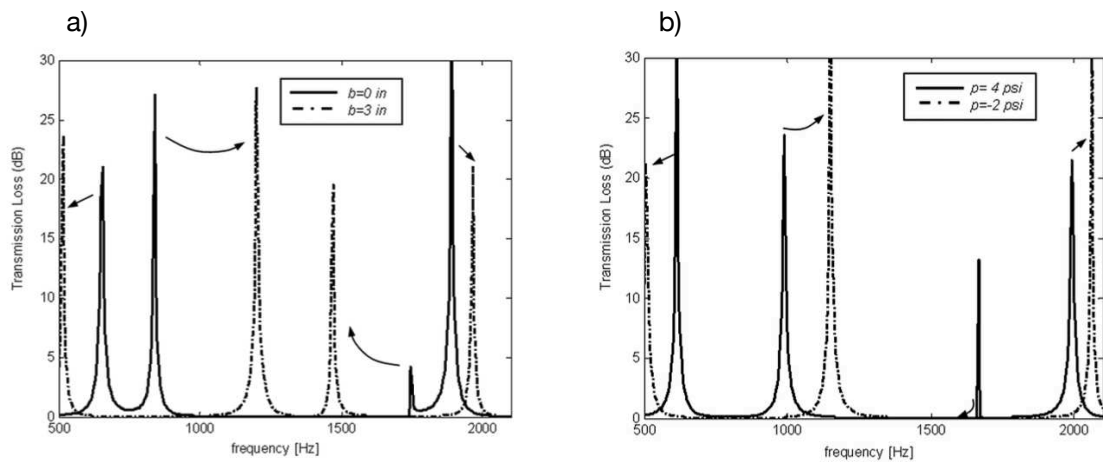


Fig. 1.8 a) Adaptive transmission loss due to ball-in HQ tube. b) Adaptive transmission loss due to diaphragm HQ tube [35].

induced delay. It allows HQ resonances to be tuned for applications with variable frequency tonal noise. The second option consists of using a constriction induced by a membrane placed inside a straight Herschel-Quincke tube, whose shape can be controlled by pressure or suction on one of its sides. Transmission losses have been evaluated in a one-dimensional tube and such adaptive systems can enhance the sound attenuation performance of HQ resonators, as shown in Fig.1.8.

The HQ interference can also be created and controlled actively, by using a piezoelectric membrane inserted into the delay branch. As an example, this configuration was studied by S. Griffin [36]. The Herschel-Quincke tube reviewed by Selamet [28] is modified by adding a pre-stressed PVDF diaphragm to form a spring-mass piston as illustrated in Fig.1.9. The used PVDF membrane behaves like a piston whose equivalent parameters can be adjusted using the applied electrical voltage, thus controlling the frequency at which attenuation occurs.

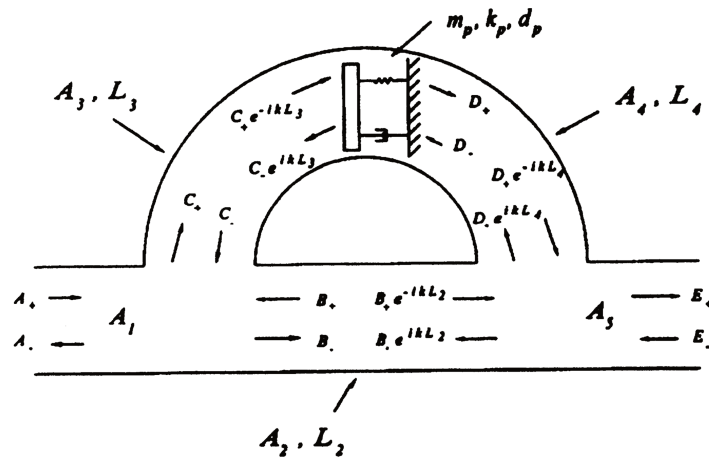


Fig. 1.9 Schematic of an adaptive Herschel-Quincke tube [36].

The transmission loss across the adaptive Herschel-Quincke tube are calculated as a function of tube geometry and piston properties. The results show that by varying the membrane voltage, the transmission loss peak of the Herschel-Quincke tube can be varied over a wide frequency range (see Fig.1.10). In this way, an adaptive Herschel-Quincke tube can be used to track time-varying tonal disturbances and maintain cancellation.

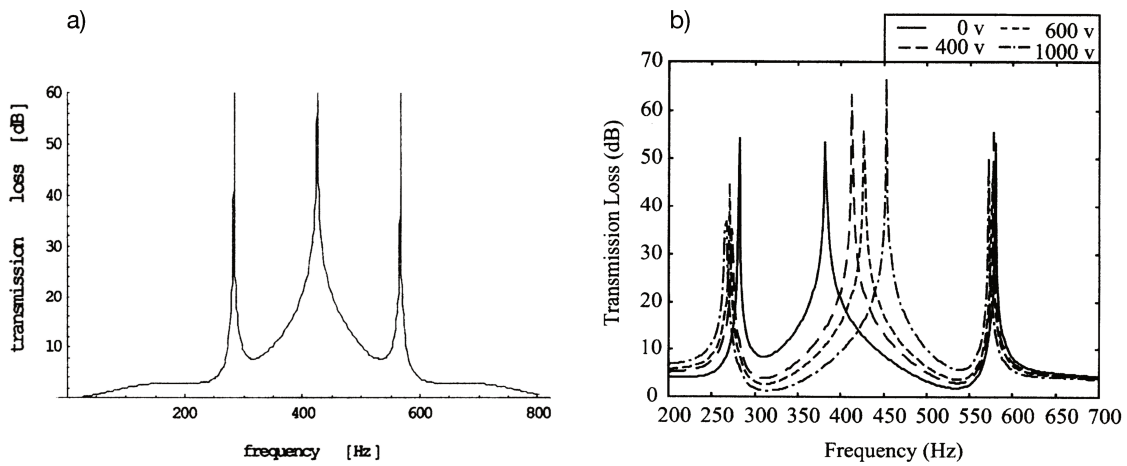


Fig. 1.10 a) Transmission loss for the classical Herschel-Quincke tube. b) Transmission loss of the adaptive Herschel-Quincke tube for different values of applied voltage [36].

Herschel-Quincke tubes can also be used to improve liners. A liner is an acoustic treatment used for aeronautical applications. A study of the performance of an HQ-

Liner system for the reduction of noise from turbofan engines was proposed by R. F. Hallez [37], R.A. Burdisso [38], J.P. Smith [39] and D. H. de la Riva [40]. The work of Hallez [37] was primarily aimed toward evaluating the noise control mechanisms involved in the HQ system and the effect of the HQ tubes on the noise radiated by the inlet of turbofan engines. The approach consists of installing circumferential arrays of HQ tubes in the inlet of the turbofan engine, as shown in Fig.1.11. An analytical technique was developed to predict the impact of Herschel-Quincke tubes on circular inlets. The results obtained from the model were compared with experimental data obtained on two real engine intakes on which the HQ system was applied. An impedance analysis has shown that the HQ system provides good reduction at discrete frequencies corresponding to the resonance of the coupled HQ tube-duct system. The dynamics of the inlet duct actually changes the resonant behavior of the pipe itself and causes the tube resonant frequencies to shift down. Then, noise control mechanisms were investigated by examining the modal amplitudes of incident, reflected and transmitted modes. This allowed to show that in the presence of the HQ system, the incident modes are not only reflected back to the fan, but also scattered to other modes of radial and circumferential order. But in order to obtain accurate results and avoid scattering of energy into propagating circumferential modes, a significantly high number of modes must be included in the calculations. And Hallez's analytical model allows to apply Herschel-Quincke tubes to a cylindrical duct in the presence of higher order modes in uniform flow, as opposed to the simple case of plane waves considered in the past.

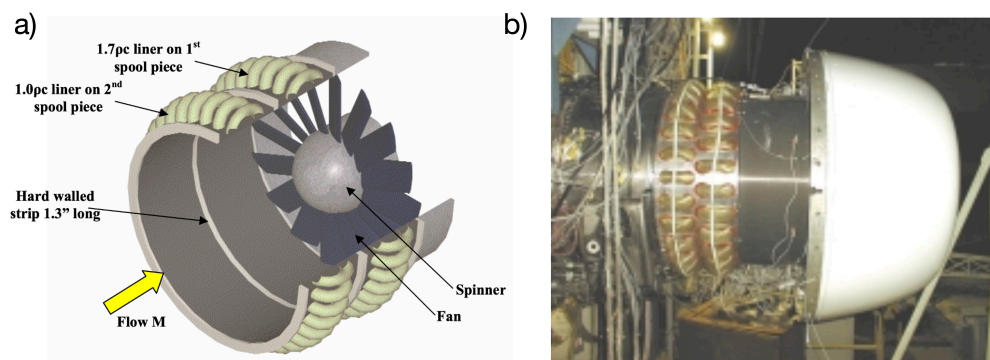


Fig. 1.11 a) Schematics of inlet multiple HQ-liner spool piece configuration [40]. b) Picture of the TFE731 inlet configured with two arrays of HQ tubes [37].

The problem of controlling the multiple higher-order modes in a two-dimensional duct was studied and extended by L.A. Brady [41]. The acoustic field inside the Herschel-Quincke tubes is assumed to consist of only plane waves, and the acoustic field in the main duct is modeled using a higher-order mode Green's function technique. The model showed that Herschel-Quincke tubes are effective in reducing both plane waves and higher-order modes. The recombination of the energy spilled between the various modes present results in destructive interference and thus sound attenuation.

The liner may also consist of a combination of a perforated plane and a honeycomb, backed with a rigid plate. The assembly results in a wall that reacts locally and induces acoustic attenuation in the aircraft jet engine. B. Poirier et al [42], [43] have proposed adding HQ filters in this context to increase acoustic attenuation. It is observed that the maximum efficiency of the membrane and that of the HQ tube are not at the same frequencies. The judicious combination of the two brings an improvement. A second arrangement consists of inserting a micro-perforated membrane inside the wall of the HQ branch itself. This combination, studied by Z.B. Wang et al. [44], involves vibroacoustic coupling, micro-perforation absorption and HQ interference. The authors show that the device improves acoustic attenuation efficiency. The authors suggest adding an acoustically transparent membrane to cover the openings to prevent whistling in case of flow through the tube.

Herschel-Quincke tubes may also find their application in automotive engineering as a vehicle exhaust system or motor. Specific embodiments are shown and described in the patent application publication of Daly et al [45]. As shown in Fig.1.12, the exhaust system consists of many separate passageways which realize passive noise cancellation. Tuning the length of these passages any target frequency may be canceled. Using Herschel-Quincke tubes, the desired noise suppression system can be achieved but they are still difficult to package in a vehicle due to their size, thus the issue of applying these tubes and using them in practice is still relevant.

Further applications of Herschel-Quincke tubes have also been studied extensively, e.g., in recent works by the authors of T. Lato [46], [47], D.-Y. Kim [48] and T. K. Papathanasiou et al. [49]. T. Lato [46] proposed a mechanism for damping pressure pulsations by an HQ device in an industrial pipeline system. The methodology of using the HQ device and verifying that it is tuned to the resonant modes of the pipeline was performed using transmission loss measurements. The experiment

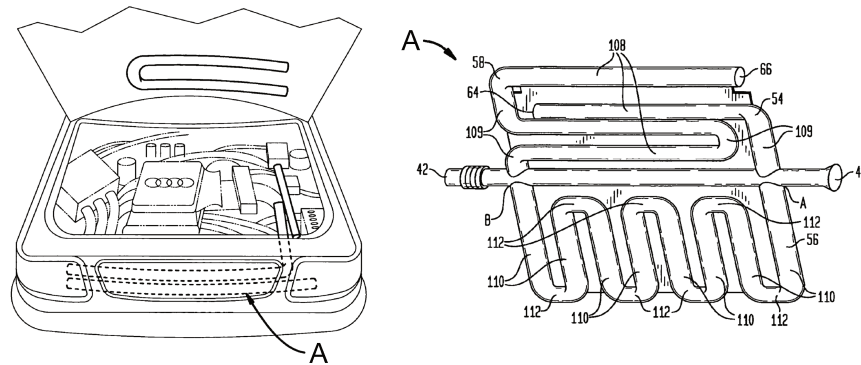


Fig. 1.12 The HQ tube arrangement used with a vehicle exhaust system and an example embodiment of the HQ tube arrangement [45].

was carried out in an air loop with the set-up shown in Fig.1.13. Experimental results of the attenuation mechanism of the HQ device indicate a reduction in transmission losses and acoustic standing wave are formed in the piping system.

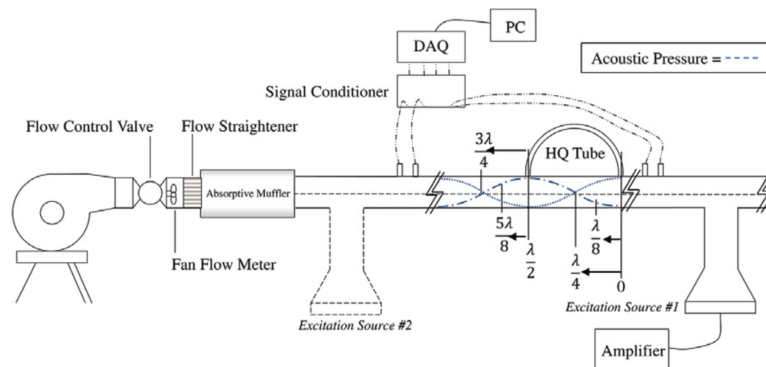


Fig. 1.13 Schematic of the experimental set-up for the air loop pipeline system [46].

D.-Y. Kim [48] investigated an acoustic metamaterial wall to develop a duct silencer. To do this, he used an array of periodic quarter-wavelength tube resonators, which in combination with the HQ device made it possible to obtain a wide bandwidth of frequency attenuation of the sound. Fig.1.14 illustrates this modified configuration of Herschel-Quincke tubes in which the phase velocities of sounds propagating in two parallel channels are different, and where the duct wall is covered by a periodic array of indented resonators. It is shown that with correct tuning of the resonator characteristics it is possible to achieve broadband noise reduction, including at low frequencies.

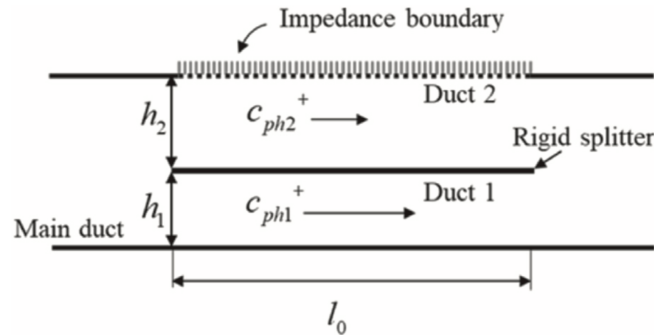


Fig. 1.14 Two parallel ducts separated by a thin rigid splitter, in which duct 1 is surrounded by rigid walls, and a wall of duct 2 is covered by the impedance boundary. Two parallel ducts constitute a virtual Herschel-Quincke tube [48].

The work by T. K. Papathanasiou [49] considers a modulated Herschel-Quincke tube based on periodicity properties similar to D.-Y. Kim [48]. Periodically placed stiffeners can change the speed of sound in the modulated tube without resorting to long branches, as has been shown in this work. And more importantly, this modulated device allows for broadband transmission loss range.

### Conclusion

The Herschel-Quincke device, widely studied for plane waves in acoustic ducts, has proven effective in suppressing vibrations at specific frequencies. However, the application of a similar passive vibration control concept for beams, rods, and plates, focusing on controlling the phase shift between two traveling waves in different paths, has not been as extensively explored. Given its simplicity and effective vibration isolation properties, the Herschel-Quincke principle is an attractive approach for this purpose.

Hints towards the generalization of the Herschel-Quincke filtering principle in discontinuous structures and its possible implementation in other configurations can be found in the monograph by D. Mead [50] and the work of E. Shoavi [51]. Mead's book [50] discusses the interaction of bending waves with discontinuities on an infinite beam, considering both external discontinuities by adding point mass, elastic spring, moment of inertia, or a combination of these, and internal discontinuities by changing the cross-section of the beam. According to Mead, in the beam cross-sectional change model, the transmitted energy is relatively sensitive

to the change in cross-section due to the impedance mismatch between the two uniform sections of the waveguide.

E. Shoavi [51] also considered a split waveguide in which the waves are out of phase and destructive interference occurs. The general results of Shoavi's work will be summarized in the following sections.

### 1.2.2 Strings

There are many different types of waves, including acoustic waves propagating in general three-dimensional space and one of the simplest cases is string oscillations [52]. String instruments (guitars, violins, etc.) provide an excellent and intuitive example of the vibration of a distributed-parameter object. Strings are also the easiest system to solve and provide a systematic way to approach other distributed-parameter structures, similar to a simple spring-mass system [4]. Therefore, as the first step, we shall use 'string' to estimate the HQ filter in elastic structures.

An attempt to analyze performance of 'split string vibration isolator', in which the HQ filtering principle is utilized, has been done by E. Shoavi [51]. He investigated the transmission of waves in strings through splitting into two or three branches, such a system is described in Fig.1.15. By analogy with the HQ acoustic tube, the interference effect can be achieved by differences in path lengths and velocities between segments (2) and (3).

Shoavi's work clearly explains and investigates the results of separated sub-branches in a string based on transmission coefficient using scattering and transfer matrix approach.

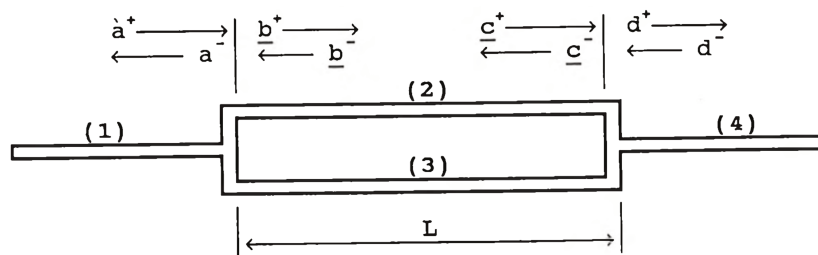


Fig. 1.15 Split string, basic configuration [51].

For analyzing the effect of vibration isolation and the transmission coefficient in split strings, Shoavi [51] used three parameters: 1) impedance mismatch, 2) balance effect and 3) interference effect.

In the first case, the impedance mismatch parameter defines the ratio between the characteristic impedance of the HQ branches, segments (2) and (3), and the impedance of the main waveguide, segment (1). This ratio can be written as

$$\beta = \frac{Z_2 + Z_3}{Z_1}, \quad (1.2.1)$$

In the second case, the two HQ branches, i.e., segments (2) and (3), may have different lengths  $L_2, L_3$  or different wave numbers  $k_2$  and  $k_3$ , then the interference parameter can be defined as

$$\mu = \frac{k_2 L}{k_3 L}, \quad (1.2.2)$$

And the last parameter is the balance parameter, which defines the ratio between the impedances of the two HQ branches, i.e., segments (2) and (3), as

$$\alpha = \frac{Z_2}{Z_3}. \quad (1.2.3)$$

Using all three of these parameters  $\beta, \mu$  and  $\alpha$ , Shoavi demonstrated the dependence of the transmission coefficient on the non-dimensional frequency when these values are changed, as shown in Fig.1.16.

As a result, he calculated that at a certain frequency, zeros occur in the transmission coefficients. The destructive interference effect generally occurs when  $\mu$  is approximately  $1/2$ , causing waves traveling through the branches propagate at different speeds, if  $\mu = 1$  no destructive interference occurs, as shown in Fig.1.16b. The impedance mismatch in the Fig.1.16a should be as large as possible in order to keep the transmission coefficient small. Fig.1.16c shows that reducing the balance effect reduces the bandwidth in which interference occurs. Also, the combined effect can exist when  $\mu = 1/2, \alpha = 1$  and the transmission coefficient varies according to different values of  $\beta$ , as shown in Fig.1.16d.

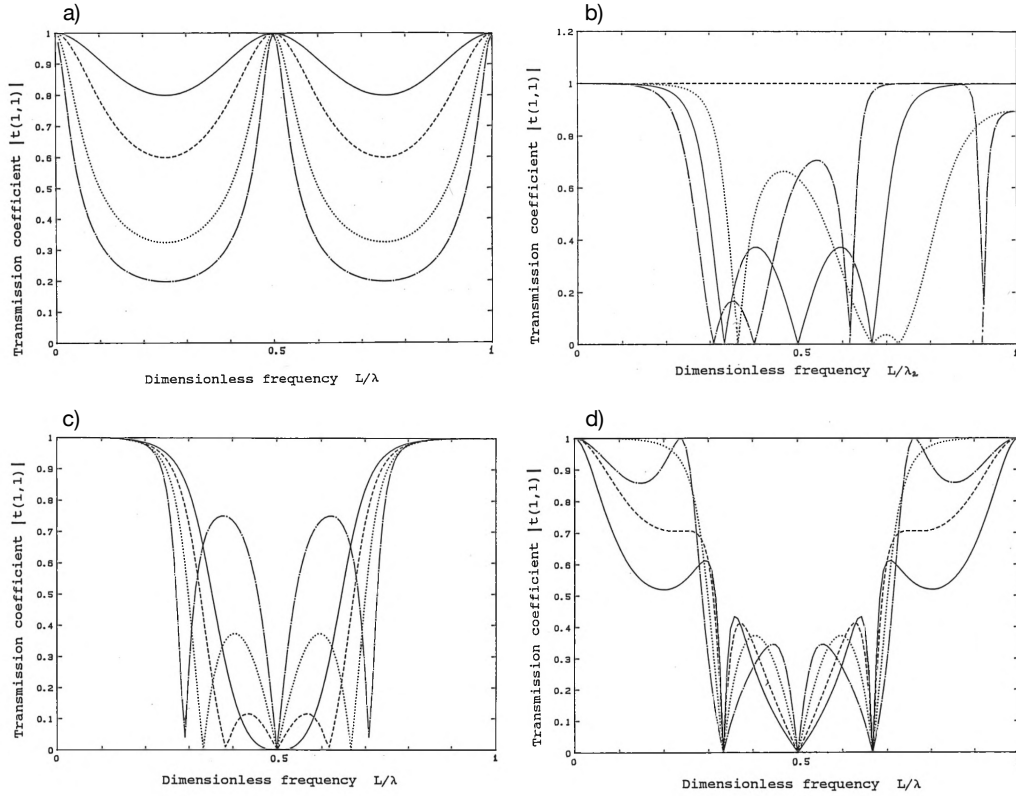


Fig. 1.16 a) Transmission coefficient for various  $\beta$ ,  $\alpha = \mu = 1$ :  $\beta = 2$  (solid line);  $\beta = 3$  (dashed line);  $\beta = 6$  (dotted line);  $\beta = 2$  (dashdotted line). b) Transmission coefficient for various  $\mu$ ,  $\alpha = \beta = 1$ :  $\mu = 0.44$  (dashdotted line);  $\mu = 0.5$  (solid line);  $\mu = 0.57$  (dotted line);  $\mu = 1.0$  (dashed line). c) Transmission coefficient for various  $\alpha$ ,  $\beta = 1$ ,  $v = 1/2$ :  $\alpha = 1/2$  (solid line);  $\alpha = 2/3$  (dashed line);  $\alpha = 1.0$  (dotted line);  $\alpha = 2$  (dashdotted line). d) Transmission coefficient for various  $\beta$ ,  $\alpha = 1$ ,  $\mu = 1/2$ :  $\beta = 1/2$  (dashdotted line);  $\beta = 1$  (dotted line);  $\beta = 2$  (dashed line);  $\beta = 3$  (solid line) [51].

### 1.2.3 Beams

The HQ filter can also be employed to attenuate bending waves in solid mechanical structures such as beams. Shoavi, having previously analyzed wave propagation in strings, conducted the initial evaluation of wave propagation in such structures.

Propagation along the beam has two main differences from its acoustic counterpart and strings: existence of evanescent bending waves and dispersive behavior of bending waves, i.e. velocity is frequency dependent.

Similar to D. Mead [50], Shoavi [51] examined scattering problems at the point of attachment and a change in cross-section, involving three wave components: the propagating bending component, near field bending component and an axial wave component. In addition, he analytically considered the split beam problem excluding axial waves, focusing on the transmission coefficient. Shoavi then experimentally confirmed the existence of zero transmission frequencies in beams using the HQ effect.

Destructive interference in split beams can be described by the same principle as in strings. However, the presence of evanescent waves and the phase velocity dependence on frequency make the analysis more difficult than for a split string.

The difference in the speed of bending waves between the two path can be controlled by a single point discontinuity, as shown in Fig.1.17. To adjust the propagating wave delay in one of the paths and the waves were  $180^\circ$  out of phase, as predicted by G.W. Stewart [26], the principle of thickness difference between segments 2 and 3  $h_2 \neq h_3$  must be satisfied. This thickness difference will provoke destructive interference at some frequencies.

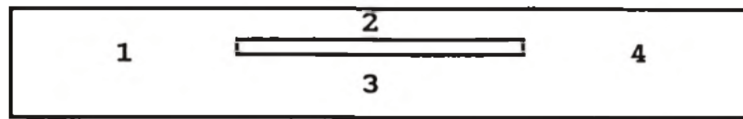


Fig. 1.17 Basic geometry of a split beam [51] .

The wave phenomenon in a split beam can be described as follow: when a wave is incident upon two or more discontinuities mounted on a waveguide, it is scattered. The wave component transmitted through the first discontinuity is incident upon the second one and is scattered again. The internal reflected waves undergo a phase change as they propagate between the discontinuities and when they are reflected at the discontinuities. If the total phase change as a wave travels once around the discontinuities and back is a multiple of  $2\pi$  then successive reflections interfere constructively. However if the total phase change is  $\pi$  plus a multiple of  $2\pi$  then successive reflections interfere destructively. The total transmission is then generally small. Since the phase change associated with reflections from the discontinuities.

In the analysis presented by Shoavi [51], two methods have been proposed to calculate the transmission coefficient for split beams, namely the scattering matrix assembly method and the combined method with transfer and scattering matrices.

For both analyses, the continuity equations, which relate to transverse and axial displacement and slope, and the equations of equilibrium, which relate to shear force and moment, at each of the joints of the split sections of the beam must be compiled.

The parameters describing the transmission problem in a split beam include an interference parameter Eq.1.2.2 with the same HQ length, a balance parameter Eq.1.2.3, which describes the behavior of the two HQ branches in a split beam, an impedance mismatch parameters between the split region (segments 2 and 3) and the main beam (segment 1), and a wave number mismatch parameter denoted as  $\gamma$ .

The characteristic impedance  $Z_o$  of bending waves in a beam is calculated as

$$Z_o = \frac{2}{\omega} EIk_j^3, \quad j = 1, 2, 3, 4 \quad (1.2.4)$$

The wave number mismatch  $\gamma$  parameter is [51]

$$\gamma = \frac{k_2}{k_1}. \quad (1.2.5)$$

By analogy with HQ filter adaptation in strings, Shoavi demonstrated the results shown in Fig.1.18. This figure illustrates the dependence of the transmission coefficient on the non-dimensional frequency at various parameters  $\beta, \mu, \alpha, \gamma$ . The destructive analysis of the HQ device in beams is similar to that shown in Fig.1.16, i.e., the zeros occur in the transmission coefficient. Shoavi investigated the design properties of a vibration isolator in a split beam. He found a suitable cross-sectional ratio and correct length for the split beam. Small changes in  $\beta, \mu, \alpha, \gamma$  significantly alter the phase difference of waves traveling through the two HQ branches, thereby affecting the transmission coefficient, as shown in Fig.1.18.

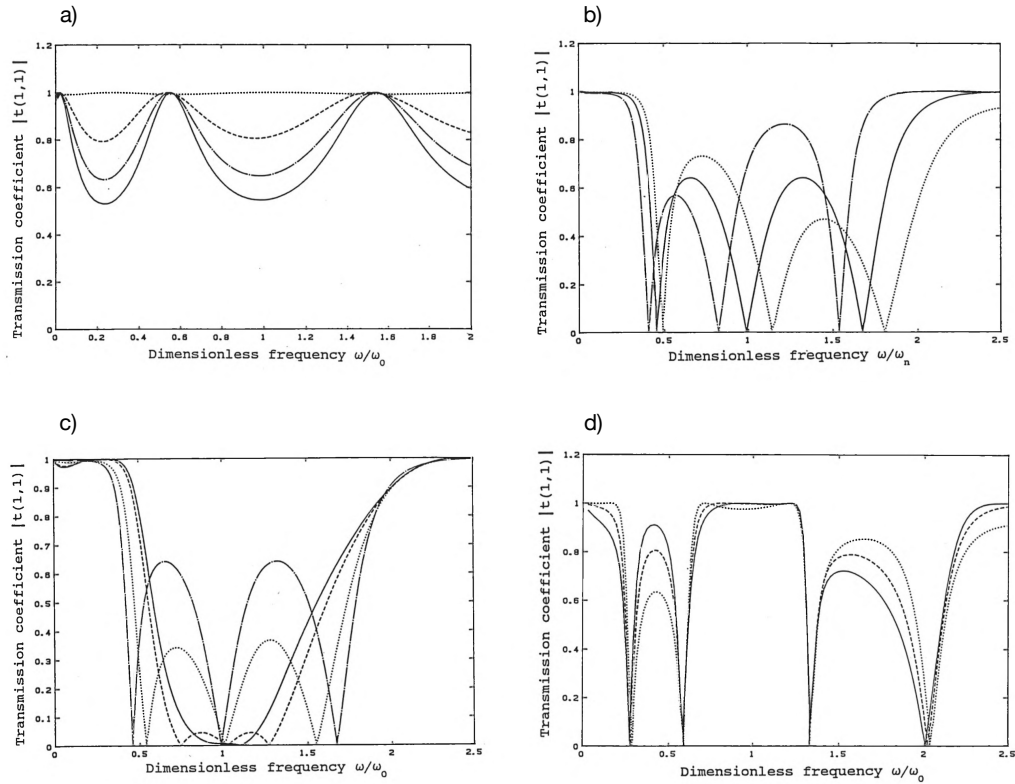


Fig. 1.18 a) Effects of various impedance mismatch values.  $\alpha = \beta = 1$ ,  $\gamma = 0.875$ ,  $\beta = 10$  (solid line);  $\beta = 5$  (dashed line);  $\beta = 1$  (dotted line);  $\beta = 0.1$  (dashdotted line). b) Effects of the interference parameter  $\mu$ :  $\alpha = \beta = 1$ ,  $\gamma = 0.875$ ,  $\mu = 0.5$  (dashdotted line);  $\mu = 0.556$  (solid line);  $\mu = 0.6$  (dotted line). c) Effects of balance,  $\mu = 0.556$ ,  $\beta = 1$ ,  $\gamma = 0.875$ :  $\alpha = 0.3$  (solid line);  $\alpha = 0.35$  (dashed line);  $\alpha = 0.6$  (dotted line);  $\alpha = 1$  (dashdotted line). d) Effects of wavenumber mismatch,  $\alpha = \beta = 1$ ,  $\mu = 0.25$ ,  $\gamma = 1$  (solid line);  $\gamma = 0.8$  (dashed line);  $\gamma = 0.6$  (dotted line) [51].

Shoavi's work has demonstrated that the HQ filter offers good prospects in vibration isolation of a mechanical elastic structure such as rods and beams, and achieving optimal vibration isolation requires meticulous design to isolate the vibrations of one part of the structure from another in the desired frequency range.

### 1.3 THESIS GOALS AND PLAN

The main goal of this thesis is to adapt the HQ principle for elastic waves in mechanical structures such as rods, beams and plates. Despite the significant work of E. Shoavi, which gave a great contribution and idea to the development of HQ analysis for elastic beams and strings, we consider this principle for elastic

beams in the case where bending and longitudinal waves coexist simultaneously. In particular, a theoretical model based on the Timoshenko beam theory will be developed to achieve this goal. Then, the attenuation mechanism of the HQ device in the resonant waveguide is studied by first numerical testing. In more detail, we will find that there are two groups of modes of the HQ device. These are out-of-phase and in-phase modes. An energy flux analysis will then be presented describing the presence of standing waves that are localized in the HQ filter. And a rather significant part of the work, is to conduct the experimental part using the advanced measurement techniques of the 3Dvib experimental platform. All the analyses performed will be compared with each other and will derive the fundamental results of HQ filter.

The adaptation of such a device might be unique to cylindrical coordinates. And the objective of this part of the work will be to integrate the HQ principle into an elastic plate. The realization of this goal will be carried out with the basis of Kirchhoff-Love plate theory.

The HQ device can then be combined with a periodic chain to produce stop bands. In addition, this device can be controlled by changing the number of traveling waves in the paths, namely by increasing the number of HQ branches or cells. The main objectives of this simulations are to transfer the concept of HQ filter from the problem of vibration attenuation at narrow frequency bands to wide frequency bands.

This manuscript embodies five self-contained chapters. The current Chapter 1 provides an introduction to the work, including background, motivation and scope of work. A summary of the remaining chapters is summarized here and briefly illustrated in the Fig.1.19.

Chapter 2 provides a detailed analysis of the first analytical results of the filtering properties of HQ system in rods. The longitudinal waves are considered exclusively. Three problems are formulated to find the zero transmission frequencies at which destructive interference takes place. Different characteristics of the phase velocities and stiffnesses between the two HQ segments are presented to show the influence on the zero transmission frequencies.

Chapter 3 presents the results of HQ filter in beams. The analysis based on Timoshenko beam theory for the flexural waves. The contribution of longitudinal waves is also taken into account. The zero transmission frequencies are calculated by using the analytical wave model and compared with the COMSOL validation

and experimental results. The eigenfrequency problem in complex plane shows the existence of out-of-phase and in-phase modes. Further, the energy flux analysis reveals the effect of energy circulation and the presence of standing waves in the HQ filter. Finally, various parametric studies of HQ device in beams are also shown.

Chapter 4 describes the implementation of the HQ filter in plates. The Kirchhoff-Love assumption of the classical (technical) plate theory is considered. The analysis consist of a zero transmission problem, then a forcing problem. The first results show the effect of attenuation of elastic waves in the HQ plate. However, analyzing the insertion loss reveals the problem of amplification of wave amplitudes in a semi-infinite HQ plate. This problem is not a particular case and can be considered for any constrained system subjected to external excitation. The last section of this Chapter describes sandwich panels and the inner core effect.

Chapter 5 studies different concepts of HQ filter to improve its vibration isolating effect. The analysis consists of considering series, parallel and mixed HQ arrangements and integrating the periodic structure using Floquet theory to achieve broadband attenuation.

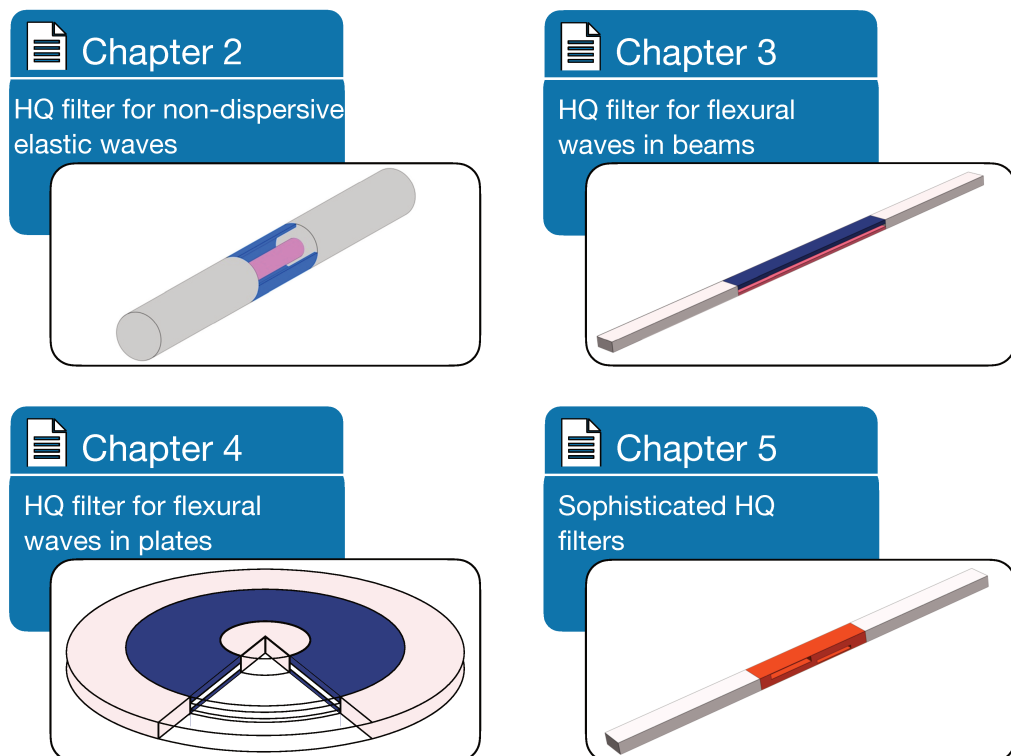


Fig. 1.19 Thesis plan



---

## HERSCHEL-QUINCKE FILTER FOR NON-DISPERSIVE ELASTIC WAVES

---

This Chapter is focused mainly on wave propagation in rods with HQ insertion. Analysis that can be handled in this manner include the first results on the transmission properties of HQ filter for elastic waves. We will analyze two independent types of waves that can be excited in solid HQ rods. The first group are longitudinal waves of compression-expansion and the second group corresponds to torsional waves.

As shown in Chapter 1, the operational principle of HQ filters is destructive interference of waves travelling in the main and side branches of a waveguide. In the classical case of an acoustic waveguide, these branches are filled with the same medium, which supports propagation of non-dispersive waves. Then the only tool to generate destructive interference is a difference in lengths of these branches.

In vibroacoustic applications, the energy transmission is associated with axial, torsion and flexural waves. This Chapter is concerned with the suppression of axial and torsion waves using HQ filtering effect. Although waves of these types are non-dispersive (as acoustic ones), it is entirely possible to design a HQ filter as a combination of two branches of different materials, see Fig.2.1. As soon as wave speeds in segments 1 and 2 are different due to material contrast, destructive interference of axial or torsion waves travelling in these branches emerges. Notably, the material of segment 2 may remain the same as the host rod (shaft). For consistency, it should be noted that the limitation to cylindrical shape of a host rod and a HQ filter applies only for torsion waves. HQ filtering of axial waves applies for a broader range of shapes of cross-section. However, the condition of an absence of generation of flexural waves at the interfaces of HQ filter and the host rod must be obeyed.

## 2.1 WAVE MODEL FOR AXIAL WAVES IN RODS

Among the types of vibrations exhibited by an elastic strings or rods, its longitudinal and torsional vibrations are the simplest to analyze. And the HQ filtering principle may be utilised for suppression of propagation of dilatation and torsion waves in the layout shown in Fig.2.1 as soon as we allow material properties of 'blue' and 'pink' segments to be different.

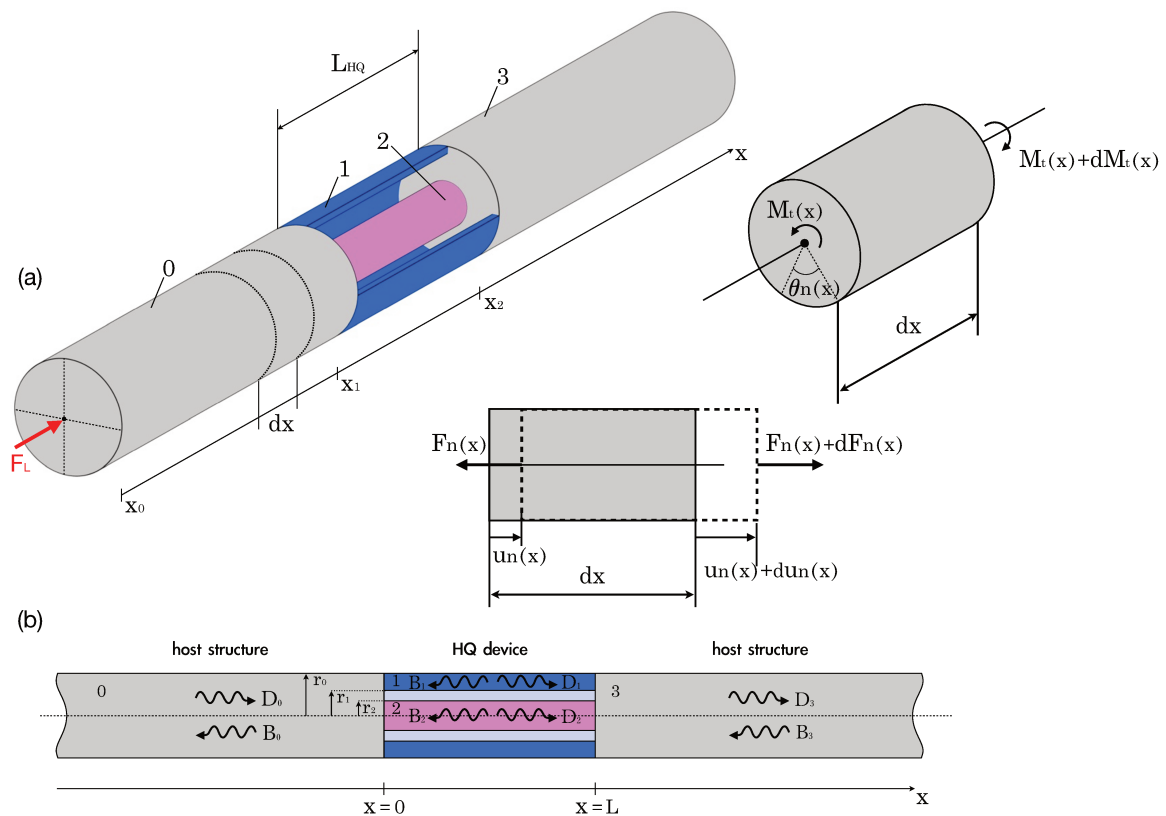


Fig. 2.1 a) Scheme of an HQ filter for longitudinal and torsional waves in rods. b) Description of longitudinal waves amplitudes in each sub-zone, where the waves propagate in homogeneous semi-infinite segments 0 and 3 and the discontinuity between segments 1 and 2 which is called HQ filter.

Both groups of waves have a phase velocity  $\omega/k$  whose is frequency independent and hence non-dispersive. In dealing with longitudinal and torsional vibrations, we will assume that the rod consist of a number of regional elements shown in Fig.2.1, where 0 and 3 segments are an unsplit regions, segment 1 represents the outer cylindrical hollow rod, and segment 2 represents the small inner rod.

All analysis reported in this Chapter is done for plane dilatation waves in the structure shown in 2.1. The results are fully applicable for HQ filtering of torsion waves in shafts of a circular cross-section as soon as an axial displacement  $u_n(x)$  and an axial stiffness  $E_n A_n$  are replaced with a rotation angle  $\theta_n(x)$  and a torsion stiffness  $G_n J_n$ , respectively.

To analyse the behaviour of HQ filter, we introduce three alternative formulations of the wave suppression problem and demonstrate their equivalence to each other:

- In the first formulation, we consider an infinite rod equipped with HQ filter and introduce an incident time-harmonic wave of the unit amplitude, which impinges on HQ filter. Hereafter, this problem will be referred to as the ‘unit amplitude incoming wave problem’, as shown in Fig.2.2a.
- In the second formulation, we consider a semi-infinite rod with a time-harmonic force of the unit amplitude acting at its free edge, as shown in Fig.2.2b. Hereafter, this problem will be referred to as the ‘unit amplitude forcing problem’.
- In the third formulation, we consider the ‘zero transmission frequency’ problem, as shown in Fig.2.2c. In its formulation, we assume the absence (i.e., zero amplitude) of outgoing wave in segment 3 (see Fig.2.1c) and identify frequencies, at which it occurs.

Therefore, the frequencies at which wave propagation in segment 3 is impossible can be found from any of these formulations. The analysis of this effect constitutes the subject of this Chapter.

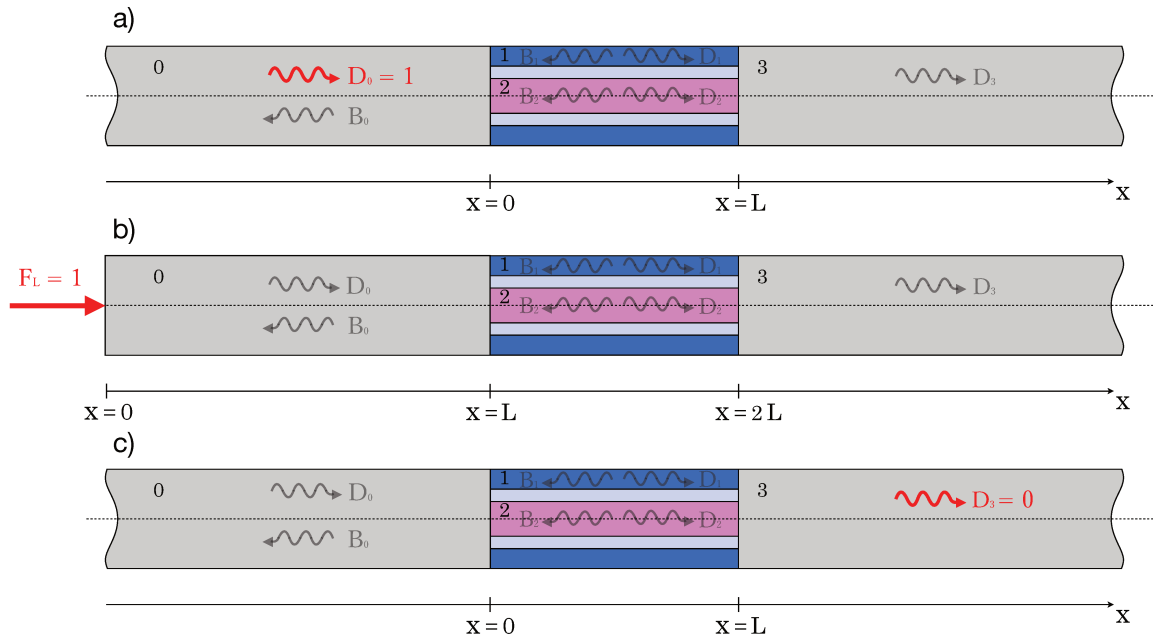


Fig. 2.2 Three typical formulations: a) Unit amplitude incoming wave problem. b) Forced problem. c) Zero transmission frequency problem.

## 2.2 ANALYSIS OF THE FILTERING PROPERTIES

### 2.2.1 Unit incoming wave problem

The aim of this section is to calculate the scattering coefficients of the HQ device, in particular the longitudinal wave transmission coefficient. The particles in every cross sections move only in the axial direction of the rod. The longitudinal extensions and compressions that take place during such a vibration of the rod will be accompanied by some lateral deformation.

We assume that Sommerfeld radiation condition takes place  $B_3 = 0$  and the unit incoming wave has a right-handed direction in segment 0, then part of the wave will be reflected due to the discontinuity in segments 1-2 and the rest will be transmitted to its far side as shown in Fig. 2.1b. When the transmitted wave is incident upon the segment 3, multiple reflections take place between the 1 and 2 segments. At certain frequencies the internally reflected waves will interfere constructively, and energy incident upon discontinuities will be fully transmitted. And at other frequencies, the reflected waves will interfere destructively which will lead to zero transmission of waves to the right hand side of the split region.

In each segment of an infinite rod shown in Figure 2.1, time-harmonic wave propagation at the frequency  $\omega$  is governed by the Helmholtz equation :

$$\frac{d^2 u_n(x)}{dx^2} + \frac{\omega^2}{c_n^2} u_n(x) = 0, \quad n = 0, 1, 2, 3 \quad (2.2.1)$$

where the speed of longitudinal wave propagation is the ratio of the material's modulus  $E_n$  to its mass density  $\rho_n$  as

$$c_n = \sqrt{\frac{E_n}{\rho_n}}, \quad (2.2.2)$$

Semi-infinite segments are made of the same material, so that  $E_3 = E_0, \rho_3 = \rho_0$ . Disregarding the time-harmonic term  $e^{-j\omega t}$ , the one-dimensional solution of the longitudinal displacement field in any point  $x$  is:

$$u_n(x) = D_n e^{jk_{dim}x} + B_n e^{-jk_{dim}x}, \quad (2.2.3)$$

The positive and negative going waves have amplitudes  $D_n$  and  $B_n$ , as shown in Fig.2.1b. As defined by Sommerfeld radiation condition,  $B_3 = 0$ . The frequency dependent wave number  $k_{dim}$  is defined as:

$$k_{dim} = \frac{\omega}{c_n}, \quad (2.2.4)$$

The longitudinal force is:

$$F_n(x) = E_n A_n \frac{du_n(x)}{dx}, \quad (2.2.5)$$

where the surface area of segments are  $A_0 = A_3 = \pi r_0^2, A_1 = \pi r_0^2 - \pi r_1^2, A_2 = \pi r_2^2$ .

The continuity conditions at the interfaces are:

$$u_0(0) = u_1(0) = u_2(0), \quad (2.2.6a)$$

$$u_3(L) = u_1(L) = u_2(L), \quad (2.2.6b)$$

The equilibrium conditions at the interfaces are:

$$F_0(o) = F_1(o) + F_2(o), \quad (2.2.7a)$$

$$F_3(L) = F_1(L) + F_2(L), \quad (2.2.7b)$$

Subsequently, we consider a non-dimensionalization scheme, where the axial coordinate is scaled to the radius of the 'main' rod,  $x = \frac{x^{dim}}{r_o}$ , the non-dimensional frequency is  $\Omega = \frac{\omega r_o}{c_o}$ , and other non-dimensional parameters, such as the ratio of sound velocities  $\alpha_n = \frac{c_o}{c_n}$ , stiffness ratio  $\beta_n = \frac{E_n A_n}{E_o A_o}$ , scaling length  $L = \frac{L^{dim}}{r_o}$ .

The amplitudes of the six waves generated by the discontinuity are to be found in terms of the amplitude of the incident wave  $D_o = 1$ . This can be done by satisfying the interaction conditions given in equations 2.2.6, 2.2.7. Where the vector of unspecified complex wave amplitudes and specified incident amplitude vector on the left side of the region o at the interface lead to the following relationship

$$\mathbf{K} = \mathbf{L} \cdot \mathbf{U}, \quad (2.2.8)$$

In the equation 2.2.8,  $\mathbf{L}$  represents the dynamic matrix between the specified amplitude vector  $\mathbf{K}$  and unspecified amplitude vector  $\mathbf{U}$

$$\mathbf{L} = \begin{bmatrix} -e^{-jkx_1} & e^{jkx_1} & e^{-jkx_1} & 0 & 0 & 0 \\ -e^{-jkx_1} & 0 & 0 & e^{jkx_1} & e^{-jkx_1} & 0 \\ 0 & e^{jkx_2} & e^{-jkx_2} & 0 & 0 & -e^{jkx_2} \\ 0 & 0 & 0 & e^{jkx_2} & e^{-jkx_2} & -e^{jkx_2} \\ \beta_o j k e^{-jkx_1} & \beta_1 j k e^{jkx_1} & -\beta_1 j k e^{-jkx_1} & \beta_2 j k e^{jkx_1} & -\beta_2 j k e^{-jkx_1} & 0 \\ 0 & \beta_1 j k e^{jkx_2} & -\beta_1 j k e^{-jkx_2} & \beta_2 j k e^{jkx_2} & -\beta_2 j k e^{-jkx_2} & -\beta_3 j k e^{jkx_2} \end{bmatrix},$$

and

$$\mathbf{K}^T = [D_o e^{jkx_o}; D_o e^{jkx_o}; 0; 0; D_o \beta_o j k e^{jkx_o}; 0],$$

$$\mathbf{U}^T = [B_o; D_1; B_1; D_2; B_3; D_3],$$

Then the amplitudes of the reflected wave  $B_0$  and the transmitted wave  $D_3$  can be found from the Equation 2.2.8 as

$$B_0 = \frac{2\alpha_1\alpha_2\beta_1\beta_2 \cdot [\cos(\alpha_1L\Omega)\cos(\alpha_2L\Omega) - 1] - [\alpha_1^2\beta_1^2 + \alpha_2^2\beta_2^2 - 1] \cdot \sin(\alpha_1L\Omega)\sin(\alpha_2L\Omega)}{\Delta}, \quad (2.2.9)$$

$$D_3 = \frac{2je^{-jL\Omega} \cdot [\alpha_2\beta_2 \sin(\alpha_1L\Omega) + \alpha_1\beta_1 \sin(\alpha_2L\Omega)]}{\Delta}, \quad (2.2.10)$$

where,

$$\Delta = 2\alpha_1\alpha_2\beta_1\beta_2 - 2\alpha_1\beta_1 \cos(\alpha_1L\Omega)[\alpha_2\beta_2 \cos(\alpha_2L\Omega) - j \sin(\alpha_2L\Omega)] + \sin(\alpha_1L\Omega) [2j\alpha_2\beta_2 \cos(\alpha_2L\Omega) + (1 + \alpha_1^2\beta_1^2 + \alpha_2^2\beta_2^2) \sin(\alpha_2L\Omega)]$$

As was pointed out earlier, a wave is incident upon a discontinuity such as HQ filter can be scattered. The proportion of the incident wave which is reflected at the intersection between segments 0 and 1-2 (see Fig.2.1) is the wave amplitudes reflection ratio R, and the proportion of the incident wave which is transmitted at the segment 3 is transmission ratio T. Hence, the transmission and reflection coefficient with Sommerfeld radiation condition yield the expressions

$$T = \frac{D_3}{D_0}, \quad (2.2.11)$$

$$R = \frac{B_0}{D_0}, \quad (2.2.12)$$

Since the incoming wave is  $D_0 = 1$  and substituting the Equations 2.2.9, 2.2.10 into the Equations 2.2.11, 2.2.12, we obtain

$$T = \frac{2je^{-jL\Omega} \cdot [\alpha_2\beta_2 \sin(\alpha_1L\Omega) + \alpha_1\beta_1 \sin(\alpha_2L\Omega)]}{\Delta}, \quad (2.2.13)$$

$$R = \frac{2\alpha_1\alpha_2\beta_1\beta_2 \cdot [\cos(\alpha_1L\Omega)\cos(\alpha_2L\Omega) - 1] - [\alpha_1^2\beta_1^2 + \alpha_2^2\beta_2^2 - 1] \cdot \sin(\alpha_1L\Omega)\sin(\alpha_2L\Omega)}{\Delta}, \quad (2.2.14)$$

The expression in the numerator of the Eq.2.2.13 cannot be equal zero, and the zero transmission frequencies are found from equation

$$\alpha_2\beta_2 \sin(\alpha_1 L\Omega) + \alpha_1\beta_1 \sin(\alpha_2 L\Omega) = 0. \quad (2.2.15)$$

For any root of this equation, we reconstruct a shape of forced vibration. It gives a standing wave in all segments of an infinite rod, because there is no energy transmission in the system when  $D_3 = 0$ .

Fig.2.3a shows the transmission and reflection coefficient as a function of non-dimensional frequency for an undamped system. For the chosen parameters:

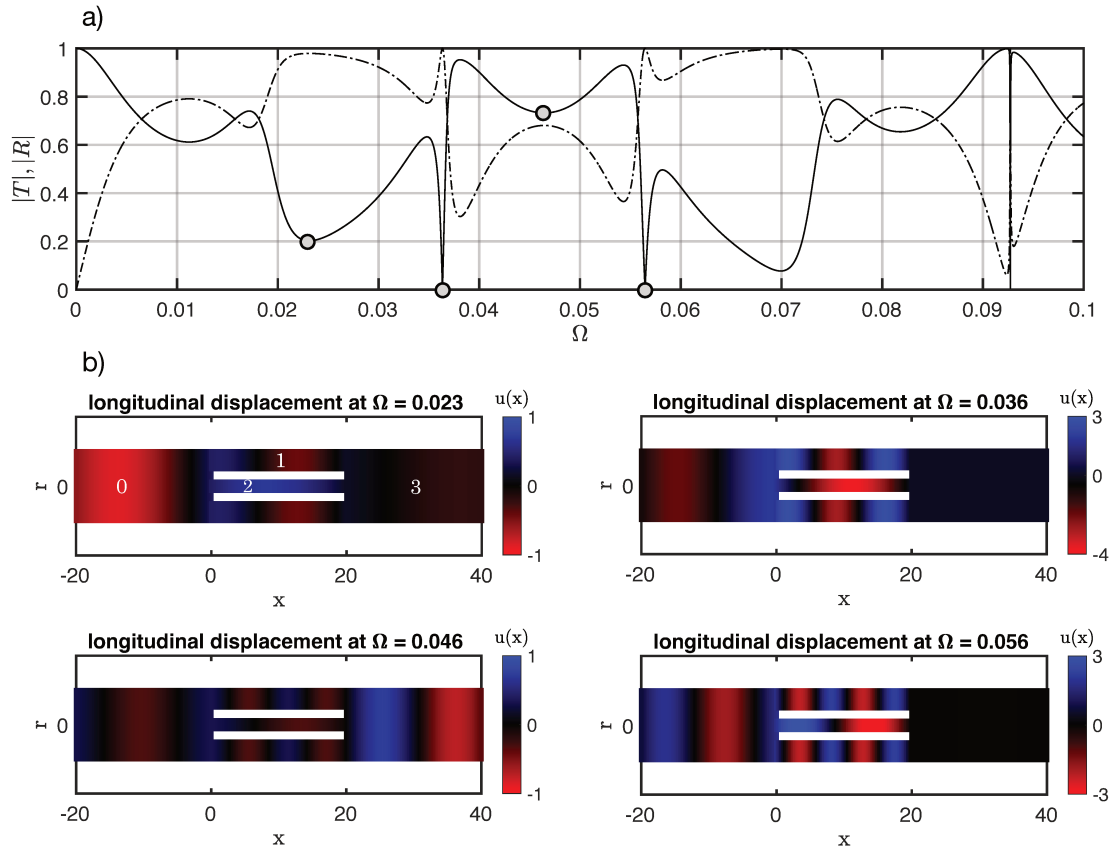


Fig. 2.3 a) The frequency dependence  $\Omega$  of the transmission coefficient (black solid line) and reflection coefficient (black dash-dotted line) at the ratio of sound velocities  $\alpha_0 = \alpha_3 = 1, \alpha_1 = 1.9, \alpha_2 = 0.8$ , stiffness ratio  $\beta_0 = \beta_3 = 1, \beta_1 = 0.7, \beta_2 = 1.2$ . b) Longitudinal displacement field for selected frequencies  $\Omega$  and for each rod elements 0,1,2,3.

the ratio of sound velocities between segments  $\alpha_0 = \alpha_3 = 1, \alpha_1 = 1.9, \alpha_2 = 0.8$ , the stiffness ratio of segments  $\beta_0 = \beta_3 = 1, \beta_1 = 0.7, \beta_2 = 1.2$  and scaled length

$L = 20$ , the transmission coefficient reaches zero at a specific frequency, ensuring full vibration isolation of the segment 3 and a complete destructive interference of waves at  $x = L$ , see Fig.2.1. For a conservative system, a transmission coefficient equal to zero, roots of the Equation 2.2.15, corresponds to a reflection coefficient equal to one.

At the selected frequencies  $\Omega$ , the real values of the longitudinal displacement fields  $u(x)$  are presented in Fig.2.3b. For zero transmission frequency, the longitudinal displacement is zero in the element 3, while for non-zero transmission frequency it is not.

### 2.2.2 Forced problem

The forced problem can be formulated for a semi-infinite rod in the same manner as the unit amplitude incoming wave problem. The semi-infinite rod with four segments excited by a force of the unit amplitude  $F_L$ , acting at an arbitrarily selected endpoint  $x_0 = 0$  in segment 0 as shown in Fig.2.2b, then a propagating wave is generated which is reflected and transmitted at the point  $x_1 = L$ , segments 1 and 2, and stops destructively due to the phase velocity difference at the point  $x_2 = 2L$ , segment 3.

The scattering parameters T and R can be determined from the continuity and equilibrium equations from Eqs.2.2.6, 2.2.7 and the new boundary condition

$$F_L = E_0 A_0 \frac{du(x)}{dx}, \quad x = x_0 \quad (2.2.16)$$

Putting a new boundary condition 2.2.16 into Equation 2.2.8, a new system of inhomogeneous equations with respect to the wave amplitudes in 2.2.3 can be expressed in the form

$$\mathbf{K}^* = \mathbf{L}^* \cdot \mathbf{U}^*, \quad (2.2.17)$$

The left-hand vector of Equation 2.2.17 is the forcing vector

$$\mathbf{K}^{*T} = [0; \quad 0; \quad 0; \quad 0; \quad 0; \quad F_L; \quad 0],$$

The right-hand vector

$$\mathbf{U}^{*T} = [D_0; B_0; D_1; B_1; D_2; B_2; D_3],$$

The new matrix with a new line representing the axial force and a new column representing the generated wave  $D_0$  has the form

$$\mathbf{L}^* = \begin{bmatrix} -e^{jkx_1} & -e^{-jkx_1} & e^{jkx_1} & e^{-jkx_1} & 0 & 0 & 0 \\ -e^{jkx_1} & -e^{-jkx_1} & 0 & 0 & e^{jkx_1} & e^{-jkx_1} & 0 \\ 0 & 0 & e^{jkx_2} & e^{-jkx_2} & 0 & 0 & -e^{jkx_2} \\ 0 & 0 & 0 & 0 & e^{jkx_2} & e^{-jkx_2} & -e^{jkx_2} \\ -\beta_0 j k e^{jkx_1} & \beta_0 j k e^{-jkx_1} & \beta_1 j k e^{jkx_1} & -\beta_1 j k e^{-jkx_1} & \beta_2 j k e^{jkx_1} & -\beta_2 j k e^{-jkx_1} & 0 \\ 0 & 0 & \beta_1 j k e^{jkx_2} & -\beta_1 j k e^{-jkx_2} & \beta_2 j k e^{jkx_2} & -\beta_2 j k e^{-jkx_2} & -\beta_3 j k e^{jkx_2} \\ -\beta_0 j k e^{jkx_0} & \beta_0 j k e^{-jkx_0} & 0 & 0 & 0 & 0 & 0 \end{bmatrix},$$

The amplitude of the incoming, reflected and outgoing wave in this case becomes

$$D_0 = \frac{1}{\Delta_1} [-2j\alpha_1\alpha_2\beta_1\beta_2 + 2\alpha_1\beta_1 \cos(\alpha_1 L\Omega)[j\alpha_2\beta_2 \cos(\alpha_2 L\Omega) + \sin(\alpha_2 L\Omega)] \\ + \sin(\alpha_1 L\Omega)[2\alpha_2\beta_2 \cos(\alpha_2 L\Omega) - j(1 + \alpha_1^2\beta_1^2 + \alpha_2^2\beta_2^2) \sin(\alpha_2 L\Omega)], \quad (2.2.18)$$

$$B_0 = \frac{-2j\alpha_1\alpha_2\beta_1\beta_2 (-1 + \cos(\alpha_1 L\Omega) \cos(\alpha_2 L\Omega)) + j (-1 + \alpha_1^2\beta_1^2 + \alpha_2^2\beta_2^2) \sin(\alpha_1 L\Omega) \sin(\alpha_2 L\Omega)}{\Delta_1}, \quad (2.2.19)$$

$$D_3 = \frac{j e^{-jL\Omega} \cdot [\alpha_2\beta_2 \sin(\alpha_1 L\Omega) + \alpha_1\beta_1 \sin(\alpha_2 L\Omega)]}{\Delta_2}, \quad (2.2.20)$$

$\Delta_1$  and  $\Delta_2$ , also have an explicit analytical form

$$\Delta_1 = 2\Omega(\cos(\Omega x_0)(2\alpha_1\alpha_2\beta_1\beta_2 + \alpha_1\beta_1 \cos(\alpha_1 L\Omega)(-2\alpha_2\beta_2 \cos(\alpha_2 L\Omega) \\ + j \sin(\alpha_2 L\Omega)) + \sin(\alpha_1 L\Omega)(j\alpha_2\beta_2 \cos(\alpha_2 L\Omega) + (\alpha_1^2\beta_1^2 + \alpha_2^2\beta_2^2) \sin(\alpha_2 L\Omega))) \\ + (\alpha_2\beta_2 \cos(\alpha_2 L\Omega) \sin(\alpha_1 L\Omega) + (\alpha_1\beta_1 \cos(\alpha_1 L\Omega) - j \sin(\alpha_1 L\Omega)) \sin(\alpha_2 L\Omega)) \sin(\Omega x_0)),$$

and

$$\Delta_2 = \Omega \cos(\Omega x_0)(2\alpha_1\alpha_2\beta_1\beta_2 + \alpha_1\beta_1 \cos(\alpha_1 L\Omega)(-2\alpha_2\beta_2 \cos(\alpha_2 L\Omega) \\ + j \sin(\alpha_2 L\Omega)) + \sin(\alpha_1 L\Omega)(j\alpha_2\beta_2 \cos(\alpha_2 L\Omega) + (\alpha_1^2\beta_1^2 + \alpha_2^2\beta_2^2) \sin(\alpha_2 L\Omega)))$$

$$+\Omega(\alpha_2\beta_2 \cos(\alpha_2L\Omega) \sin(\alpha_1L\Omega) + (\alpha_1\beta_1 \cos(\alpha_1L\Omega) - j \sin(\alpha_1L\Omega)) \sin(\alpha_2L\Omega)) \sin(\Omega x_0)$$

For a rod undergoing axial force, the transmission and reflection parameters can be determined from the Equations 2.2.11 and 2.2.12. As expected, the zero transmission frequencies from 2.2.20 cannot be dependent upon excitation type and they are determined from Equation 2.2.15. These frequencies of the forced problem correspond to the frequencies shown in Fig.2.3.

### 2.2.3 Zero transmission frequency problem and parametric studies

In fact, the ‘zero transmission frequency’ problem is readily formulated with no reference to excitation conditions, i.e., as an eigenvalue problem. Indeed, the conditions  $D_3 = 0$  and  $B_3 = 0$  mean that  $u_3(x) \equiv 0$ . Then conditions 2.2.6b become  $u_1(L) = 0, u_2(L) = 0$ . The condition 2.2.7b reduces to  $F_1(L) + F_2(L) = 0$ . Finally, condition 2.2.7a gives:  $u_1(0) = u_2(0)$ . Now we have set up a system of four homogeneous linear algebraic equations with respect to four amplitudes  $D_1, D_2, B_1, B_2$ . Equating to zero the determinant of this system yields the zero transmission frequency equation 2.2.15.

For any root of this equation, we construct an eigenmode as a standing wave in both segments of an HQ device, which is defined up to the undetermined wave amplitude, say,  $D_1$ . Next, we employ remaining two conditions,

$$u_0(0) = u_1(0) \tag{2.2.21a}$$

$$F_0(0) = F_1(0) + F_2(0) \tag{2.2.21b}$$

This is a system of two homogeneous linear algebraic equations with respect to three amplitudes  $D_0, D_1, B_0$ . For an incident wave of the unit amplitude,  $D_0 = 1$ , the end result is elementary:

$$u_0(x) = \cos(\Omega x) + \alpha_1\beta_1 \left[ -\cot(\alpha_1L\Omega) + \frac{\cos(\alpha_2L\Omega)}{\sin(\alpha_1L\Omega)} \right] \sin(\Omega x) \tag{2.2.22a}$$

$$u_1(x) = \frac{\sin(\alpha_1\Omega(L-x))}{\sin(\alpha_1L\Omega)} \tag{2.2.22b}$$

$$u_2(x) = \frac{\sin(\alpha_2\Omega(L-x))}{\sin(\alpha_2L\Omega)} \tag{2.2.22c}$$

Of course, this result may be obtained by equating to zero the determinant of six equations 2.2.6, 2.2.7 formulated for the full set of wave amplitudes  $D_0, D_1, D_2, B_0, B_1, B_2$  with scaling the eigenmode with an incident wave of the unit amplitude,  $D_0 = 1$ .

To gain an insight into the physical mechanism of the filtering phenomenon at zero transmission frequencies, it is helpful to notice that  $F_1(L) = -F_2(L)$ . It means that, at any instant of time, segments of HQ device at its right edge are loaded in opposite directions, and the net force is zero, as well as  $u_1(L) = 0$  and  $u_2(L) = 0$ .

Analysis of roots of Equation 2.2.15 is presented in Fig.2.4. The zero transmission frequency was calculated as the non-dimensional length of the HQ insertion dependent on the non-dimensional frequency at fixed values of the ratio of sound velocities  $\alpha_1 = 1.9, \alpha_2 = 0.8$  and stiffness ratio  $\beta_1 = 0.7, \beta_2 = 1.2$ . The roots of the zero transmission frequency equation at scaled length  $L = 20$  correspond exactly to the zero peaks of the T in Fig.2.3. From Fig.2.4 it follows that the zero transmission frequencies are controlled by changing the parameter  $L$ , namely as soon as  $L$  increases, the zeros transmission frequencies are shifted towards the low frequency range.

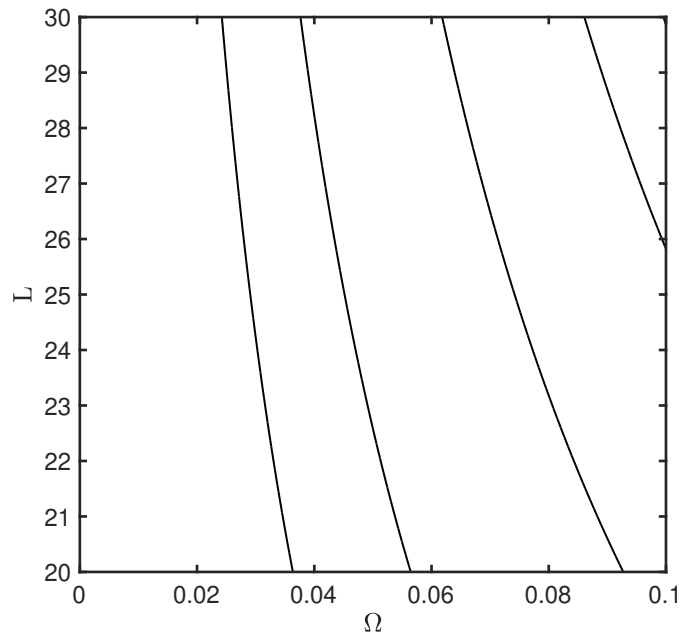


Fig. 2.4 Zero transmission frequencies as a function of non-dimensional frequency  $\Omega$  dependence on non-dimensional length. At the ratio of sound velocities  $\alpha_0 = \alpha_3 = 1, \alpha_1 = 1.9, \alpha_2 = 0.8$  and stiffness ratio  $\beta_0 = \beta_3 = 1, \beta_1 = 0.7, \beta_2 = 1.2$ .

A parametric study of the zero transmission frequency as a frequency dependence on the ratio of sound velocities in segment 1 is presented in Fig.2.5. For fixed values of the scaled length  $L = 28$ , ratio of sound velocities and stiffnesses  $\alpha_2 = 1$ ,  $\beta_2 = 0.2$ , it follows that a significant contribution to the shift of zero transmission frequencies is made by the low stiffness value  $\beta_1$  in segment 1 (see black and pink colored bar). Namely, if the stiffness ratio of  $\beta_1$  decreases with decreasing of the ratio of sound velocities  $\alpha_1$ , the zero transmission frequencies are considerably shifted, and vice versa. However, when  $\alpha_1$  is an integer, i.e.,  $\alpha_1 = 1, 2, 3, \dots$ , the zero transmission frequencies are independent of the choice of the parameter  $\beta_1$ . If the parameters  $\alpha_1 = \alpha_2 = \alpha$ , then the equation 2.2.15 is transformed to equation  $(\beta_1 + \beta_2)\alpha \sin(\alpha\Omega L) = 0$  and if  $2\alpha_1 = \alpha_2$ , the equation 2.2.15 becomes  $(\beta_1 + 2\beta_2 \cos(\alpha\Omega L))\alpha \sin(\alpha\Omega L) = 0$ . Since the parameters  $\beta_2, \beta_1$  are given and are not zero, the zero transmission frequency equation for integer values of  $\alpha_1$  and  $\alpha_2$  can be found as  $\sin(\alpha\Omega L) = 0$ . It is also the case for any  $\alpha_2 = n\alpha_1$  or  $\alpha_2 = \frac{1}{n}\alpha_1$  at  $n = 1, 2, 3, \dots$ , see [53] Section 4.21. This equation characterises standing waves and the effect of HQ interference is dictated by the presence of trapped modes, which are discussed in the following Section 2.2.4. In practice, we can establish any appropriate materials to achieve the desired zero transmission frequencies.

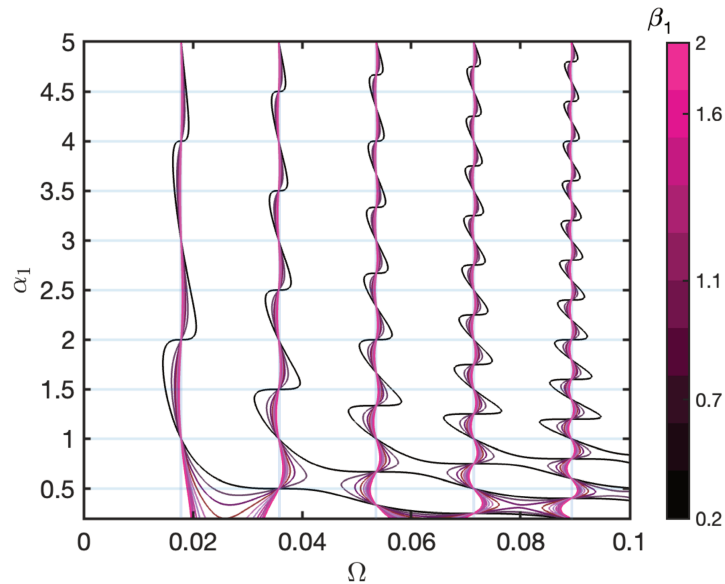


Fig. 2.5 Zero transmission frequency dependence on the ratio of sound velocities  $\alpha_1$  for different stiffness ratio  $\beta_1$  (right colored bar). Fixed values  $\alpha_2 = 1$ ,  $\beta_2 = 0.2$  and scaled length  $L = 28$ .

The grid lines in Fig.2.5 highlight the location of the 'focal points' of the zero transmission frequency. The vertical lines are defined by the condition  $\sin(n\alpha_2\Omega L) = 0$ ,  $n = 1, 2, 3, \dots$ . The blue horizontal lines define the relation  $\alpha_1 = \frac{n\alpha_2}{2}$ ,  $n = 1, 2, 3, \dots$

#### 2.2.4 The trapped mode case

As long as  $\alpha_1 \neq \alpha_2$  and, therefore,  $c_1 \neq c_2$ , the zero transmission effect is attributed to the destructive interference of waves travelling in parallel segments of the HQ device. However, Equation 2.2.15 predicts the same effect for  $\alpha_1 = \alpha_2 = \alpha$  at the frequency  $\Omega = \frac{n\pi}{\alpha L}$ ,  $n = 1, 2, 3, \dots$ . Then formulas 2.2.22 become not applicable, and this case requires a more careful analysis.

Substitution  $\Omega = \frac{n\pi}{\alpha L}$  to 2.2.3 gives  $u_1(x) = D_1 \exp\left(j\frac{n\pi x}{L}\right) + B_1 \exp\left(-j\frac{n\pi x}{L}\right)$ , and, as  $u_1(L) = 0$ , we have  $B_1 = -D_1$ , so that  $u_1(x) = D_1 \sin\frac{n\pi x}{L}$ . The same result is obtained for the segment 2:  $u_2(x) = D_2 \sin\frac{n\pi x}{L}$ . Naturally, these are the eigenmodes of HQ segments with fixed ends. As is well known, these localized (or trapped) eigenmodes exist in infinite waveguides [54], [55].

For an incident wave, Equation 2.2.6a at  $\Omega = \frac{n\pi}{\alpha L}$  is reduced to  $u_0(o) = D_o + B_o = u_1(o) = u_2(o) = 0$ , and  $D_o = -B_o$ . It means that, in the segment 0, we have a standing wave  $u_0(x) = D_o \sin\left(\frac{n\pi x}{L}\right)$ . Thus, the transmission coefficient is zero, while reflection coefficient is one. However, the amplitude of transmitted wave in the solution of the forcing problem is defined by equation 2.2.10. In this formula, both the numerator and the denominator vanish at  $\Omega = \frac{n\pi}{\alpha L}$ ,  $n = 1, 2, 3, \dots$  when  $\alpha_1 = \alpha_2 = \alpha$ . Then the L'Hospital rule gives  $D_3 = (-1)^n \exp\left(-j\frac{n\pi}{\alpha}\right)$ . It means that the transmission coefficient is one, and reflection coefficient is zero.

To resolve this non-uniqueness, we repeat solving of the incoming wave forcing problem at  $\Omega = \frac{n\pi}{\alpha L}$ ,  $n = 1, 2, 3, \dots$ . Equations 2.2.6a, 2.2.7a at  $x = 0$  become

$$D_1 + B_1 = D_o + B_o \quad (2.2.23a)$$

$$D_2 + B_2 = D_o + B_o \quad (2.2.23b)$$

$$\alpha\beta_1(D_1 - B_1) + \alpha\beta_2(D_2 - B_2) = D_o - B_o \quad (2.2.23c)$$

Equations 2.2.6b, 2.2.7b at  $x = L$  are (the identity  $\cos(n\pi) = (-1)^n$ ,  $n = 1, 2, 3, \dots$  is used)

$$D_1 + B_1 = (-1)^n D_3 e^{jn\pi/\alpha} \quad (2.2.24a)$$

$$D_2 + B_2 = (-1)^n D_3 e^{jn\pi/\alpha} \quad (2.2.24b)$$

$$\alpha\beta_1(D_1 - B_1) + \alpha\beta_2(D_2 - B_2) = (-1)^n D_3 e^{jn\pi/\alpha} \quad (2.2.24c)$$

Left hand sides of Equation 2.2.23 and 2.2.24 are the same, and we obtain direct relation between the amplitudes of incident (in segment 1) and transmitted (to segment 3) waves.

From Equations 2.2.23a and 2.2.24a, it follows that

$$D_0 + B_0 = (-1)^n D_3 e^{jn\pi/\alpha} \quad (2.2.25a)$$

From Equations 2.2.23c and 2.2.24c, we have

$$D_0 - B_0 = (-1)^n D_3 e^{jn\pi/\alpha} \quad (2.2.25b)$$

(observe that Equations 2.2.23b and 2.2.24b, give 2.2.25a)

Solution of equations 2.2.25 gives  $B_0 = 0$  and there is no wave reflection from an HQ device. Then  $D_3 = (-1)^n D_0 \exp\left(-j\frac{n\pi}{\alpha}\right)$  and the transmission coefficient equals one. So, the reflection and transmission coefficients correspond to the full transparency of the HQ filter at its resonant frequencies.

However, a shape of forced vibrations of components of an HQ device at these frequencies is not uniquely defined. Indeed, the sets of equations at  $x = 0$  and  $x = L$  are exactly the same

$$D_1 + B_1 = 1 \quad (2.2.26a)$$

$$D_2 + B_2 = 1 \quad (2.2.26b)$$

$$\alpha\beta_1(D_1 - B_1) + \alpha\beta_2(D_2 - B_2) = 1 \quad (2.2.26c)$$

Then the amplitudes of vibrations of two segments of HQ device are linked to each other as

$$\alpha\beta_1(2D_1 - 1) + \alpha\beta_2(2D_2 - 1) = 1 \quad (2.2.27)$$

This relation allows arbitrarily large, resonant vibrations of HQ device with its segments moving in anti-phase to each other ( $D_1 \rightarrow \infty, D_2 \rightarrow -\infty$ ) excited by an incoming wave of the unit amplitude. Then the ratio  $\left|\frac{D_0}{D_1}\right| \sim \left|\frac{D_0}{D_2}\right| \rightarrow 0$ , and, with this scaling, the amplitude of transmitted wave also vanishes.

In this work, we employ a standard ‘steady-state’ problem formulation. To figure out the actual response of an HQ device in these resonant excitation conditions, the problem should be re-formulated as a transient one in the time domain, as it has been done in, for example,[55, 56]. Accomplishment of this challenging task lies beyond the scope of this work.

### 2.3 ADAPTATION TO TORSIONAL WAVES

The HQ rod model for torsional waves is shown in Fig.2.1 The equation of motion for the torsional vibration of the circular form rods is the same as the longitudinal vibration of the bars discussed in one-dimensional wave equation for lateral vibration of string Eq.2.2.1

$$\frac{d^2\theta_n(x)}{dx^2} + \frac{\omega^2}{c_n^2}\theta_n(x) = 0, \quad c_n = \sqrt{\frac{G_n}{\rho_n}}, \quad n = 0, 1, 2, 3 \quad (2.3.1)$$

where  $G_n$  is the Coulomb shear modulus, respectively.

The wave number  $k_{dim}$  is defined as:

$$k_{dim} = \frac{\omega}{c_n}, \quad (2.3.2)$$

The angle of twist of the cross-section is:

$$\theta_n(x) = D'_n e^{jk_{dim}x} + B'_n e^{-jk_{dim}x}, \quad (2.3.3)$$

And the twisting moment takes the form

$$M_t(x) = G_n J_n(x) \frac{d\theta_n}{dx}, \quad (2.3.4)$$

where  $G_n J_n(x)$  is the torsional stiffness, with  $J_n(x) = \frac{\pi}{32} d^4$  denoting the polar moment of inertia of the cross section in the case of a circular section. The continuity and equilibrium conditions at the interface are:

$$\left\{ \begin{array}{l} \theta_0(o) = \theta_1(o), \\ \theta_0(o) = \theta_2(o), \\ \theta_3(L) = \theta_1(L), \\ \theta_3(L) = \theta_2(L), \\ M_{t0}(o) = M_{t1}(o) + M_{t2}(o), \\ M_{t3}(L) = M_{t1}(L) + M_{t2}(L). \end{array} \right. \quad (2.3.5)$$

Using the unit amplitude incoming wave problem  $D'_0 = 1$  and introducing non-dimensional parameters:  $\gamma_n = \frac{a_o}{a_n}$  and  $\psi_n = \frac{G_n J_n}{G_o J_o}$ , the system of linear equations according to the unknown torsional amplitudes  $B'_0, D'_1, B'_1, D'_2, B'_3, D'_3$  can be determined as

$$\mathbf{T} = \mathbf{W} \cdot \mathbf{S}, \quad (2.3.6)$$

where, the dynamic matrix

$$\mathbf{W} = \begin{bmatrix} -e^{-jkx_1} & e^{jkx_1} & e^{-jkx_1} & 0 & 0 & 0 \\ -e^{-jkx_1} & 0 & 0 & e^{jkx_1} & e^{-jkx_1} & 0 \\ 0 & e^{jkx_2} & e^{-jkx_2} & 0 & 0 & -e^{jkx_2} \\ 0 & 0 & 0 & e^{jkx_2} & e^{-jkx_2} & -e^{jkx_2} \\ \psi_0 j k e^{-jkx_1} & \psi_1 j k e^{jkx_1} & -\psi_1 j k e^{-jkx_1} & \psi_2 j k e^{jkx_1} & -\psi_2 j k e^{-jkx_1} & 0 \\ 0 & \psi_1 j k e^{jkx_2} & -\psi_1 j k e^{-jkx_2} & \psi_2 j k e^{jkx_2} & -\psi_2 j k e^{-jkx_2} & -\psi_3 j k e^{jkx_2} \end{bmatrix},$$

and vectors

$$\mathbf{T}^T = [D'_0 e^{jkx_0}; \quad D'_0 e^{jkx_0}; \quad 0; \quad 0; \quad D'_0 \psi_0 j k e^{jkx_0}; \quad 0],$$

$$S^T = [B'_0; D'_1; B'_1; D'_2; B'_2; D'_3],$$

From Equations 2.2.11 and 2.2.12, the transmission and reflection coefficient can be found as

$$T = \frac{D'_3}{D'_0}, \quad (2.3.7)$$

$$R = \frac{B'_0}{D'_0}. \quad (2.3.8)$$

The frequency dependence on the transmission and reflection coefficient is plotted for the chosen non-dimensional parameters  $\gamma_0 = \gamma_3 = 1, \gamma_1 = 0.5, \gamma_2 = 2.5, \psi_0 = \psi_3 = 1, \psi_1 = 2.5, \psi_2 = 0.5$  and  $L = 30$ . As a result, we can see that the T parameter tends to zero at one particular frequency and no transmitted energy takes place. The results are similar to the case of longitudinal waves.

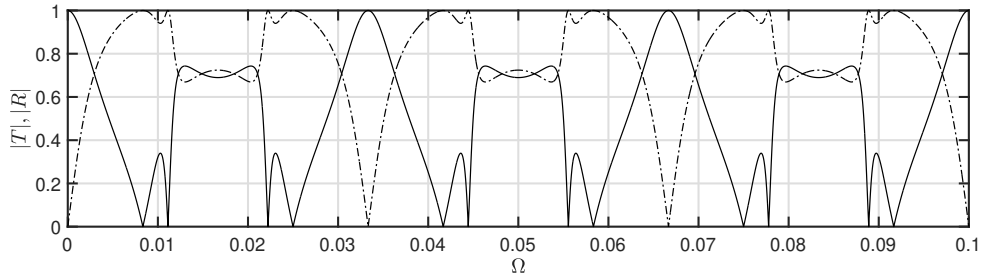


Fig. 2.6 Transmission coefficient (black solid line) and reflection coefficient (black dash-dotted line) at the ratio of sound velocities and the stiffness ratio  $\gamma_0 = \gamma_3 = 1, \gamma_1 = 0.5, \gamma_2 = 2.5, \psi_0 = \psi_3 = 1, \psi_1 = 2.5, \psi_2 = 0.5$ .

## 2.4 CONCLUSION

The HQ filter in the rod has been effectively analyzed. We found that there are certain frequencies at which the transmission coefficient is zero. When the transmission coefficient is zero, destructive interference occurs at the output of the HQ device, resulting in no energy transfer.

Three problems have been formulated to find the same zero transmission frequencies of the HQ filter in rods. These are the unit amplitude incoming waves problem, forced problem and zero transmission frequency problem. Indeed, the

straightforward equation of the zero transmission frequencies is defined only through the wave velocity and the stiffness of the segments. Therefore, any HQ waveguide system with elastic longitudinal waves, characterized by differences in velocities and stiffnesses of the two HQ segments, can be described by this equation without establishing force equations and continuity equations.

A parametric study was carried out for zero transmission frequencies. As a result, the characteristic behavior of zero transmission frequency was found, where the velocity ratio between segments 0 and 1 can take any integer values, then the effect of trapped modes was also observed.

In addition, the zero transmission frequency problem cannot be limited in the analysis of longitudinal waves, we can also consider this problem for other classes of waves such as bending waves. In both analysis for longitudinal and torsion waves has been considered the two pair of propagating waves in each sub-zone, where they can scatter along the HQ filter, resulting in the destructive interference. The sound speed of these waves is independent of frequency, which is not the case for bending waves, where the speed of bending waves is frequency dependent. The complexity of the bending wave analysis is the presence of evanescent waves. Analyses of this difficulty will be discussed in the next Chapter 3.



---

## HQ FILTERS FOR FLEXURAL WAVES IN BEAMS

---

The perspectives and techniques that have been developed in the previous Chapter 2 will now be applied to calculation of wave propagation in solid HQ beam. In this case, the destructive interference does not require a length difference between the main and the side branches made of the same material. It is achieved due to a difference in thickness of branches, which entails a difference in flexural wave propagation speeds. In contrast to longitudinal waves, the bending wave velocity is frequency dependent and near-field waves are present.

### 3.1 MODELS OF THE HQ VIBRATION FILTER FOR BENDING WAVES

#### 3.1.1 *Wave based model with coupled longitudinal and bending motions*

The system shown in Fig.3.1 consists of an infinite beam of height  $h$  and width  $b$ , which is locally divided into two thinner parallel beams of the same length  $L$  but different thicknesses  $h_1 \neq h_2$ . This difference in thickness causes interference between the bending waves due to the contrast in bending stiffness between the two branches, and coupling between the bending waves and the longitudinal waves due to the non-symmetry of the thickness of the host beam.

The aim of this section is to calculate the bending wave transmission coefficient. The wave model is developed by considering both the Timoshenko beam equation [57–61] to describe the bending motion and a wave equation to describe the longitudinal motion [62].

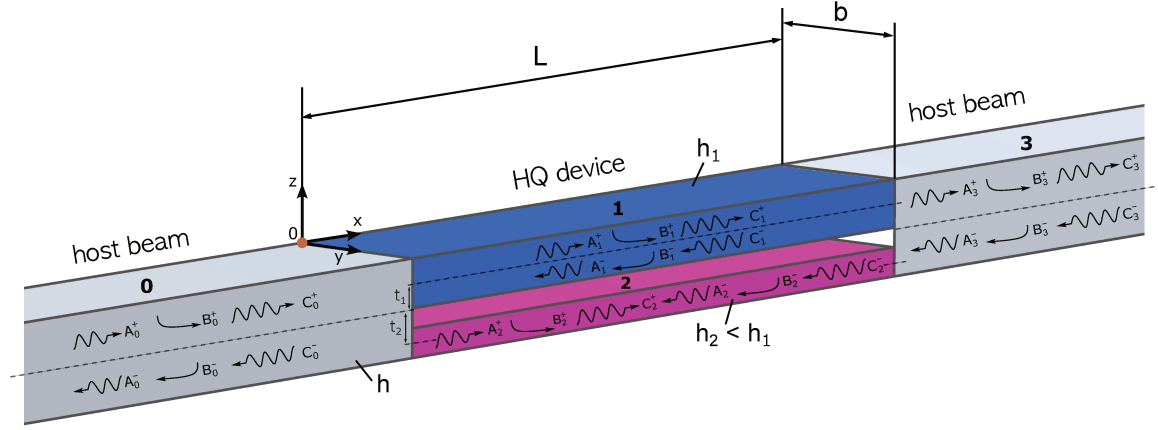


Fig. 3.1 Scheme of an HQ filter embedded into an infinite host beam, made up of two parallel beams of the same length but different thicknesses. The wave amplitudes are denoted  $A_k^-, A_k^+$  and  $B_k^-, B_k^+$  for propagating and evanescent bending waves, and  $C_k^-, C_k^+$  for longitudinal waves.

Assuming harmonic motion with  $e^{-j\omega t}$ , the governing equations are

$$\begin{cases} \kappa GS \left( \frac{d^2 w}{dx^2} - \frac{d\theta}{dx} \right) - \rho S \omega^2 w = 0, \\ EI \frac{d^2 \theta}{dx^2} + \kappa GS \left( \frac{dw}{dx} - \theta \right) - \rho I \omega^2 \theta = 0, \\ \frac{d^2 u}{dx^2} - \frac{\omega^2}{c_L^2} u = 0. \end{cases} \quad (3.1.1)$$

where  $w(x), u(x)$  are the transverse and longitudinal displacements,  $\theta(x)$  is the rotation angle,  $\gamma(x) = \frac{dw}{dx} - \theta(x)$  the shear angle. The parameter  $\rho$  is the density of the beam material,  $E = E_0(1 + j\eta)$  is the complex Young's modulus with  $E_0$  the elastic constant and  $\eta$  the material loss factor,  $\nu$  is the Poisson's ratio and  $G = \frac{E}{2(1 + \nu)}$  is the shear modulus. The bending stiffness is given by  $EI_n = E \frac{bh_n^3}{12}$  and  $\kappa = \frac{10(1 + \nu)}{12 + 11\nu} \approx \frac{5}{6}$  is the shear deformation coefficient for the rectangular section of the beam studied.

For each beam segment, the bending displacement, slope and longitudinal displacement are expressed as wave expansions ( $n = 0, 1, 2, 3$  designating the beam

segments, as shown on Fig.3.1.)

$$\begin{cases} w_n(x) = A_n^+ e^{jk_{b1}x} + A_n^- e^{-jk_{b1}x} + B_n^+ e^{-k_{b2}x} + B_n^- e^{k_{b2}x}, \\ \theta_n(x) = N_1 A_n^+ e^{jk_{b1}x} + N_2 A_n^- e^{-jk_{b1}x} + N_3 B_n^+ e^{-k_{b2}x} + N_4 B_n^- e^{k_{b2}x}, \\ u_n(x) = C_n^+ e^{jk_a x} + C_n^- e^{-jk_a x}, \end{cases} \quad (3.1.2)$$

where the wavenumbers are given by

$$\begin{cases} k_{b1} = \frac{1}{\sqrt{2}} \sqrt{\frac{\sqrt{I}(E + G\kappa)\omega^2\rho - \omega\sqrt{\rho}\sqrt{4SEG^2\kappa^2 + I(E - G\kappa)^2\omega^2\rho}}{EG\sqrt{I}\kappa}}, \\ k_{b2} = \frac{1}{\sqrt{2}} \sqrt{\frac{\sqrt{I}(E + G\kappa)\omega^2\rho + \omega\sqrt{\rho}\sqrt{4SEG^2\kappa^2 + I(E - G\kappa)^2\omega^2\rho}}{EG\sqrt{I}\kappa}}, \\ k_a = \sqrt{\frac{\rho}{E}}\omega. \end{cases} \quad (3.1.3)$$

The wave amplitudes  $A_n^\pm$ ,  $B_n^\pm$ ,  $C_n^\pm$  are unknown at this stage. The coefficients  $N_p$  with  $p = 1 \dots 4$  are given by  $N_p = \frac{\bar{\theta}}{\bar{w}} = \frac{\rho\omega^2 - \kappa G k_p^2}{jk_p \kappa G}$ .

$$\begin{cases} M_n(x) = EI \frac{d\theta(x)}{dx}, \\ F_n(x) = \kappa GS \left( \frac{dw(x)}{dx} - \theta(x) \right), \\ L_n(x) = ES \frac{du(x)}{dx}. \end{cases} \quad (3.1.4)$$

At  $x = x_0 = 0$  (at the HQ input), continuity and equilibrium conditions lead to, respectively,

$$\begin{cases} w_0(x_0) = w_1(x_0), \\ w_0(x_0) = w_2(x_0), \\ \theta_0(x_0) = \theta_1(x_0), \\ \theta_0(x_0) = \theta_2(x_0), \\ u_0(x_0) = u_1(x_0) - t_1 \tan(\theta_1(x_0)), \\ u_0(x_0) = u_2(x_0) + t_2 \tan(\theta_2(x_0)), \end{cases} \quad (3.1.5)$$

we consider small amplitudes of vibrations, so that  $\tan(\theta_{1,2}(x_0)) = \theta_{1,2}(x_0)$ ,

$$\begin{cases} M_0(x_0) = M_1(x_0) + M_2(x_0) + t_1 L_1(x_0) - t_2 L_2(x_0), \\ F_0(x_0) = F_1(x_0) + F_2(x_0), \\ L_0(x_0) = L_1(x_0) + L_2(x_0). \end{cases} \quad (3.1.6)$$

Similar equations are also considered at  $x = x_0 + L$ , i.e. at the right end of the HQ device. In these equations, the coupling between the bending and longitudinal waves is described by the terms proportional to  $t_1$  and  $t_2$  (see Fig.3.1). In the following, Sommerfeld conditions in beam segment 3 are assumed and lead to  $A_3^- = B_3^- = C_3^- = 0$ . In order to study the scattering properties of the HQ filter, an incident propagating flexural wave of the unit amplitude is assumed in beam segment 0 such that  $A_0^+ = 1$  and  $B_0^+ = C_0^+ = 0$ . Substitution of Eq.3.1.2 into Eq.3.1.4, applying Eqs.3.1.5, 3.1.6 and isolating the terms depending on  $A_0^+$  at the right hand side finally lead to a set of 18 linear equations with respect to wave amplitudes written in matrix form

$$\mathbf{\Lambda} = \mathbf{M}\mathbf{\Phi}, \quad (3.1.7)$$

where

$$\mathbf{\Lambda}^T = [A_0^+; A_0^+; N_1 A_0^+; N_1 A_0^+; E I N_1 k_1 A_0^+; \kappa G S (k_1 - N_1) A_0^+; 0; 0; 0; 0; 0; 0; 0; 0; 0; 0; 0; 0], \quad (3.1.8)$$

and

$$\mathbf{\Phi}^T = [A_0^-; B_0^-; A_1^+; A_1^-; B_1^+; B_1^-; A_2^+; A_2^-; B_2^+; B_2^-; A_3^+; B_3^+; C_0^-; C_1^+; C_1^-; C_2^+; C_2^-; C_3^+]. \quad (3.1.9)$$

The  $18 \times 18$  matrix  $\mathbf{M}$  is given in appendix A. The vector  $\Phi^T$  contains the unknown wave amplitudes that are obtained by solving Eq.3.1.7. Finally, the reflection and transmission coefficients of the HQ filter for bending waves are given by

$$\mathbf{R} = \frac{A_0^-}{A_0^+}, \quad \mathbf{T} = \frac{A_3^+}{A_0^+}. \quad (3.1.10)$$

### 3.1.2 3D Finite Element model of the HQ filter

A 3D finite element model is developed using COMSOL solid mechanics software to validate the wave-based semi-analytical model. The geometry of the simulated systems follows Fig. 3.1 with  $L = 200\text{mm}$ ,  $h = 10\text{mm}$ ,  $h_1 = 4\text{mm}$ ,  $h_2 = 3\text{mm}$  and  $b = 10\text{mm}$ . The total length of the beam is  $1000\text{ mm}$ . The aluminium material parameters are considered:  $E_0 = 70\text{GPa}$ ,  $\eta = 0$ ,  $\rho = 2700\text{kg.m}^{-3}$  and  $\nu = 0.3$ , according to the definitions given after Eq.3.1.1. At the left end ( $x < 0$ ), a transverse line of force is applied so that incoming bending wave is generated. At the opposite right-hand end, a Perfectly Matched Layer (PML) is defined in order to simulate the infinite length of the beam, as we considered earlier. To solve the problem, a mesh of 1932 nodes is used with 3D elastic linear theory (solid mechanics package), considering 3 elements in the thickness, 2 elements in the width and a mesh size of 5 mm along the x axis.

The coefficients R and T defined in Eq.3.1.10 are calculated from the simulated values of the beam vibration field: the z-displacement response  $w(x_k)$  is picked out on the neutral line of the beam ( $y = 0$  and  $z = 0$ ) at 4 abscissas upstream ( $x_k < 0$  with  $k = 1$  to 4, where  $x_1 = -100\text{mm}$ ,  $x_2 = x_1 - 10\text{mm}$ ,  $x_3 = x_1 - 30\text{mm}$ ,  $x_4 = x_1 - 60\text{mm}$ ) and downstream ( $x_k > L$  with  $k = 5$  to 8, where  $x_5 = L + 100\text{mm}$ ,  $x_6 = x_5 + 10\text{mm}$ ,  $x_7 = x_5 + 30\text{mm}$ ,  $x_8 = x_5 + 60\text{mm}$ ) of the HQ filter. For each of the 8 responses, we consider a wave decomposition according to Eq.3.1.2, which leads to the following matrix problem

$$\begin{bmatrix} w(x_1) \\ \vdots \\ w(x_4) \\ w(x_5) \\ \vdots \\ w(x_8) \end{bmatrix} = \begin{bmatrix} e^{-jk_{b1}x_1} & e^{jk_{b1}x_1} & e^{-k_{b2}x_1} & e^{k_{b2}x_1} & 0 & 0 & 0 & 0 \\ \vdots & \vdots \\ e^{-jk_{b1}x_4} & e^{jk_{b1}x_4} & e^{-k_{b2}x_4} & e^{k_{b2}x_4} & 0 & 0 & 0 & 0 \\ 0 & 0 & 0 & 0 & e^{-jk_{b1}x_5} & e^{jk_{b1}x_5} & e^{-k_{b2}x_5} & e^{k_{b2}x_5} \\ \vdots & \vdots \\ 0 & 0 & 0 & 0 & e^{-jk_{b1}x_8} & e^{jk_{b1}x_8} & e^{-k_{b2}x_8} & e^{k_{b2}x_8} \end{bmatrix} \begin{bmatrix} A_0^+ \\ \vdots \\ B_0^- \\ A_3^+ \\ \vdots \\ B_3^- \end{bmatrix} \quad (3.1.11)$$

The reflection and transmission coefficients  $R$  and  $T$ , as defined in Eq.3.1.10, are finally obtained by solving Eq.3.1.11. Fig.3.2 shows the  $R$  and  $T$  coefficients of the HQ filter obtained both from the analytical model described in Section 3.1.1 with (black line) or without (gray line) considering the coupling between bending and longitudinal waves and from the finite element reference model (blue circles).

$T$  is close to 1 over the range [0-2500]Hz except at some selected frequencies where it displays deep drops. At these frequencies, the FEM simulated displacement field shows a phase opposition for the bending motion in the two parallel HQ beams, leading to a destructive interference quite similar to the one involved in the HQ acoustic tubes (see the displacement fields at 430Hz and 1155Hz in Fig.3.2). Outside the drops, the displacement field as the one at 1560Hz in Fig.3.2 displays no particular phase relation between the two parallel HQ beams so that no filtering effect is obtained.

The good agreement between the results of the coupled wave model (black line) and the reference FEM model (blue circles) over the whole frequency range under study shows the relevance of considering the coupling between longitudinal and bending waves. Indeed, outside the  $T$  drops, significant discrepancies can appear when the bending/longitudinal wave coupling is ignored in the wave model (grey line). However, the frequency of the drops are well captured by such a purely bending wave model, as the destructive interference effect is driven by bending motion. As an additional comment, results shows an expected overestimation of the  $T$  drop frequencies no matter whether the bending/longitudinal wave coupling is considered or not. Modeling of the structure with 3D solid elements makes it more compliant as compared with its model, which employs the plane cross-sections assumption. This assumption is used in each of the two coupled one-dimensional

models: a classical wave equation for longitudinal motions and a Timoshenko model for bending waves. In the Timoshenko model, the possible warping of the beam's cross-section are ignored. However, such warping can be produced due to the complex dynamics at the HQ branches junctions to the host beam and to the non-symmetry in the beam's thickness (the two branches of the HQ filter, by definition, have different thicknesses).

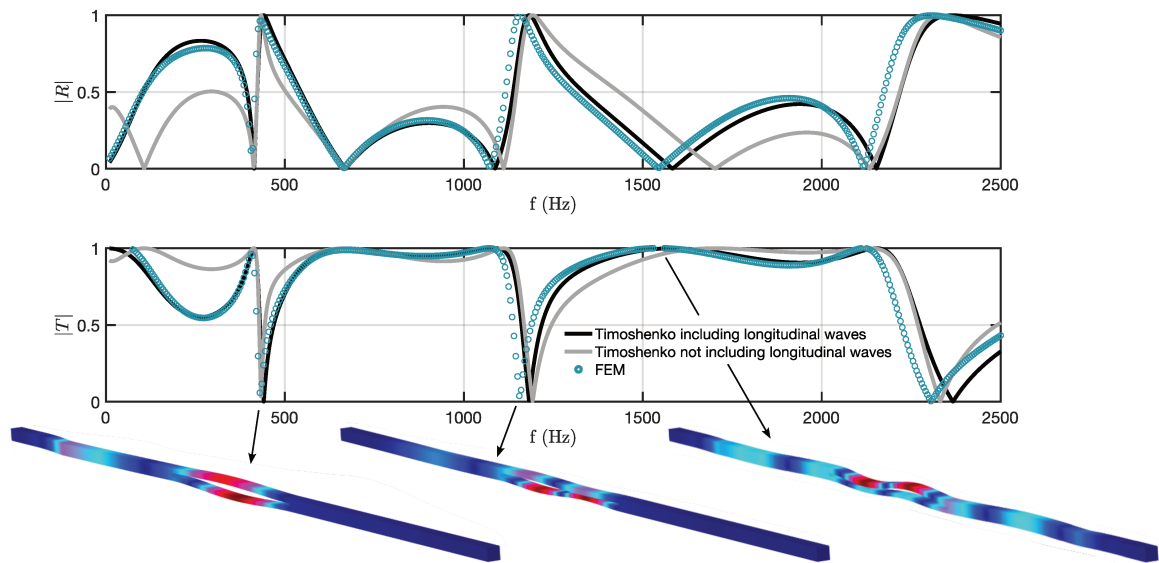


Fig. 3.2 Reflection coefficient  $|R|$  and transmission coefficient  $|T|$  obtained from the Timoshenko beam model including (black line) or not (gray line) the coupling with longitudinal motion and the finite element method (blue circles). The frequencies of the  $T$  drops are 433 Hz, 1193 Hz, 2331 Hz for Timoshenko not including longitudinal waves ; 441 Hz, 1182 Hz, 2369 Hz for Timoshenko including longitudinal waves ; 430 Hz, 1155 Hz, 2305 Hz for FEM.

## 3.2 ANALYSIS OF THE PERFORMANCES OF THE HQ FILTER

### 3.2.1 Energy flow

The wave model formulated in Section 3.1 facilitates analysis of the energy flow in the structure shown in Fig.3.1. Since the involvement of longitudinal waves is deemed to be insignificant in the frequency range presented in Fig.3.2, the energy flow analysis in this subsection is done within Timoshenko beam model. In this

case, the period-averaged energy flux is defined as [63]:

$$E(x) = \frac{1}{2} [\text{Re}[F_n(x) \cdot v_n^*(x)] + \text{Re}[M_n(x) \cdot \chi_n^*(x)]], \quad (3.2.1)$$

where  $*$  denotes the complex conjugate, the velocity  $v_n(x) = -i\omega w_n(x)$  and the angular velocity  $\chi_n(x) = -i\omega\theta_n(x)$ , respectively.

The results of the energy flux analysis are assembled in Fig.3.3. Obviously, the energy flux remains constant at any cross-section of the structure, as dictated by the energy conservation law. The Fig.3.3a shows the total energy flux  $E$  (black line) and its partition between the segments one  $E_{HQ_1}$  (blue line) and two  $E_{HQ_2}$  (blue dashed line) in the HQ device.

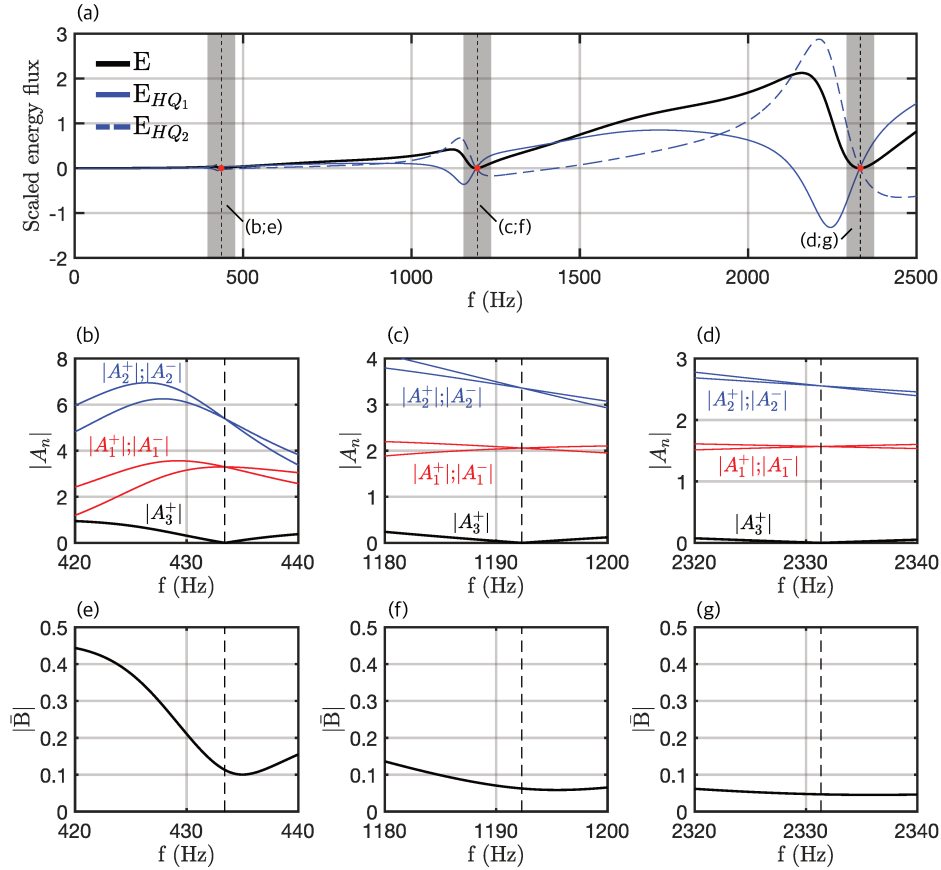


Fig. 3.3 a) Total energy flux (black line) and the energy flux in the upper  $E_{HQ_1}$  (blue line) and the lower HQ strand  $E_{HQ_2}$  (blue dashed line). b),c)d) Crossing at the zero transmission frequency of the absolute value of the amplitudes  $A_1^+$ ,  $A_1^-$ ,  $A_2^+$ ,  $A_2^-$  and  $A_3^+$ . e),f),g) The amplitude of evanescent wave  $|\bar{B}|$  at  $x = x_0 + L$  and around the zero transmission frequency.

At the zero transmission frequencies, the total energy flux and energy fluxes in each segment of the structure vanish. It manifests formation of standing waves and implies that the amplitude of reflected wave in the segment 0,  $A_0^-$  equals the amplitude of incoming waves  $\frac{A_0^-}{A_0^+} = 1$ .

The evolution of energy transmission is generic, and it is illustrated in Fig.3.3a. The energy flux in a thick (upper) segment becomes positive as soon as the excitation frequency exceeds the zero transmission one, whereas in a thin (lower) segment it becomes negative. Thus, the energy circulation inside the HQ device is generated on top of the positive net energy flux. As the excitation frequency continues to grow, both segments begin to convey the energy in the same direction. However, at a certain frequency, the energy flux in a thick (upper) segment becomes negative, and circulation is recovered, but in the reversed direction. As soon as the magnitudes of both these fluxes become equal to zero, the next zero transmission frequency emerges.

Figs.3.3b,c,d illustrate frequency dependences of the amplitudes of travelling waves in segments 1-3 in the ranges shadowed in Fig.3.3a. These amplitudes are scaled by the amplitude of incoming wave  $A_0^+$ . At zero transmission frequencies, amplitudes of the left-going and right-going waves in these segments equal each other, and standing waves are formed. The absence of the travelling wave in segment 3 does not mean its left end has a zero displacement. Fig.3.3e,f,g illustrates the frequency dependence of amplitude evanescent wave  $\bar{B}$  at  $x = x_0 + L$ . It becomes very small at zero transmission frequencies (the scaling to  $A_0^+$  should be observed). However, this evanescent wave does not convey energy, and vibration amplitudes decay exponentially in segment 3.

### 3.2.2 Modal Analysis of an infinite beam with the HQ filter

It is a common practice to put results of harmonic analysis of a mechanical system into the framework of its modal analysis. This section focuses on the analysis of the local modes of an infinite beam including an HQ filter. The length of the filter is kept the same as in the previous section. These local modes result from the resonant behavior of the HQ filter branches. The coupling between the branches and the host beam involves radiation into the host medium and thus induces damping of the local modes. Eigenfrequencies and eigenshapes are obtained from the following

condition

$$\text{Det}[\mathbf{M}] = 0, \quad (3.2.2)$$

where  $\mathbf{M}$  is given by Eq.3.1.7. The first 6 eigenfrequencies and eigenshapes are shown in Fig.3.4. The eigenfrequencies  $f_n$  are complex valued due to energy leakage from the HQ filter into the infinite host beam. A small (resp. large) imaginary part of  $f_n$  corresponds to a small (resp. large) leakage. The damping coefficient  $\xi_n$  and the real natural frequency  $f_{rn}$  in the absence of material losses are related to the complex eigenfrequency  $f_n$  by the following relations

$$\Re(f_n) = f_{rn} \sqrt{1 - \xi_n^2}, \quad \Im(f_n) = 2\xi_n f_{rn}, \quad (3.2.3)$$

The complex natural frequencies shown in Fig. 3.4a can be divided into two groups: A first group corresponds to almost real eigenfrequencies (see  $f_1, f_3, f_5$ ). The associated eigenshapes are almost entirely localized within the HQ filter: the amplitude of the eigenshape oscillations is much greater inside than outside the HQ insert (see Fig. 3.4b, left-hand column). For this set of modes, the eigenshapes are symmetrical with respect to the center of the HQ filter. This symmetry induces a cut-off between the fields radiated by the two HQ branches, reducing the efficiency of radiation in the host beam. The resulting damping is quite low, and the local mode is well confined. The second group corresponds to eigenfrequencies with large imaginary parts, leading to substantial leakage (see  $f_2, f_4, f_6$ ) resulting in oscillations of same range of amplitude both inside and outside the HQ insert (see Fig. 3.4b, right column). For this set of modes, the eigenshapes are antisymmetric toward the center of the HQ filter, which favors the radiation of the two HQ branches into the host beam. The resulting modal damping coefficient is quite high and the local mode is not strongly confined but clearly extends outside the HQ filter.

The modal analysis performed in this subsection demonstrates close similarity between operational mode shapes of forced vibrations at zero transmission frequencies and eigemodes of an infinite beam with HQ device. However, the purely real zero transmission frequencies are just reasonably close to the complex-valued eigenfrequencies. Therefore, the eigenvalue problem, which exactly corresponds to the forcing problem considered in Section 3.1, should be formulated differently.

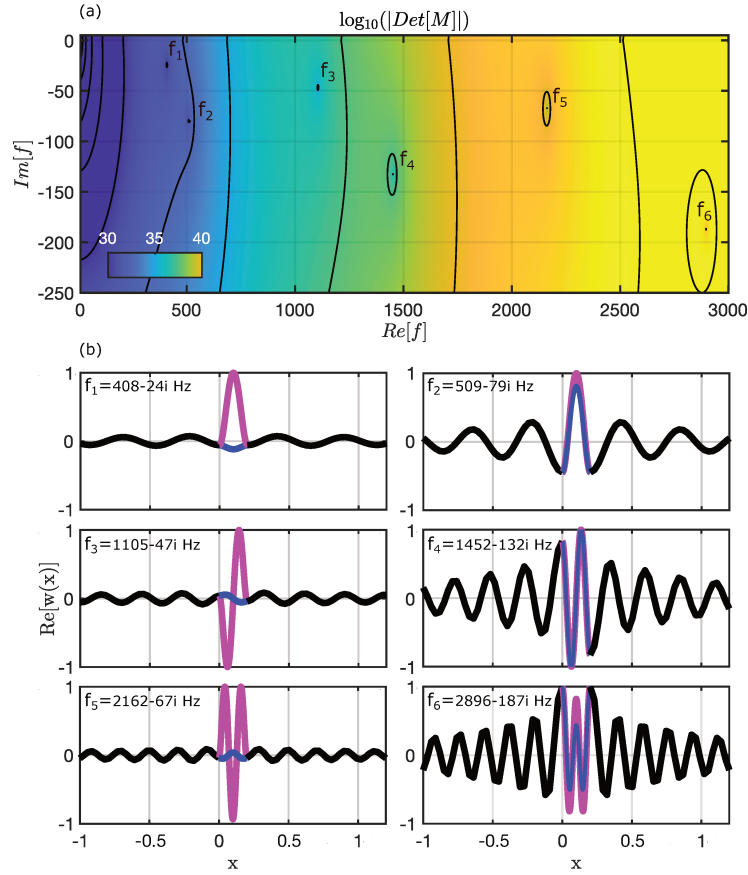


Fig. 3.4 a) Complex eigenfrequencies  $f_m$  of the HQ filter represented by points in the complex frequency plane. The colour and isolines describe the variations in  $|Det(M)|$ . Each point indicates a zero of  $|Det(M)|$ . b) Real parts of antisymmetric eigenshapes (displacements with smallest imaginary part  $f_1, f_3, f_5$ ) and symmetric eigenshapes (largest imaginary part of  $f_2, f_4, f_6$ ). Magenta, blue and black are associated to the upper HQ branch, the lower HQ branch and the host beam respectively.

3.3 AN ALTERNATIVE FORMULATION OF THE PROBLEM AND PARAMETRIC ANALYSES OF LOCATION OF THE ZERO-TRANSMISSION FREQUENCIES

In the previous section, the transmission coefficient  $|T|$  is obtained from Eq.3.1.10 by setting the incident wave amplitude  $A_0^+$  equal to 1. Then solving the forcing problem by a 'frequency sweep' permits to find zero-transmission frequencies as defined by formula Eq.3.1.10. This method is perfectly valid, but it might suggest that the filtering properties of a HQ device vary depending on excitation conditions. To determine the frequencies at which exact zero transmission occurs ( $|T|=0$ ), we reformulate the problem by setting the amplitude of the transmitted wave  $A_3^+$  to

zero (11th component of  $\Phi$ ) and leaving the amplitude of the incident wave  $A_0^+$  unspecified. Taking into account these conditions, Eq.3.1.7 can be rewritten in the form

$$\mathbf{M}'\Phi' = 0, \quad (3.3.1)$$

where  $\Phi'$  is obtained from  $\Phi$  by replacing its 11th component by  $A_0^+$  :

$$\Phi'^T = [A_0^-; B_0^-; A_1^+; A_1^-; B_1^+; B_1^-; A_2^+; A_2^-; B_2^+; B_2^-; A_3^+; B_3^+; C_0^-; C_1^+; C_1^-; C_2^+; C_2^-; C_3^+].$$

The matrix  $\mathbf{M}'$  is obtained from  $\mathbf{M}$  by replacing its 11th column by vector  $C$ , where

$$C^T = [1; 1; N_1; N_1; E I N_1 k_1; \kappa G S(k_1 - N_1); 0; 0; 0; 0; 0; 0; 0; 0; 0; 0; 0; 0; 0].$$

This is the eigenfrequency, or eigenvalue problem, which corresponds to the forcing problem solved earlier. Equation 3.3.1 has a nontrivial solution when  $Det[\mathbf{M}'] = 0$ . It provides the frequencies, at which the transmission coefficient  $|T|$  is zero. Eigenvectors are determined up to a scaling factor. If scaling is chosen as the amplitude of incoming wave  $A_0^+$ , then the wave coefficients obtained by solving Eq.3.1.7 at zero transmission frequencies are recovered. In the absence of material losses, these frequencies are purely real. As soon as material losses are taken into account, they become complex-valued.

The location of the zero transmission frequencies depends on the physical and geometric parameters of the HQ device. Fig.3.5a illustrates parametric studies of performance of this device in the framework of Timoshenko beam model. In this Figure, zero transmission frequencies correspond to poles of the function  $\log_{10}(|Det[\mathbf{M}']|)$ . The background colours demonstrate orders of magnitude of this function in vicinity of zero transmission frequencies. First, the influence of the length  $L$  in the absence of material losses is described by the trajectories of two purely real zero transmission frequencies (marker square) introduced by varying the length of the HQ filter from 20cm to 30cm (see the colour scale in the first column, upper-right corner of Fig.3.5a).

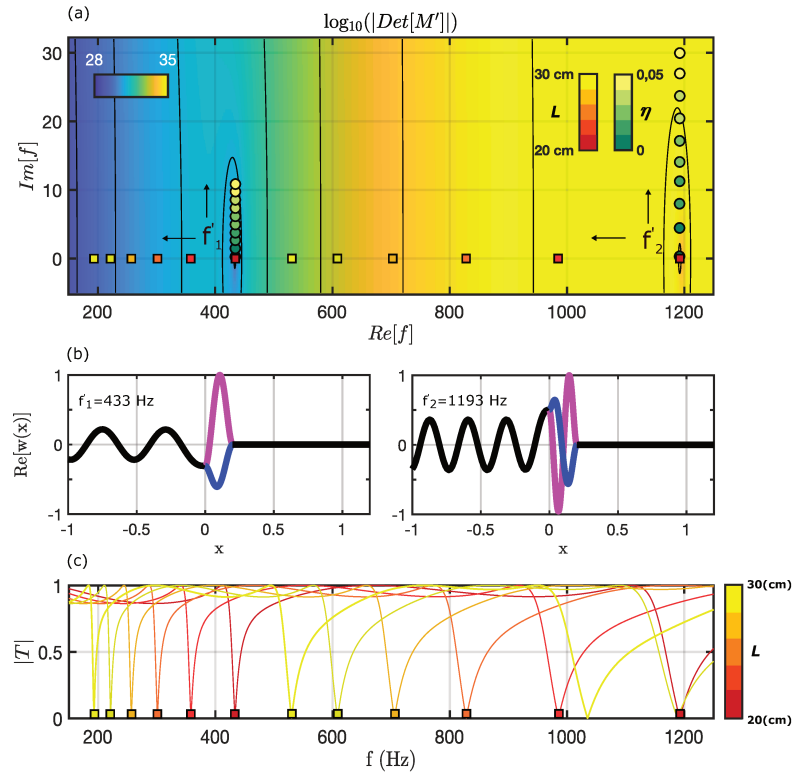


Fig. 3.5 a) Complex plane showing the zero transmission frequencies of the HQ device for specified values of length  $L$  and loss factor  $\eta$ . b) Vibration mode shapes at zero transmission frequencies for  $L = 20\text{cm}$  when  $\eta = 0$ . c) The frequency dependence of the transmission coefficient  $|T|$  when changing the length  $L$  in solving the forcing problem (3.1.7) when  $\eta = 0$ .

The deflection shapes at zero transmission frequencies are presented in Fig.3.5b. As already shown in subsection 3.2, due to the absence of energy transmission to infinity in the right semi-infinite segment of the beam, the mode shape in the left semi-infinite segment is a standing wave. Increasing the length  $L$  from 20cm to 30cm shifts the zero transmission to the low frequencies, demonstrating the direct control of frequency by the length of the HQ device. This property is also confirmed in Fig.3.5c, as it demonstrates that the drops of  $|T|$  are at the same abscissa as the zero transmission points in Fig.3.5a.

Next, Fig.3.6a shows the zero transmission frequencies (in the absence of the material losses) if thickness of one HQ branch varies while other is kept constant.

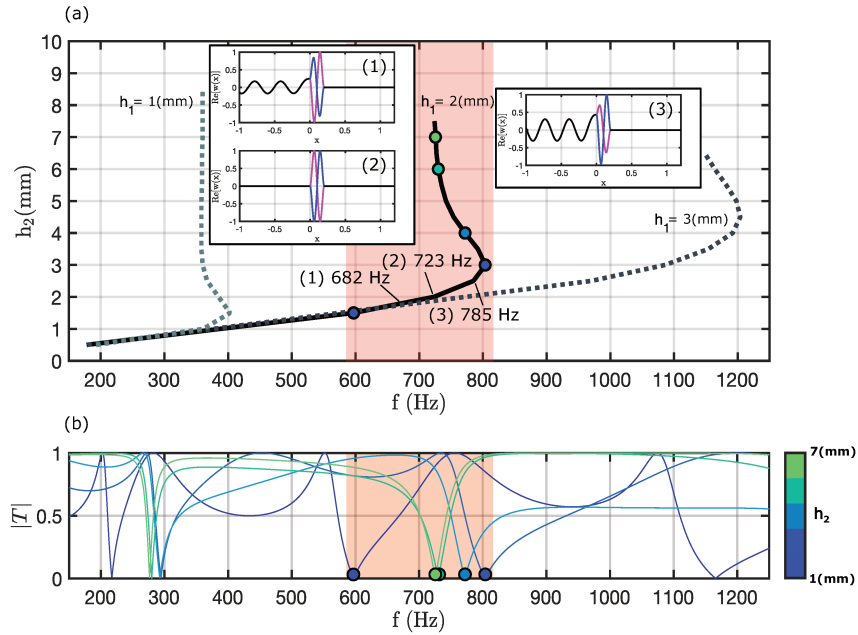


Fig. 3.6 a) Parametric study of the second zero transmission frequencies when changing the ratio of thickness, when  $h_1 = 1\text{mm}$  (grey dotted line),  $h_1 = 2\text{mm}$  (black line),  $h_1 = 3\text{mm}$  (black dotted line). The shape modes represent for the cases  $h_1 \neq h_2$  at 682 Hz, 785 Hz and  $h_1 = h_2$  at 723 Hz. b) The frequency dependence of the transmission coefficient for several values of thickness  $h_2$  while  $h_1$  is 2mm from solving the forcing problem (3.1.7).

For this parametric analysis, the length  $L$  of the HQ device is fixed as 20cm and  $h_1 = 2\text{mm}$ . Relation between the zero transmission frequencies and  $h_2$  is represented in Fig. 3.6a.

As seen from Fig.3.6a, the ratio  $h_2/h_1$  efficiently controls the location of zero transmission frequencies as long as the condition  $h_2 < h_1$  holds. When  $h_2$  becomes larger than  $h_1$ , its further growth weakly affects location of the zero transmission frequency. In the case  $h_1 = h_2$ , zero transmission occurs exactly at the purely real eigenfrequency of a trapped mode of an infinite beam with the HQ device [55, 54]. This eigenfrequency is readily obtained from Eq.3.2.2. The vibration deflection shapes at zero transmission frequencies for  $h_2 = 1.8\text{mm}$ ,  $h_2 = 2\text{mm}$  and  $h_2 = 2.5\text{mm}$  are shown in Fig.3.6a. For  $h_2 \neq h_1$ , these shapes are similar to those in Fig.3.5b. When  $h_2 = h_1$ , the vibration deflection shape at zero transmission is the same as the resonant mode shape of the HQ filter.

For consistency, in Fig.3.6b we present the frequency dependence of transmission coefficient for the discrete values of  $h_2$  defined by different colours, (see the column

to the right in Fig.3.6b. The zero transmission frequencies obtained from solution of forcing problem perfectly agree with solution of Eq. 3.3.1.

As seen in Fig.3.5a, increasing the loss factor  $\eta$  from 0 to 0.05 (see the colour scale in the second column, upper-right corner of Fig.3.5a shifts the zero transmission frequencies to the upper part of the complex plane, demonstrating the direct control of the damping of the local modes by the material loss factor (marker circle). In

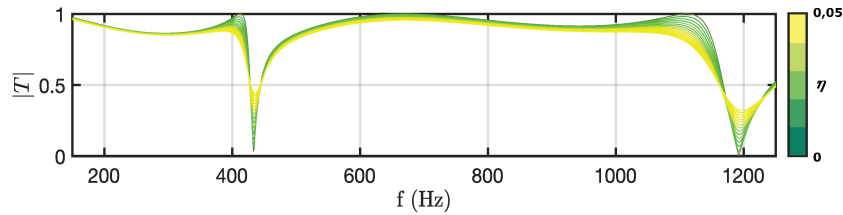


Fig. 3.7 The frequency dependence of the transmission coefficient  $|T|$  when changing loss factor  $\eta$  in solving the forcing problem (3.1.7) when  $L = 20\text{cm}$ .

Fig. 3.7, frequency dependence of transmission coefficient obtained from solution of forcing problem with  $\eta \neq 0$  is presented. As expected, transmission coefficient grows when loss factor increases because an incoming wave has been assumed to have a purely real frequency. To attain zero transmission coefficient, an incoming wave should have a complex-valued frequency, which depends on material loss factor as shown in Fig.3.5a.

### 3.4 EXPERIMENTAL VALIDATION

#### 3.4.1 Setup and signal processing

An experimental demonstration of the HQ effect for bending waves is carried out using the setup shown in Fig.3.8. It consists of a vertical beam, 10mm thick and wide and 2000mm long, suspended at its top end to a rigid frame and excited at its bottom end by a shaker with a swept sine. The HQ filter of dimensions  $h_1 = 4\text{mm}$ ,  $h_2 = 3\text{mm}$ ,  $L = 200\text{mm}$  is located at the mid length of the host beam. The response of the beam is measured using the 3Dvib experimental platform located at "Technocampus Acoustique et Matière" in Le Mans, France. This platform includes a 3D infrared Polytec Scanning Vibrometer mounted on a 5-meter robotic arm (RoboVib with PSV500 Xtra). Thanks to its micron-level positioning repeatability, this robotic arm allows scanning of the beam at different positions defined for the

robot. Each scan is performed along a mesh grid with a step size set at 3mm. At the end of the robot's movement process, each intermediate scan is concatenated to generate the complete velocity field of the beam, including the front and back faces of the beam around the HQ filter. Although the velocity components ( $x$ ,  $y$ ,  $z$ ) are known through this process, only the out-of-plane  $z$ -component will undergo post-processing.

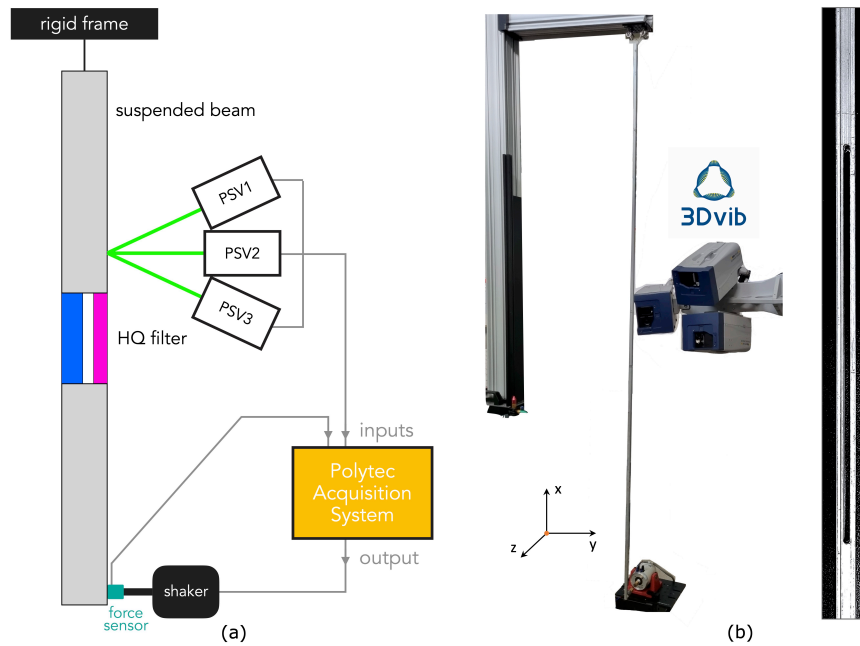


Fig. 3.8 a) Scheme and (b) photograph of the experimental setup and zoomed view of the HQ filter (right side)

### 3.4.2 Results

The experimental results are reported in Fig.3.9. A first evidence of the HQ filtering effect is figured out when comparing the cross mobility, defined as the velocity response at the top end divided by the force excitation at the bottom end, in cases the HQ device is implemented (red line) or not (blue line) in the host beam (see Fig.3.9a). In the frequency ranges where a transmission drop is expected from the model, the mobility displays strong dips meaning that the top end is efficiently isolated from the source. Notice that additional resonances also appears in the HQ beam case due to reflection effects provided by the HQ at the beam mid length.

The transmission coefficient, defined by Eq.3.1.10, is evaluated from the inversion of Eq.3.1.11 as for the FEM reference model, in which  $w(x_i)$  corresponds to the mean displacement measured at abscissa  $x_i$  over the 3 mesh points of the beam width, so as to minimize the contribution of unwanted torsional motion in the signals. To improve identification quality, 20 abscissas between  $x_1 = -20\text{cm}$  and  $x_{20} = 0\text{cm}$  as well as between  $x_{21} = 20\text{cm}$  and  $x_{40} = 40\text{cm}$ , are considered on the left and right sides of the HQ insert respectively, leading to an overdetermined linear system solved by a pseudo-inverse of the  $8 \times 40$  matrix in Eq. 3.1.11.

The 1D Timoshenko and FEM models have been used to determine wave amplitudes of forced vibrations of the beam shown in Fig.3.8, and the coefficients T

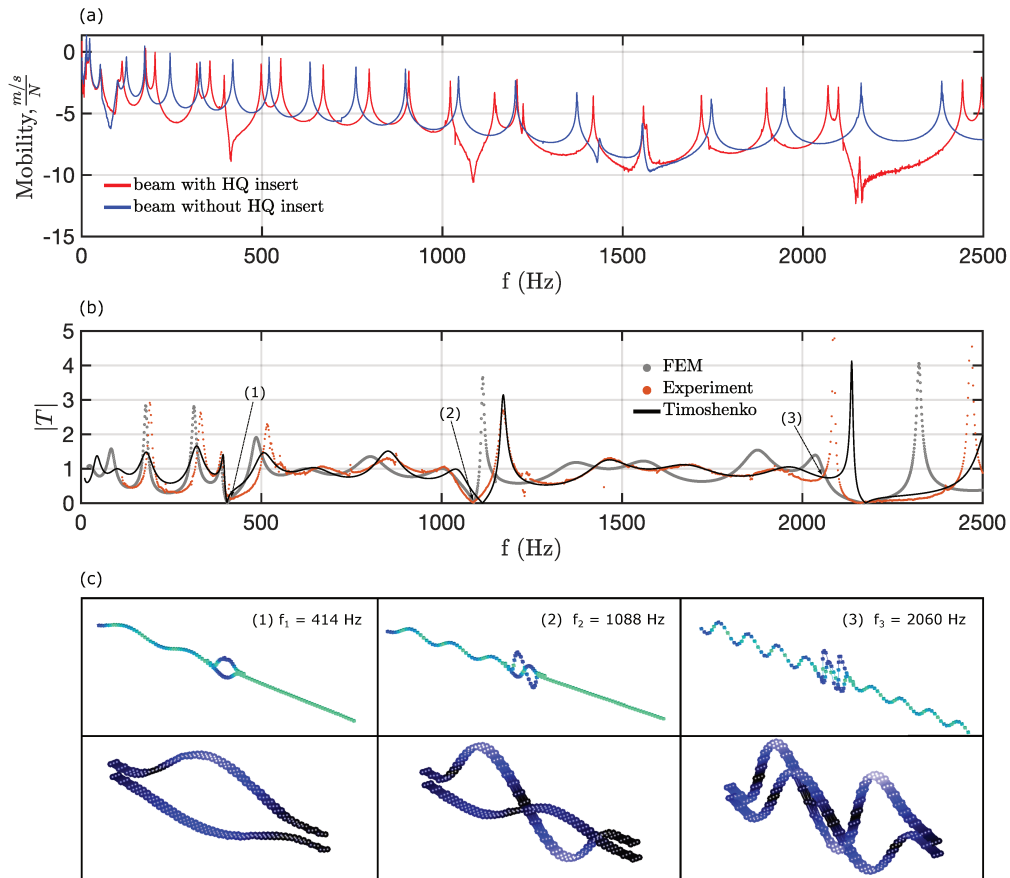


Fig. 3.9 a) Cross mobility between the response at the top end and the force at the bottom end of the host beam with or without the HQ filter. b) Results of the transmission coefficient for FEM, Timoshenko and Experimental analysis. c) Local mode analysis of HQ beams using 3Dvib.

obtained by these means have been compared with the experimental transmission coefficient. In the former case, the radiation and decay conditions are replaced

with conventional free end conditions by equating forces and moments to zero. At the left end, a point transverse force is applied. The physical and geometrical parameters are taken to be the same as in the experiment. We generate a new system of equations in the form Eq.3.1.7 by replacing the matrix  $M$  by the new matrix  $M''$ . Then, we find the coefficient  $T$  by Eq.3.1.10. To set up the free edge model in the FEM, we use the same solution as in Section 3.1.2, but without considering PML.

The Fig. 3.9b shows the agreement of zero transmission frequencies between the experimental (red dots) and numerical results for both the 1D wave model (black line) and the 3D FEM model (gray dots) of a finite beam. Unlike the frequency-dependence of the transmission coefficient for an infinite beam, shown in Fig. 3.2, in this case its behaviour is 'polluted' by reflections of waves at the end cross-sections of the beam. These disturbances can lead to incorrect estimates of  $T$  greater than 1, which are seen in Fig. 3.9b. However, the positions of zero-transmission frequencies remain unaffected. At the first two drops at  $f_1 = 414\text{Hz}$  and  $f_2 = 1088\text{Hz}$  respectively, the experimental operating shapes well display the filtering efficiency: the wave field is nearly zero downstream the HQ device. Moreover, the zoomed view of the deflecting shape inside the HQ device shows the resonance of a local mode with phase opposition between the two parallel beam segments, as predicted by the models. On the other hand, at the frequency  $f_3 = 2060\text{Hz}$  where no HQ filtering effect is expected (see Fig. 3.9c), the deflection shapes of the two parallel beam segments show no particular phase relationship. In an infinite beam, this leads to a transmitted wave field downstream of the HQ filter.

Although these experimental results confirm the principle of HQ filtering for bending wave and the main related phenomena, some discrepancies are observed outside the drops. In particular secondary drops appears in the experimental results. To determine the reasons for this, Fig. 3.10 shows complementary FEM

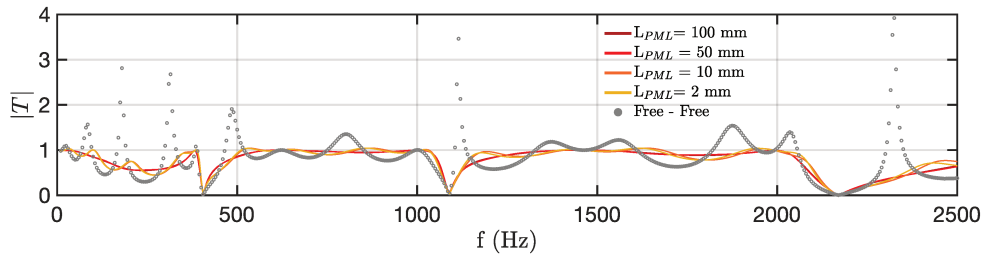


Fig. 3.10 The impact of PML accounting on the transmission coefficient in COMSOL calculations. The PML length value is set from 100 mm to 0 mm (i.e. free-free boundary conditions).

results where the length of the PML is varied so that the reflection at the beam ends becomes non zero. Results show that secondary dips increase while the PML length decreases, i.e. the reflection at the ends increases. Hence, these secondary drops appears to be identification artefacts due to stationary waves induced at the sample beam edges.

### 3.5 CLASSIFICATION OF 2 PARALLEL BRANCH CONFIGURATIONS

Several classes can be identified to generalize the configuration with two parallel branches and an internal discontinuity, leading to different types of transmission properties. A split beam with two parallel branches can be classified as presented in the Table 3.1:

- Thick symmetrical model, i.e., the height of two parallel HQ branches is the same  $h_2 = h_3$  and in some cases, as high as the height of the host beam  $h_2 + h_3 \leq h_1$ .
- Thin symmetrical model, i.e., the height of two parallel HQ branches is the same  $h_2 = h_3$  and their heights are very small compared to the height of the host beam  $h_{2,3} \ll h_1$ .
- Thick non-symmetrical model, i.e., the height of two parallel HQ branches is not the same  $h_2 \neq h_3$  and in some cases, as high as the height of the host beam  $h_2 + h_3 \leq h_1$ .
- Thin non-symmetric model, i.e., the height of two parallel HQ branches is not the same  $h_2 \neq h_3$  and their heights are very small compared to the height of the host beam  $h_{2,3} \ll h_1$ .

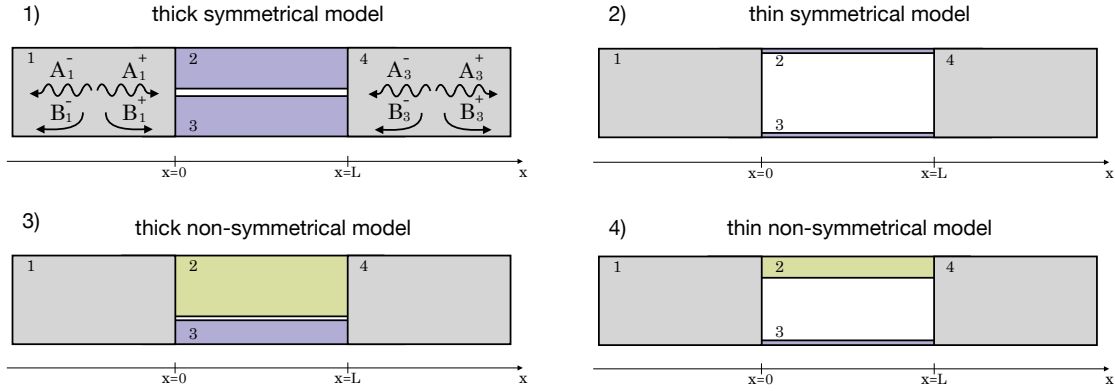


Table 3.1 Classification of two parallel branch systems: 1) thick symmetrical model, 2) thin symmetrical model, 3) thick non-symmetrical model, 4) thin non-symmetrical model.

Fig.3.11 shows the frequency dependence of the transmission coefficient and complex eigenfrequencies for all four classes. The transmission coefficient of the thin and thick symmetrical model does not exhibit any dips in the transmission coefficient, however the eigenfrequencies of these configurations are purely real, which corresponds to the case of trapped modes, [55, 54]. For the thin and thick non-symmetrical model, there are certain frequencies at which dips in the transmission coefficient occur, and the complex eigenfrequencies have both a small imaginary part, which is related to the dip in the transmission coefficient, and a large imaginary part, which is related to the strong energy leakage.

When the contrast between the two parallel HQ heights and host beam height is small  $h_{2,3} \leq h_1$ , the transmission coefficient is close to one, and there are a small number of dips in the transmission coefficient and eigenfrequencies on the complex plane. When the contrast between the two parallel HQ heights and host beam height is large  $h_{2,3} \ll h_1$ , the transmission coefficient is low, i.e., close to zero, and more dips and eigenfrequencies occur.

The analysis of thin and thick non-symmetrical model, which correspond to HQ filter in beams, shows that the thin non-symmetrical model has a strong filtering effect in the beam than the thick non-symmetrical model, however the balance between low transmission coefficient and high stiffness of the model should be considered. The thin and thick symmetrical model can produce the trapped modes, where the strong resonance will be localized in two parallel branches (see

Chapter 2). The thin symmetrical model will have more of these modes and a lower transmission coefficient than the thick symmetrical model.

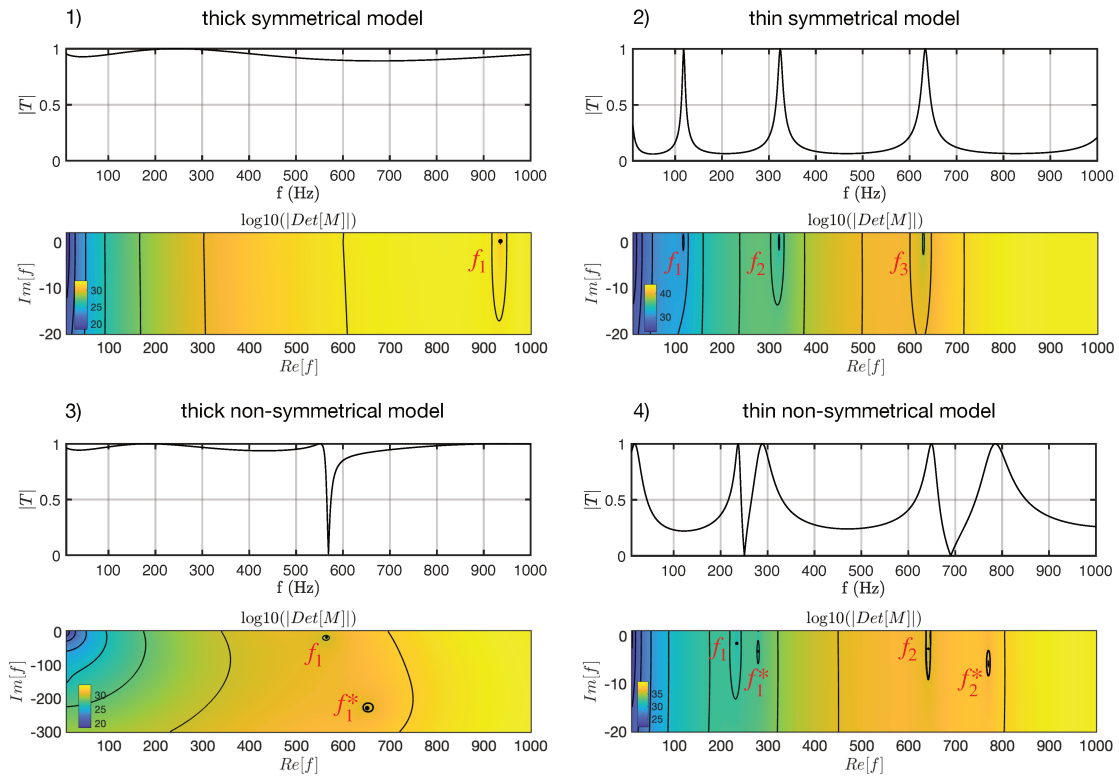


Fig. 3.11 Transmission coefficient and eigenfrequencies on the complex plane for four models.

### 3.6 CONCLUSION

The filtering properties of the beam-integrated HQ device which consists of two branches of equal length but different thickness are analysed. The difference in bending wave speeds in the two branches can at a discrete set of frequencies create o-transmission effect, resulting from destructive interference of these waves at the interfaces between components of HQ device. Computations of the reflection coefficient  $R$  and transmission coefficient  $T$  of the bending waves are done semi-analytically (using a wave model based on Timoshenko theory) and numerically (using the finite element code Comsol), and prove the device's efficiency. Measurements of  $R$  and  $T$  using a laser vibrometer clearly validate the simulations.

The energy flux analysis demonstrates the co-existence of two regimes of wave motion. In certain frequency ranges, it is unidirectional in both segments, while in other ranges energy fluxes are in opposite directions with the net flux always remaining non-negative. The frequencies, which separate these ranges, are the zero transmission frequencies. They define the formation of a standing wave in the whole beam.

It can be seen that the zero transmission frequencies are close to the real part of the eigenfrequencies of the HQ modes for which the two branches move in phase opposition (symmetrical modes). The differences between these two sets of frequencies are small and are not studied here. Instead, an alternative formulation of the eigenvalue problem is proposed and it is proved that the zero transmission frequencies are its eigenvalues. Respectively, the eigenvectors of this problem are the mode shapes of forced vibrations at these frequencies. It can also be seen that the vibration deflection shapes at zero transmission frequencies are close to the real part of the symmetrical eigenmodes, confirming the destructive interference of the fields radiated by the two branches.

Parametric variations including length, thickness and loss factor are performed around a nominal configuration and show how the zero transmission and hence the performance of the HQ filter can be controlled. A generalization of parallel branch configurations was presented by comparing symmetrical and non-symmetrical models with different branch heights. The results showed that the non-symmetrical model with thin HQ branches has a better filtering effect.

On balance, this chapter has demonstrated semi-analytically, numerically and experimentally the applicability of the HQ filtering effect to suppress propagation of flexural waves and provided the interpretation of this effect in terms of energy fluxes. These results constitute the novelty of the reported work.

---

## HQ FILTERS FOR FLEXURAL WAVES IN PLATES

---

This chapter introduces the analysis of the 2D plate using the HQ filter. We concentrate on physically elastic thin plates of circular shape. The previous chapters considered models of rods, beams, where their displacements are a function of a single coordinate,  $x$ . This section considers plates with displacements that are functions of two polar coordinates. Then, the concept of HQ can be easily transferred from beam theory to plate theory. Accordingly, the Kirchhoff-Love framework of the classical (technical) plate theory is assumed to be valid. From this, the transmission and energy flow features of HQ plates can be analyzed.

### 4.1 MODEL OF THE HQ VIBRATION FILTER IN A CIRCULAR PLATE

A split plate is capable of isolating vibrations in a similar manner to the split rod or beam. According to the principle of HQ filter, if the phase change experienced by waves travelling along the two branches is different, strong destructive interference takes place. We consider the HQ plate model which is described in Fig.4.1. The model consists of an infinite elastic plate into which two co-centric annular plates of equal radial length  $R_2$  but different thicknesses  $h_2$  and  $h_3$  are embedded. The system of polar coordinates has its origin in the common centre of these two annular inserts. The radius of an inner circular plate is  $R_1$ . The conventional decay and the Sommerfeld radiation conditions are formulated at infinity. The interfacial condition between sections are presented in the equation 4.1.7.

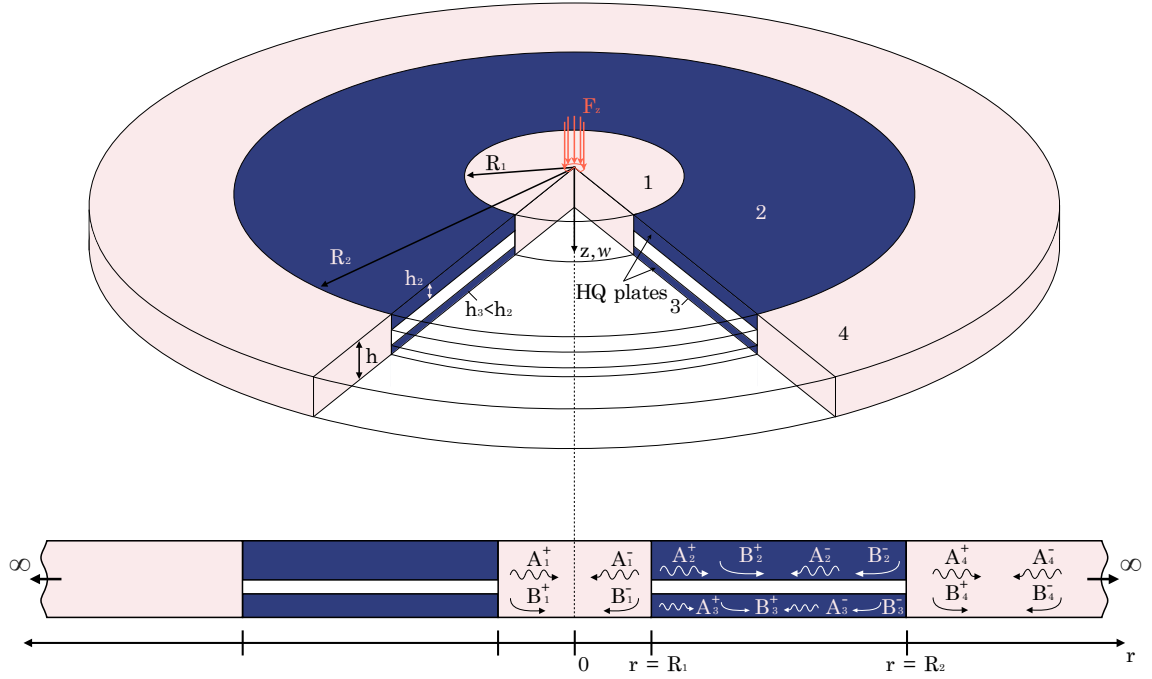


Fig. 4.1 Scheme of an HQ filter embedded into an infinite host structure, made up of two parallel plates of the same length but different thicknesses.

Let  $w_m(r, \theta, t)$  represent the displacement in the  $z$  direction of each of the four segments in Fig.4.1. Then the equation of motion in polar coordinates has the form [52, 64–66]

$$D\nabla^4 w_m(r, \theta, t) + \rho h_m \frac{\partial^2 w_m(r, \theta, t)}{\partial t^2} = 0, \quad 0 \leq \theta \leq 2\pi, \quad \begin{cases} 0 < r \leq R_1 & \text{for } m = 1 \\ R_1 \leq r \leq R_2 & \text{for } m = 2, 3 \\ r \geq R_2 & \text{for } m = 4 \end{cases} \quad (4.1.1)$$

where the operator  $\nabla^4$ , called the biharmonic operator

$$\nabla^4(\dots) = \nabla^2(\dots)\nabla^2(\dots) = \left( \frac{\partial^2}{\partial r^2} + \frac{1}{r} \frac{\partial}{\partial r} + \frac{1}{r^2} \frac{\partial^2}{\partial \theta^2} \right) \left( \frac{\partial^2(\dots)}{\partial r^2} + \frac{1}{r} \frac{\partial(\dots)}{\partial r} + \frac{1}{r^2} \frac{\partial^2(\dots)}{\partial \theta^2} \right), \quad (4.1.2)$$

The bending stiffness of the plate given by  $D = \frac{Eh_m^3}{12(1-\nu^2)}$ , is defined in terms of Poisson's ratio and the plate thickness  $h_m$ ,  $E$  is the Young's modulus,  $\rho$  is the mass density, respectively. We assume the same material whatever  $m = 1, 2, 3, 4$ .

Assuming a time harmonic solution with frequency  $\omega$  as  $e^{-j\omega t}$ , the wave number is [67, 68]

$$k_m^4 = \frac{\rho h_m \omega^2}{D}, \quad (4.1.3)$$

The general form of the scattered field can be represented as [52, 64–66]

$$w_{nm}(r, \theta) = \sum_{n=0}^{\infty} \left[ A_{nm}^+ H_n^{(1)}(k_m r) + A_{nm}^- H_n^{(2)}(k_m r) + B_{nm}^+ I_n(k_m r) + B_{nm}^- K_n(k_m r) \right] \cos(n\theta), \quad (4.1.4)$$

where  $H_n^{(1)}(kr)$  and  $H_n^{(2)}(kr)$  are called Hankel functions,  $I_n$  and  $K_n$  are modified Bessel functions of the first and second kind, respectively. Connection formulas [53, 69, 70]

$$\begin{aligned} H_n^{(1)}(k_m r) &= J_n(k_m r) + jY_n(k_m r), \\ H_n^{(2)}(k_m r) &= J_n(k_m r) - jY_n(k_m r) \end{aligned} \quad (4.1.5)$$

Also,  $A_{nm}^+$ ,  $A_{nm}^-$ ,  $B_{nm}^+$  and  $B_{nm}^-$  are amplitudes to be determined, as shown in Fig.4.1.

The solution of  $H_n^{(1)'}(kr)$ ,  $H_n^{(2)'}(kr)$  and  $I_n'(kr)$ ,  $K_n'(kr)$  and the subsequent second, third derivatives see [53, 69, 70].

The moment and shear force are related to the transverse displacement by [66, 71–74]

$$\begin{aligned} M_{nm} &= -D \left[ \frac{\partial^2 w_{nm}}{\partial r^2} + \nu \left( \frac{1}{r} \frac{\partial w_{nm}}{\partial r} + \frac{1}{r^2} \frac{\partial^2 w_{nm}}{\partial \theta^2} \right) \right] = -D \left[ \frac{\partial^2 w_{nm}}{\partial r^2} + \nu \left( \frac{1}{r} \frac{\partial w_{nm}}{\partial r} - \frac{n^2}{r^2} w_{nm} \right) \right], \quad \forall n, \\ V_{nm} &= -D \left[ \frac{\partial}{\partial r} \nabla^2 w_{nm} + \frac{1-\nu}{r} \frac{\partial}{\partial \theta_{nm}} \left( \frac{1}{r} \frac{\partial^2 w_{nm}}{\partial r \partial \theta_{nm}} - \frac{1}{r^2} \frac{\partial w_{nm}}{\partial \theta_{nm}} \right) \right] = \\ &\quad -D \left[ \frac{\partial^3 w_{nm}}{\partial r^3} + \frac{1}{r} \frac{\partial^2 w_{nm}}{\partial r^2} - \frac{1}{r^2} \frac{\partial w_{nm}}{\partial r} (1 + (2-\nu)n^2) + \frac{(3-\nu)n^2}{r^3} w_{nm} \right] \end{aligned} \quad (4.1.6)$$

where order  $n$  corresponds to the number of nodal diameters,  $r$  is radius.

The continuity and equilibrium conditions has

$$\left\{ \begin{array}{ll} w_{n1}(R_1) = w_{n2}(R_1), & w_{n1}(R_1) = w_{n3}(R_1), \\ \theta_{n1}(R_1) = \theta_{n2}(R_1), & \theta_{n1}(R_1) = \theta_{n3}(R_1), \\ w_{n4}(R_2) = w_{n2}(R_2), & w_{n4}(R_2) = w_{n3}(R_2), \\ \theta_{n4}(R_2) = \theta_{n2}(R_2), & \theta_{n4}(R_2) = \theta_{n3}(R_2), \\ M_{n1}(R_1) = M_{n2}(R_1) + M_{n3}(R_1), & M_{n4}(R_2) = M_{n2}(R_2) + M_{n3}(R_2), \\ V_{n1}(R_1) = V_{n2}(R_1) + V_{n3}(R_1), & V_{n4}(R_2) = V_{n2}(R_2) + V_{n3}(R_2) \end{array} \right. \quad (4.1.7)$$

where, the values of  $R_1$  and  $R_2$  are taken from the Fig.4.1.

#### 4.2 ANALYSIS OF THE FILTERING PROPERTIES OF THE HQ PLATE

Solution ansatz 4.1.4 has been formulated to study propagation of free waves in polar coordinates. When a plate is exposed to time-harmonic forcing  $F_z(r, \theta)$ , its decomposition in angular coordinate gives

$$F_z(r, \theta) = \sum_{n=0}^{\infty} F_{n1}(r) \cos(n\theta), \quad (4.2.1)$$

Thus, both the free vibration problem and the forced vibration problem are factorized into the set of sub-problems for each individual circumferential wavenumber  $n$ , which defines how many nodal diameters the set of modes has. Then, for each  $n$ -spectrum of waves, problem formulation becomes one-dimensional, and solution is sought as 4.2.1

$$w_{nm}(r) = A_{nm}^+ H_n^{(1)}(k_m r) + A_{nm}^- H_n^{(2)}(k_m r) + B_{nm}^+ I_n(k_m r) + B_{nm}^- K_n(k_m r), \quad (4.2.2)$$

The frequencies at which the transmission coefficient is equal to zero do not depend on the way of force application, we solve the problem of finding the zero transmission frequency, as has been done in Chapter 2. We specify the amplitude of outgoing wave in segment 4 as  $A_{n4}^+ = 0$ . Thereby, we have the equations 4.2.2 for amplitudes in the inner plate,  $A_{n1}^+, A_{n1}^-, B_{n1}^+, B_{n1}^-$ , the HQ segments,  $A_{n2}^+, A_{n2}^-, B_{n2}^+, B_{n2}^-$ ,  $A_{n3}^+, A_{n3}^-, B_{n3}^+, B_{n3}^-$  and the semi-infinite segment 4,  $B_{n4}^+$ . The plus or minus sign in the amplitudes determines the direction of the wave, where the positive direction

is toward infinite space and the negative direction is toward the center of the HQ plate and the index number below corresponds to the section number (see Fig.4.1).

In equations 4.2.2, there are 13 unknown amplitudes, and we have a overdetermined system  $\Lambda = M\Phi$  and we must lower its order. It is done by regularization of solution. Displacement at  $R = 0$  must be finite, while  $H_n^{(1)}, H_n^{(2)}$  and  $K_n$  are singular at  $R = 0$ . To remove the singularity of displacement at the origin of system of coordinates, we express the amplitude of the evanescence wave  $B_{n1}^-$  through the expansion for  $K_n(k_m r)$  to obtain a complete closed system of unknown amplitudes.

The regularization principle implies that, for any infinitely small argument  $k_m r \rightarrow 0$ , the solution should not diverge to a singularity despite that 4.2.2 has both the regular part  $J_n(k_m r)$  and singular part  $Y_n(k_m r), K_n(k_m r)$ . Hence, we can combine the asymptotic formulation of the small argument of  $Y_n(k_m r), J_n(k_m r)$  and  $I_n(k_m r), K_n(k_m r)$  [53]

$$Y_n(k_m r) = -\frac{\left(\frac{1}{2}k_m r\right)^{-n}}{\pi} + \frac{2}{\pi} \ln\left(\frac{1}{2}k_m r\right) J_n(k_m r) \quad (4.2.3a)$$

$$J_n(k_m r) = \left(\frac{1}{2}k_m r\right)^n \frac{1}{\Gamma(n+1)} \quad (4.2.3b)$$

$$I_n(k_m r) = \left(\frac{1}{2}k_m r\right)^n \frac{1}{\Gamma(n+1)} \quad (4.2.3c)$$

$$K_n(k_m r) = \frac{1}{2} \left(\frac{1}{2}k_m r\right)^{-n} + (-1)^{n+1} \ln\left(\frac{1}{2}k_m r\right) I_n(k_m r) \quad (4.2.3d)$$

Substituting Eqs.4.2.3, 4.1.5 into the amplitude decomposition of Eq.4.2.2 yields

$$\begin{aligned} & A_{nm}^+ \left[ \left(\frac{1}{2}k_m r\right)^n \frac{1}{\Gamma(n+1)} + j \left( -\frac{\left(\frac{1}{2}k_m r\right)^{-n}}{\pi} + \frac{2}{\pi} \ln\left(\frac{1}{2}k_m r\right) J_n(k_m r) \right) \right] + \\ & A_{nm}^- \left[ \left(\frac{1}{2}k_m r\right)^n \frac{1}{\Gamma(n+1)} - j \left( -\frac{\left(\frac{1}{2}k_m r\right)^{-n}}{\pi} + \frac{2}{\pi} \ln\left(\frac{1}{2}k_m r\right) J_n(k_m r) \right) \right] + \\ & B_{nm}^+ I_n(k_m r) + B_{nm}^- \left[ \frac{1}{2} \left(\frac{1}{2}k_m r\right)^{-n} + (-1)^{n+1} \ln\left(\frac{1}{2}k_m r\right) I_n(k_m r) \right] = 0 \end{aligned} \quad (4.2.4)$$

Since  $I_n(k_m r)$  is finite at  $r = 0$ , we neglect it and after balancing the terms in Eq.4.2.2, which tend to  $\infty$ , we obtain

$$B_{nm}^- = j \frac{2}{\pi} (A_{nm}^+ - A_{nm}^-) \quad (4.2.5)$$

Equation 4.2.5 can be applied for any  $n$ .

From the Eq.4.2.2 and considering wave propagation in the inner segment of a plate, where this part of the solution tends to zero, we have

$$w_{n1}(r) = A_{n1}^+ \left[ H_n^{(1)}(k_1 r) + j \frac{2}{\pi} K_n(k_1 r) \right] + A_{n1}^- \left[ H_n^{(2)}(k_1 r) - j \frac{2}{\pi} K_n(k_1 r) \right] + B_{n1}^+ I_n(k_1 r), \quad (4.2.6)$$

Hence, we have 12 unknown amplitudes in the system of homogeneous linear algebraic equations for any  $n$

$$H = YQ, \quad (4.2.7)$$

or

$$\begin{bmatrix} 0 \\ 0 \\ \vdots \\ 0 \\ 0 \\ \vdots \\ 0 \\ 0 \end{bmatrix} = \begin{bmatrix} -H_n^{(1)}(k_1 r) - j \frac{2}{\pi} K_n(k_1 r) & -H_n^{(2)}(k_1 r) + j \frac{2}{\pi} K_n(k_1 r) & -I_n(k_1 r) & \dots & 0 \\ -H_n^{(1)}(k_1 r) - j \frac{2}{\pi} K_n(k_1 r) & -H_n^{(2)}(k_1 r) + j \frac{2}{\pi} K_n(k_1 r) & -I_n(k_1 r) & \dots & 0 \\ \vdots & \vdots & \vdots & \vdots & \vdots \\ \dots & \dots & \dots & \dots & \dots \\ \dots & \dots & \dots & \dots & \dots \\ \vdots & \vdots & \vdots & \vdots & \vdots \\ 0 & 0 & 0 & \dots & -K_n(k_4 r) \\ 0 & 0 & 0 & \dots & -K_n(k_4 r) \end{bmatrix} \begin{bmatrix} A_{n1}^+ \\ A_{n1}^- \\ \vdots \\ B_{n2}^+ \\ B_{n2}^- \\ \vdots \\ B_{n3}^- \\ B_{n4}^- \end{bmatrix} \quad (4.2.8)$$

Condition of existence of its nontrivial solution defines equation for zero transmission frequency

$$\det|Y| = 0 \quad (4.2.9)$$

Fig.4.2a,d shows the solution of the frequency dependent equation 4.2.9 on the complex plane. The parameters of the HQ plate were chosen as follows: thicknesses  $h = 10$  mm,  $h_2 = 4$  mm,  $h_3 = 3$  mm, radii  $R_1 = 200$  mm,  $R_2 = 400$  mm and the HQ plate material is aluminium, as in the HQ beam analysis. This figure presents two cases for different  $n$ .

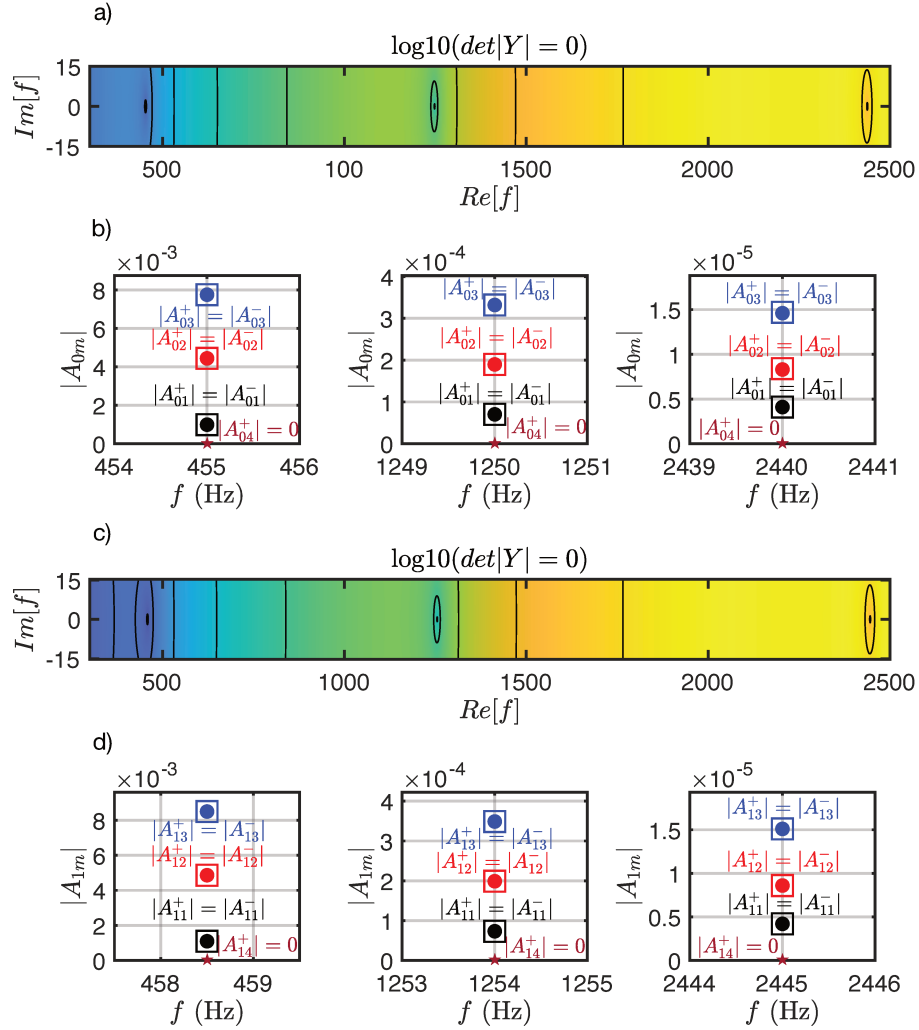


Fig. 4.2 a) Zero transmission frequency on the complex plane (black dots) for  $n = 0$  at  $f_1 = 455\text{Hz}$ ,  $f_2 = 1250\text{Hz}$ ,  $f_3 = 2440\text{Hz}$  and c) for  $n = 1$  at  $f_1 = 458.5\text{Hz}$ ,  $f_2 = 1255\text{Hz}$ ,  $f_3 = 2445\text{Hz}$ . b) Magnitude of amplitudes of positive-going waves (black, red and blue squares) and negative-going waves (black, red and blue circles) in segments 1,2,3 for  $n = 0$  and d) for  $n = 1$  at zero transmission frequencies.

The first case in Fig.4.2a represents an axisymmetric oscillation of a circular plate for  $n = 0$ . The second case in Fig.4.2c illustrates a non-axisymmetric oscillation for  $n = 1$ . We can clearly see that the solution of the equation 4.2.9 for both cases is purely real due to the absence of an outgoing wave in segment 4 and the lossless system. At the set of frequencies  $f_1 = 455\text{ Hz}$ ,  $f_2 = 1250\text{ Hz}$ ,  $f_3 = 2440\text{ Hz}$  for  $n = 0$  and  $f_1 = 458.5\text{ Hz}$ ,  $f_2 = 1255\text{ Hz}$ ,  $f_3 = 2445\text{ Hz}$  for  $n = 1$ , destructive interference of waves in segments 2 and 3 cancels propagation of a wave in segment 4, as shown in Fig.4.3. Exactly as in the case of a beam, at these frequencies standing waves

are generated in segments 1,2 and 3, as demonstrated by the magnitudes of the amplitudes of the positive-going waves (black, red, and blue squares) and negative-going waves (black, red, and blue circles) in Fig.4.2b,d. Note that for  $n = 0$ , the magnitude of the positive-going wave at zero transmission frequencies in segment 1 is:  $f_1 = 455\text{Hz}$ ,  $|A_1^+| = 9.7 \times 10^{-4}$ ,  $f_2 = 1250\text{ Hz}$ ,  $|A_1^+| = 7.03 \times 10^{-5}$ ,  $f_3 = 2440\text{Hz}$ ,  $|A_1^+| = 4.08 \times 10^{-6}$ , and for  $n = 1$ , the magnitude is:  $f_1 = 458.5\text{Hz}$ ,  $|A_1^+| = 1.1 \times 10^{-4}$ ,  $f_2 = 1255\text{Hz}$ ,  $|A_1^+| = 7.3 \times 10^{-5}$ ,  $f_3 = 2445\text{Hz}$ ,  $|A_1^+| = 4.17 \times 10^{-6}$ .

Indeed, the frequencies at which no wave propagation takes place for the case  $n = 0$  are different from those for the case  $n = 1$ , this problem is discussed in the next Section 4.3.

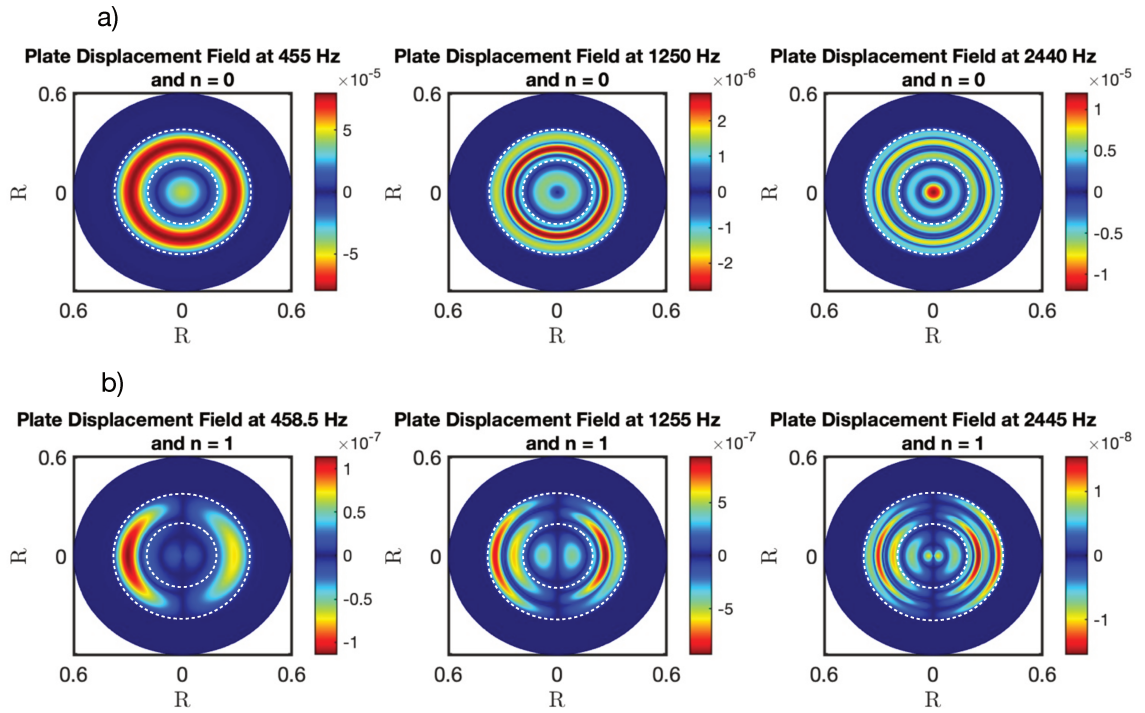


Fig. 4.3 a) Plate displacement field at zero transmission frequencies  $f_1 = 455\text{ Hz}$ ,  $f_2 = 1250\text{ Hz}$ ,  $f_3 = 2440$  for  $n = 0$  b) Plate displacement field at zero transmission frequencies  $f_1 = 458.5\text{Hz}$ ,  $f_2 = 1255\text{Hz}$ ,  $f_3 = 2445\text{Hz}$  for  $n = 1$ .

Due to reciprocity, the same zero transmission frequency is easily obtained in the reversed problem formulation. Namely, we assume the incident wave  $A_{n4}^-$  impinges on the HQ insert. Thus, the problem formulation involves following amplitudes for the inner disk  $B_{n1}^+$ , the HQ annular disk  $A_{n2}^+$ ,  $A_{n2}^-$ ,  $B_{n2}^+$ ,  $B_{n2}^-$ ,  $A_{n3}^+$ ,  $A_{n3}^-$ ,  $B_{n3}^+$ ,  $B_{n3}^-$  and

the infinite plate  $A_{n4}^+, A_{n4}^-, B_{n4}^+$ . Using the boundary conditions from Eq.4.1.7 yields

$$H' = Y'Q', \quad (4.2.10)$$

By analogy with Eq.4.2.9, we have

$$\det|Y'| = 0 \quad (4.2.11)$$

The Eq.4.2.11 gives us absolutely identical zero transmission frequency for any parameter  $n$  as in Fig.4.2.

#### 4.3 ZERO TRANSMISSION FREQUENCY FOR DIFFERENT N

As demonstrated in the previous Section, magnitudes of zero transmission frequencies are dependent upon the circumferential wavenumber  $n$ . In this Section, we explore this dependence along with the dependence of zero transmission frequencies upon a location of the HQ insert. Its length, material and thickness of its components are kept the same as in Section 4.2.

The Fig.4.4 shows the effect of the circumferential wavenumber  $n$  on the zero transmission frequency at different values of length in segment 1, i.e., at different distances from the origin of system of coordinates to circular HQ device. It is convenient to scale this distance by the thickness of the main plate,  $R_1 = \frac{R_1^{dim}}{h}$ . Fig.4.4 clearly shows that in the near field at  $R_1 = 50$  (light blue circles), the zero transmission frequency is strongly shifted towards higher frequencies as the circumferential wavenumber grows. However, in the far field at  $R_1 = 500$  (black circles), the zero transmission frequency shifts weakly as  $n$  changes and these frequencies are practically the same for any  $n$ . To explain this difference in dependence of zero transmission frequencies upon parameter  $n$ , it is sufficient to recall the large argument asymptotic presentation of Bessel functions  $H_n$  and  $K_n$ , [53] Sections 10.17.5, 10.40.10. As seen from these formulas, the leading order term for  $H_n$  features the  $n$ -dependence only in the phase and the leading order term for  $K_n$  is not dependent upon  $n$ . Therefore, if the HQ device is located at the distance  $R_1=50$  from the origin, it is placed in the 'near field' zone, in which these asymptotic expansions are not accurate, while, if the HQ device is located at the

distance  $R_1=500$  from the origin, it is placed in the 'far field' zone, in which these asymptotic expansions are valid.

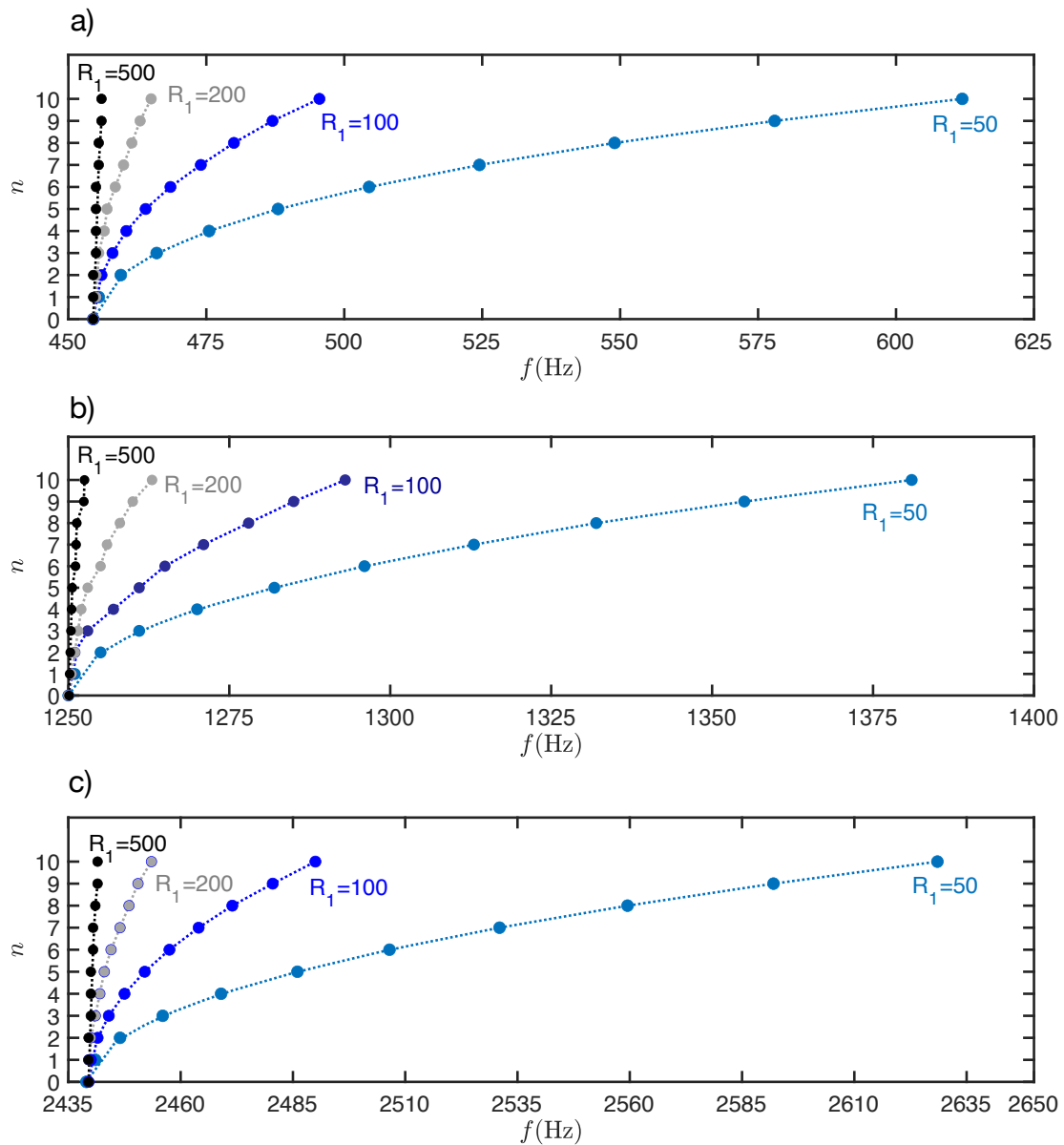


Fig. 4.4 a) Frequency dependence of the circumferential order  $n$  for the a) 1st ; b) 2nd; c) 3rd zero transmission frequency and the non-dimensional distance parameters in segment 1, i.e.,  $R_1 = 50, 100, 200, 500$ .

## 4.4 FORCED PROBLEM

This section is associated to solving the forced problem. The force of unit intensity is applied along a circle of small radius (at the orifice) in segment 1,  $R_f = 0.01\text{mm}$ , and the bending moment at the orifice remains zero. The problem formulation is to find the following amplitudes in the inner plate  $A_{n1}^+, A_{n1}^-, B_{n1}^+, B_{n1}^-$ , the HQ segment  $A_{n2}^+, A_{n2}^-, B_{n2}^+, B_{n2}^-, A_{n3}^+, A_{n3}^-, B_{n3}^+, B_{n3}^-$  and semi-infinite segment 4  $A_{n4}^+, B_{n4}^+$ , see Fig.4.1.

The boundary conditions for the semi-infinite HQ plate is introduced for any  $n$  as

$$\begin{cases} M_{n1}(R_f) = 0 \\ V_{n1}(R_f) = F_z, \end{cases} \quad (4.4.1)$$

Note that the frequency at which the transmission is zero is independent of the magnitude of the force, that implies the force can take any value. Obviously, the same holds true regarding the transmission coefficient 3.1.10.

Taking Equation 4.1.7 yields the continuity and equilibrium equations for the forced problem. The wave decomposition is taken from Equation 4.2.2. Hence, we arrive at the following set of equations for the unknown wave amplitudes

$$F = IE, \quad (4.4.2)$$

or

$$\begin{bmatrix} 0 \\ F_z \\ \vdots \\ 0 \\ 0 \\ \vdots \\ 0 \\ 0 \end{bmatrix} = \begin{bmatrix} -H_n^{(1)}(k_1 r) & -H_n^{(2)}(k_1 r) & -I_n(k_1 r) & -K_n(k_1 r) & \dots & 0 & 0 \\ -H_n^{(1)}(k_1 r) & -H_n^{(2)}(k_1 r) & -I_n(k_1 r) & -K_n(k_1 r) & \dots & 0 & 0 \\ \vdots & \vdots & \vdots & \vdots & \vdots & \vdots & \vdots \\ \dots & \dots & \dots & \dots & \dots & \dots & \dots \\ \dots & \dots & \dots & \dots & \dots & \dots & \dots \\ \vdots & \vdots & \vdots & \vdots & \vdots & \vdots & \vdots \\ 0 & 0 & 0 & 0 & \dots & -H_n^{(2)}(k_4 r) & -K_n(k_4 r) \\ 0 & 0 & 0 & 0 & \dots & -H_n^{(2)}(k_4 r) & -K_n(k_4 r) \end{bmatrix} \begin{bmatrix} A_1^+ \\ A_1^- \\ \vdots \\ B_2^- \\ A_3^+ \\ \vdots \\ A_4^- \\ B_4^- \end{bmatrix} \quad (4.4.3)$$

where the expression for the transmission coefficient can be found in the Equation 3.1.10.

### Finite Element model validation

The solution using this wave model has been also validated using FEM in COMSOL solid mechanics software. For the analysis, we use the axisymmetric solid mechanic interface and the equation of motion is formulated for the 2D cross section, where the loads are constant around the object's circumference. The HQ model consists of the following elements as shown in Fig.4.1, where the radii of inner plate is  $R_1 = 500\text{mm}$ , the two HQ plates is  $R_2 = 700\text{mm}$  with HQ thicknesses are  $h_2 = 4\text{mm}$ ,  $h_3 = 3\text{mm}$  and total thickness  $h = 10\text{mm}$ , respectively. The plate is bounded by the annular Perfectly Matched Layer in order to simulate the infinite outside radius. Aluminum has been selected as the material for the HQ plate, where  $E = 70\text{GPa}$ ,  $\rho = 2700\text{kg.m}^{-3}$ ,  $\nu = 0.3$  and lossless system. The parameters of mesh took into account 4 elements in the thickness and a mesh size of 5 mm along the  $r$ -axis. The transmission coefficient  $T$  is determined by the wave decomposition which is derived from bending displacement components  $w$ , as seen in Chapter 3, Section 3.1.2.

The Fig.4.5 depicts the frequency dependence of the transmission coefficient for the wave model of Kirchhoff plate (black line) at  $n = 0$  and FE simulation (dashdotted line). The transmission coefficient of Kirchhoff model tends to zero at the same zero transmission frequencies as in Fig.4.2a. However, neglecting transverse shear deformation of the cross-section and longitudinal waves leads to a discrepancy with zero transmission frequencies predicted by the FE model.

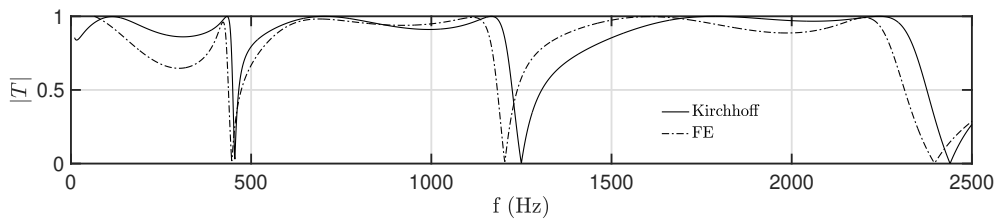


Fig. 4.5 Frequency dependence of the transmission coefficient by Kirchhoff model (solid line) and FE simulation (dashdotted line) for  $n = 0$ .

The axisymmetric deflection fields of the HQ plate model for forced problem shown in Fig.4.6. In both beam and plate analysis, zero transmission occurs at particular frequencies, where for the plate these frequencies are  $f = 455\text{Hz}$ ,  $f = 1250\text{Hz}$ ,  $f = 2440\text{Hz}$ , similar to the figure Fig.4.2a. In these frequencies the two HQ segments are in out-of-phase, resulting in standing waves in the HQ filter, the

same as in Fig.4.3a. For other frequencies  $f = 315\text{Hz}$ ,  $f = 1010\text{Hz}$ ,  $f = 1815\text{Hz}$ , the two HQ segments are in-phase and the energy is transmitted in segment 4.

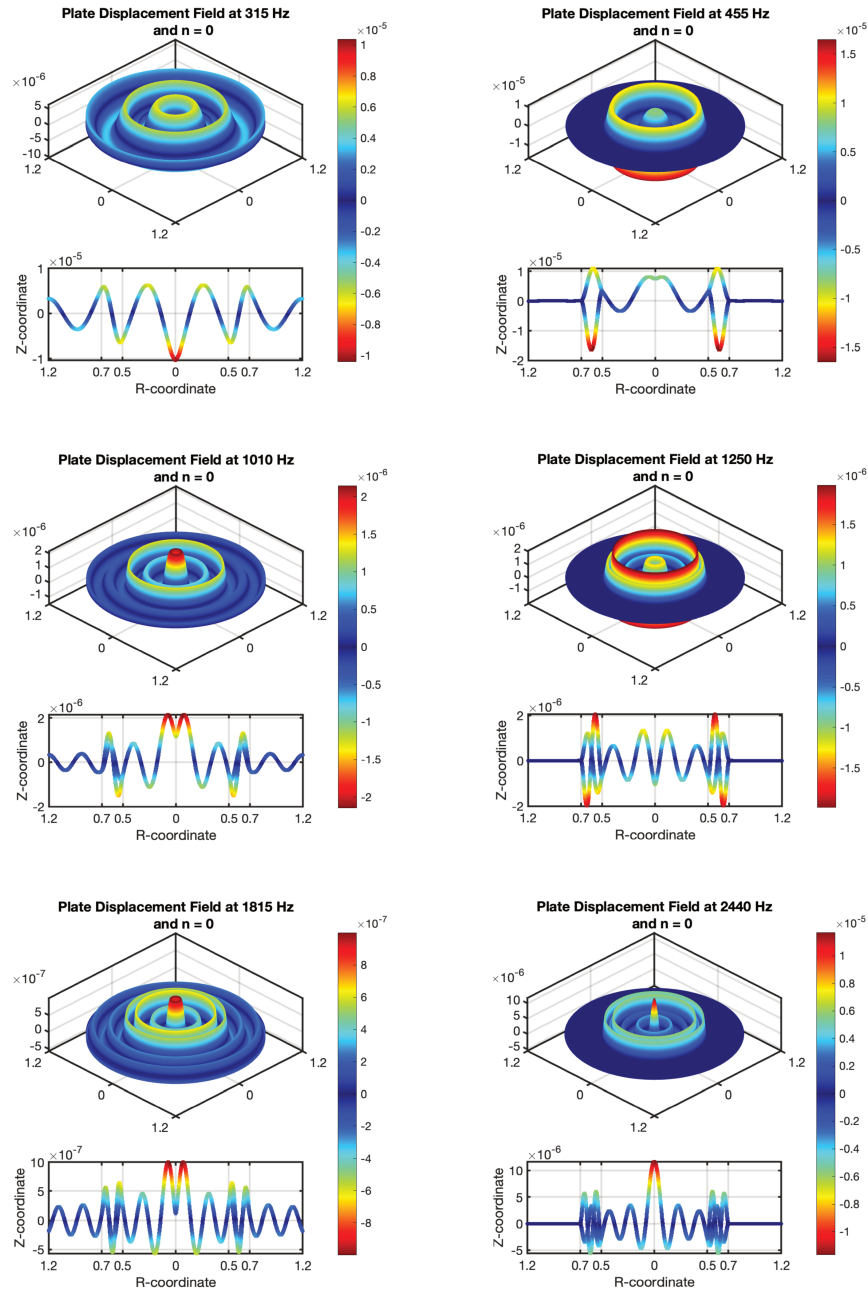


Fig. 4.6 Displacement field of the HQ plate for the forcing problem at specific frequencies and  $n = 0$ . Each displacement field represents a 3d view and a cross-sectional view of the HQ plate.

## 4.5 ENERGY FLUX AND INSERTION LOSS ANALYSIS

In this section we outline the energy flux analysis for the forced problem. The analysis of the energy flux relationship between the bending wave of a beam and a plate is similar.

For time harmonic motion, the time-averaged power is given in terms of the displacement and internal force vectors by

$$\Pi = \left[ \frac{1}{2} \text{Re}[V_{nm}(x, t) \cdot v_{nm}^*(x, t)] + \frac{1}{2} \text{Re}[M_{nm}(x, t) \cdot \chi_{nm}^*(x, t)] \right] \varphi 2\pi R_O, \quad (4.5.1)$$

where asterisk \* indicates complex conjugate,  $R_O$  is a radius of the control surface, at which the energy flux is evaluated, the velocity  $v_{nm}(x, t) = \frac{\partial w_{nm}(x, t)}{\partial t} = -j\omega w_{nm}$  and the angular velocity  $\chi_{nm}(x, t) = \frac{\partial \theta_{nm}(x, t)}{\partial t} = -j\omega \theta_{nm}$ , respectively. The coefficient  $\varphi = 1$  at  $n = 0$  and  $\varphi = 0.5$  at  $n = 1, 2, 3, \dots$  for integration over the interval  $(0, 2\pi)$ .

Fig.4.7 shows the logarithmic scale of energy flux analysis with reference power 1 Watt. The principle of conservation of energy requires that the energy flux through the system be the same at all positions. The power results in Fig.4.7a were calculated without the HQ filter  $\Pi_1$  for a uniform main plate, and the results in Fig.4.7b are power analysis for a plate with the HQ filter  $\Pi_2$ . The physical and

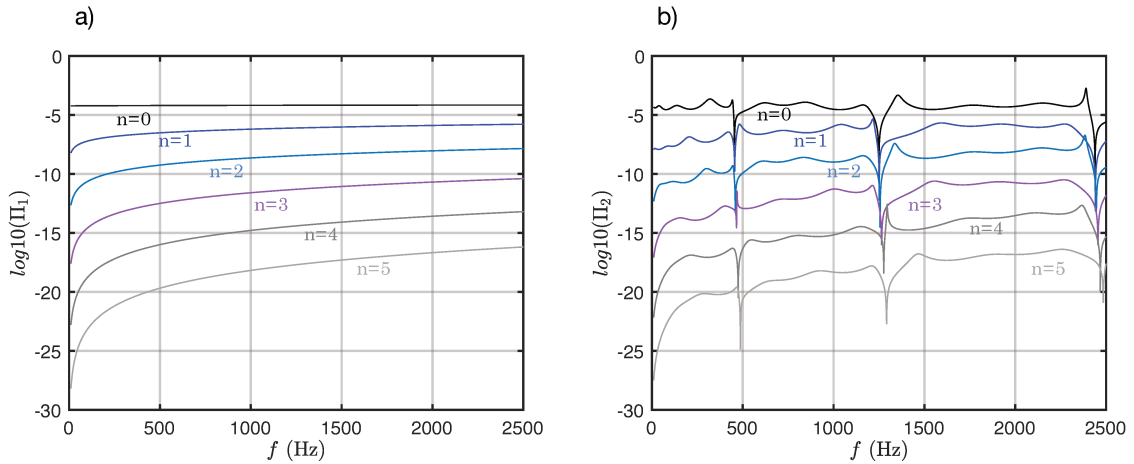


Fig. 4.7 a) Logarithmic scale of energy flux without HQ filter  $\Pi_1$  for  $n = 0 \dots 5$  b) with HQ filter  $\Pi_2$  for  $n = 0 \dots 5$ .

geometrical parameters of a plate with the HQ filter and the total thickness for a

uniform plate were chosen to be the same as in Section 4.4. Both cases have been calculated for different circumferential orders  $n$ . It can be seen that the largest energy flux corresponds to  $n = 0$  and the energy is dominantly conveyed by the axisymmetric wave. Comparing the two results between Fig.4.7a and Fig.4.7b, the energy flux in Fig.4.7b shows dips for any  $n$  at particular frequencies exactly at the zero transmission frequencies marked in Fig.4.2.

When energy fluxes are found with and without the HQ filter, as shown in Fig.4.7, then we can find how much the energy flux has been reduced by the HQ filter. The generally recognized measure of this effect is  $IL$  (Insertion Loss), defined as the logarithmic ratio of the energy flux transmitted by the system before the HQ device is installed to the energy flux after it is installed [1, 3, 75]. Hence, the Insertion Loss can be written as the logarithm on base 10 of the ratio of the sum of the energies of the participating propagating waves for all orders  $n$  with and without the HQ filter (reference intensity) in decibels

$$IL = 10 \log_{10} \frac{\sum_{n=0}^{\infty} \Pi_1}{\sum_{n=0}^{\infty} \Pi_2} \text{dB}. \quad (4.5.2)$$

Fig.4.8 depicts the typical Insertion Loss defined by the Eq.4.5.2. The maximum of the peaks corresponds to the zero transmission frequency and the lowest energy flux parameter. The negative values of Insertion Loss corresponds to the amplification effect of the HQ filter. This indicates that the energy flux in the HQ plate becomes larger at certain frequencies than the energy flux in the uniform plate.

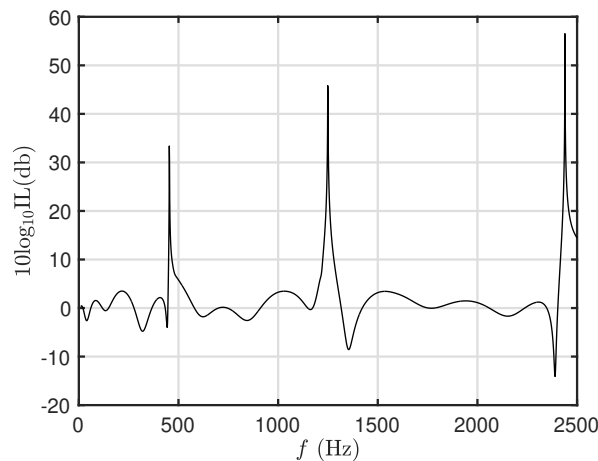


Fig. 4.8 Insertion Loss defined by the Equation 4.5.2.

## 4.6 ASSESSMENT OF PERFORMANCE OF HQ DEVICE OUTSIDE ZERO TRANSMISSION FREQUENCIES

As has been shown in Chapters 2-3 and in Section 4.4, zero transmission frequencies can be readily obtained with no reference to excitation conditions, i.e., as solutions of an eigenvalue problem.

In the previous Section, an inspection of the energy flux has revealed that, besides its complete cancellation at zero transmission frequencies, there are frequency ranges in which insertion of HQ device produces an amplification effect. To explain the mechanism of its generation, it is necessary to distinguish between two alternative formulations of the forcing problem for a plate equipped with HQ device.

In its simplest possible formulation, it is assumed that a time-harmonic travelling wave of the prescribed amplitude (with the natural choice being the unit amplitude) impinges an 'inlet' of HQ device. Then zero transmission frequencies are those at which no travelling wave is launched at the 'outlet' of HQ device. An alternative formulation of the forcing problem is to specify a point in the waveguide, where a time-harmonic force of the prescribed (for simplicity, the unit) amplitude generates the travelling wave, which impinges HQ device. As is proven in Chapter 2, the same sets of zero transmission frequencies are obtained in these formulations, and they are also available as solutions of the above-mentioned eigenvalue problem. At these frequencies, a standing wave is set up, and an energy flux in the whole waveguide is absent.

Energy fluxes obtained in the 'unit force' problem formulation for a plate with and without HQ device are reproduced in Fig.4.9 at  $n = 0$ . The 'unit wave amplitude' problem formulation implies that, instead of condition of the absence of outgoing wave in segment 4,  $A_{o4}^+ = 0$ , the condition  $A_{o1}^+ = 1$  is applied. Energy fluxes obtained in this problem formulation for a plate with and without HQ device are shown in Fig.4.9a. As clearly seen from these graphs, amplification effect is impossible in the 'unit wave amplitude' problem formulation, but it takes place in the 'unit force' formulation.

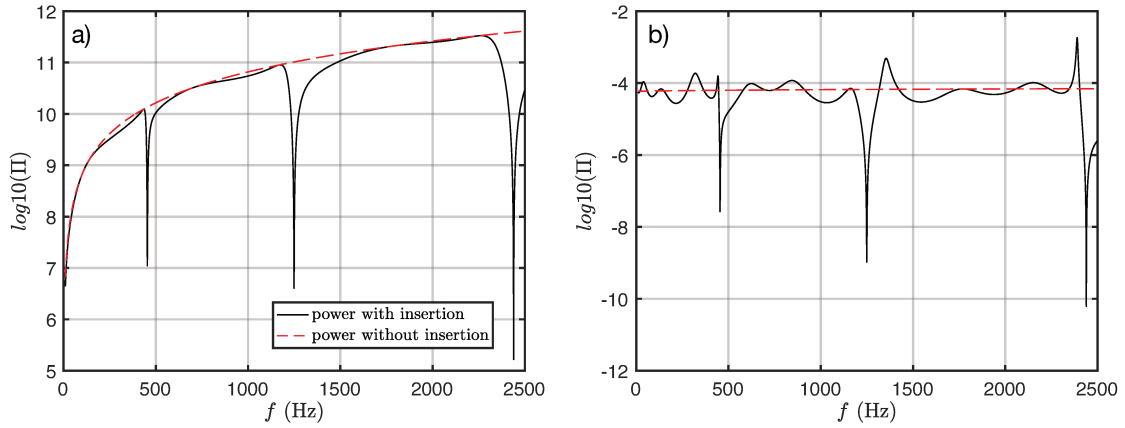


Fig. 4.9 a) Energy Flux for specified unit amplitude  $A_1^+$  problem in a uniform infinite plate (red dashed line) and in the HQ plate (black line). b) Energy Flux for the forced problem in a solid infinite plate (red dashed line) and in the HQ plate (black line).

The ‘unit force’ problem formulation for a plate means that the second equation in 4.4.1 is formulated as  $F_z = 1$ . Then the amplification frequency ranges can be readily found via calculation of input mobility at the excitation orifice. Indeed, the energy input condenses to

$$\Pi = \frac{1}{2} \text{Re} [j\omega w_{n1}^*(R_f)] \varphi 2\pi R_f, \quad (4.6.1)$$

so that

$$\Pi = \frac{1}{2} \omega \text{Im} [w_{n1}(R_f)] \varphi 2\pi R_f, \quad (4.6.2)$$

Using Eq.4.6.2, it is found that the Input Point Mobility becomes

$$Y_{R_f} = \omega \text{Im} [w_{n1}(R_f)] \varphi 2\pi R_f, \quad (4.6.3)$$

Fig.4.10 depicts the Input Point Mobility determined by the Equation 4.6.3 at  $n = 0$ . The results are presented for a uniform plate and for the HQ plate. As expected, the Input Point Mobility in the HQ plate is higher than the Input Point Mobility in the solid plate at certain frequencies, which leads to an increase in the magnitude of the incoming wave. However, at some frequencies, the mobility is zero, which corresponds to energy flux dips in Fig.4.7b. Hence, the amplification effect is driven

by orifice excitation in the central segment and the Input Point Mobility determines the energy that is pumped into the system.

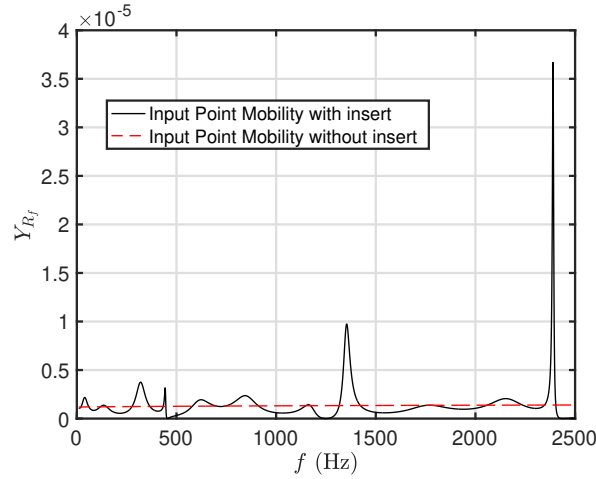


Fig. 4.10 Input Point Mobility in a uniform infinite plate (red dashed line) and in HQ plate (black line).

The position of the excitation orifice affects the magnitude of the Insertion Loss, as shown in Fig.4.11. The analysis was done for specified unit amplitude  $A_{01}^+$  problem Fig.4.11a and for the forced problem Fig.4.11b at  $n = 0$ . This excitation source at the radius of the orifice is controlled by the distance parameter  $R_1$  in segment 1 (see the black and blue color bar in Fig.4.11), where  $R_1 = \frac{R_1^{dim}}{h}$ . At the small value of  $R_1$  (black line) the Insertion Loss shifts toward the positive values and negative dips decrease in a certain frequency range, as shown in Fig.4.11. However, negative drops appear at low frequencies. As  $R_1$  increases, the Insertion Loss remains unchanged in Fig.4.11a, which is not the case in Fig.4.11b, where the Insertion Loss takes both positive and negative values at certain frequencies. The peaks of the Insertion Losses at which destructive interference take place do not change within the accuracy of the graph.

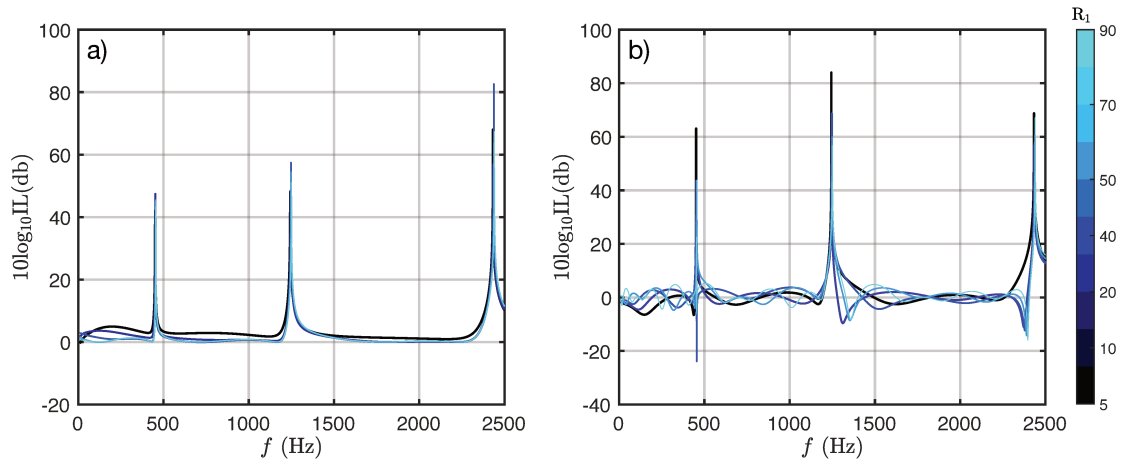


Fig. 4.11 a) Insertion Loss for specified unit amplitude  $A_{01}^+$  problem and different parameters  $R_1$ . b) Insertion Loss for the forced problem and different parameters  $R_1$ .

## 4.7 APPLICATION TO SANDWICH PANELS

### 4.7.1 Classification of HQ sandwich architectures

Sandwich plates are increasingly utilized in mechanical engineering due to their ability to offer enhanced strength and stiffness without added weight compared to metal alternatives. This allows designers to reduce weight without compromising on strength and stiffness. In the most common and practical case, such plates can be achieved by using multilayer plates in which a lightweight and relatively pliable core is joined with two stiff contralateral facings.

The HQ principle may be attractive for integration into sandwich panels due to its simplicity of realisation and its effectiveness in suppressing vibrations at particular frequencies, as was shown previously. The system can be described as it is represented in Fig.4.12, where the HQ sandwich panel is made out of 3 layers: two different skins and a pliable core.

The phase velocity difference between the two skins can be controlled by the thickness difference, as in the case of a metal plate, but can also be controlled by the effective Young's modulus as in the case of a perforated plate [76–83], (see Appendix A.2), as shown in Fig.4.12a. The difference in effective Young's modulus between the two layers  $E_1$  and  $E_2$  will lead to destructive interference and no energy transfer.

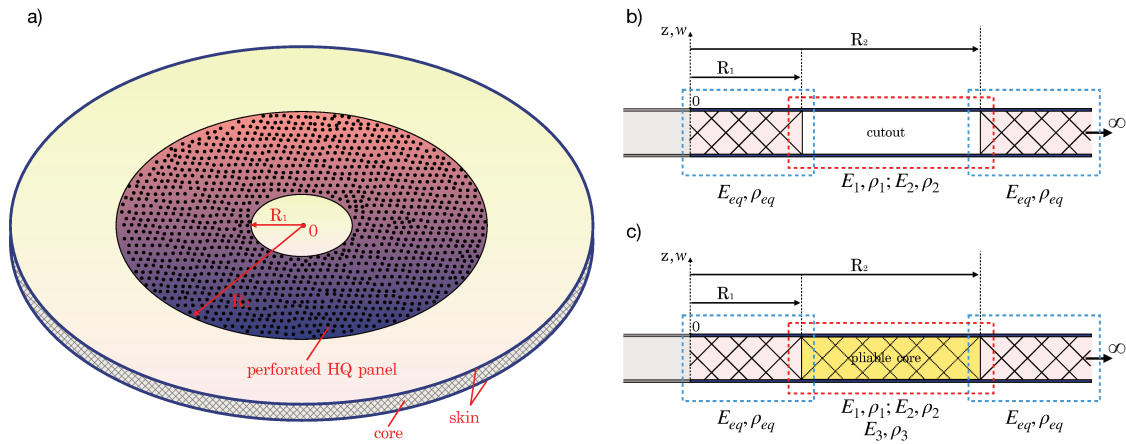


Fig. 4.12 a) Model of HQ perforated sandwich panel. b) Multilayer HQ panel with a cutout in the HQ zone. c) Multilayer HQ panel with a pliable core in the HQ zone.

Two cases of realisation of HQ sandwich plate can be considered:

- In the first case, shown in Fig.4.12b, the infinite multilayer HQ panel consists of a cutout in the HQ zone (red contour), which is similar to the HQ filter in the beam and plate, and different skins with different stiffness characteristics  $E_1, \rho_1$  and  $E_2, \rho_2$ . The left center segment and the right infinite segment have an equivalent parameter of Young's modulus and density  $E_{eq}, \rho_{eq}$ .
- In the second case, shown in Fig.4.12c, the multilayer HQ panel is made of the same different skins  $E_1, \rho_1$  and  $E_2, \rho_2$  but with a pliable core  $E_3, \rho_3$  in the HQ zone (red contour). This case is of important interest because we can see the influence of the central core on the effect of destructive interference in the HQ filter.

#### 4.7.2 Analysis of a perforated skin of HQ plate

The analysis of the skin of the HQ sandwich plate, as shown in Fig.4.12b, was carried out using a FEM in a 2D axisymmetric interface of COMSOL Solid Mechanics, as in Sections 4.4. The finite element mesh was set as 3 elements along the total thickness and a mesh size of 0.3mm along the radius of the HQ zone (red contour) and 5mm along the radius of the left central and right infinite segments. The panel characteristics were chosen as an aluminium honeycomb panel [84, 85] with an overall thickness of 6.6mm and a skin thickness of 0.3mm, radii  $R_1 = 50\text{mm}$  and

$R_2 = 150\text{mm}$ . The Young's modulus and density for the left central and right infinite segments are  $E_{eq} = 4.67\text{GPa}$ ,  $\rho_{eq} = 233\text{kg}\cdot\text{m}^{-3}$  [84], and for the upper segment are  $E_1 = 70\text{GPa}$ ,  $\rho_1 = 2700\text{kg}\cdot\text{m}^{-3}$ . The parameters of the lower segment  $E_2$ ,  $\rho_2$  can be chosen according to the difference in wave speed between the upper and lower segments. This difference should create a phase shift between two travelling wave, resulting in destructive interference at the output of the infinite segment. Whereas the wave speed in thin plate [86] is given by the expression

$$c_{B_m} = \left( \frac{E_m h^2}{12(1 - \nu^2)\rho_m} \omega^2 \right)^{1/4}, \quad m = 1, 2 \quad (4.7.1)$$

Therefore, from Equation 4.7.1, it is implied that the difference in wave speeds between the two HQ segments  $c_{B_1} \neq c_{B_2}$  can be produced by  $\frac{E_1}{\rho_1} \neq \frac{E_2}{\rho_2}$ . We assume that  $\rho_1 = \rho_2$ , then the HQ segment characteristic can be described by  $E_1 = \Psi \cdot E_2$ , where  $\Psi$  is a coefficient defining the contrast between the two elastic moduli of the HQ segments.

The transmission coefficient  $T$  was computed by the wave decomposition shown earlier in Section 3.1.2 and 4.4.

The frequency dependence of the transmission coefficient for different values of  $\Psi$  at  $n = 0$  is shown in Fig.4.13. When  $\Psi$  is one, there is no destructive interference effect and energy is transmitted. However, the dips and zero transmission frequencies occur when  $\Psi = 0.9$  and when there is a small contrast between the two elastic moduli of the HQ branches. At  $\Psi = 0.1$  the elastic moduli contrast is larger, leading to an increase in the number of zero transmission frequencies at which standing waves take place as indicated by the displacement fields for frequencies  $f_1 = 257\text{Hz}$ ,  $f_2 = 733\text{Hz}$ ,  $f_3 = 1595\text{Hz}$ .

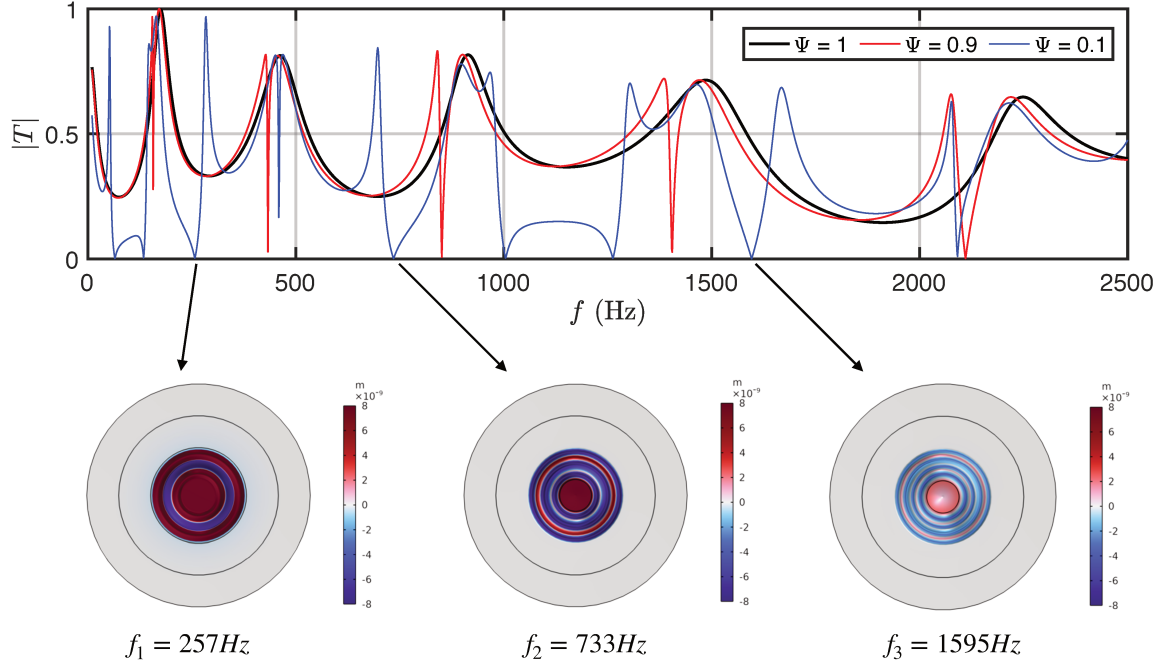


Fig. 4.13 Frequency dependence of the transmission coefficient at different coefficient  $\Psi$  determining the contrast between the two elastic moduli of HQ segments. Displacement field for zero transmission frequency at  $\Psi = 0.1$  and  $n = 0$ .

#### 4.7.3 Limitation due to the core

This section mainly focuses on the effect of the core of the HQ sandwich panel between the two HQ segments, as illustrated in Fig.4.12c. The analysis was done using the FEM as in the previous Section 4.7.2. For the simulation, we adjust a new core region that has a new material characteristic  $E_3 = 0.055\text{GPa}$ ,  $\rho_3 = 37\text{kg}\cdot\text{m}^{-3}$ . The characteristics of the two HQ branches at which zero transmission frequencies exist were chosen from Section 4.7.2 for the first branch as  $E_1 = 70\text{GPa}$ ,  $\rho_1 = 2700\text{kg}\cdot\text{m}^{-3}$  and for the second branch as  $E_2 = 0.1E_1$ ,  $\rho_2 = \rho_1$ , the equivalent parameters are  $E_{eq} = 10.5\text{GPa}$ ,  $\rho_{eq} = 436.5\text{kg}\cdot\text{m}^{-3}$ . The remaining parameters and the evaluation of  $T$  coefficient are in accordance with Section 4.7.2.

Fig.4.14 demonstrates the effect of the core in the HQ zone on the frequency dependence of the transmission coefficient. The core parameter is controlled by Young's modulus as  $E_\zeta = \zeta \cdot E_3$ , where  $\zeta$  is a coefficient determining the core resistance in the HQ zone. From Fig.4.14, it is evident that the core has a significant effect on creating destructive interference between the two HQ segments. When the

resistance is large, e.g.,  $\zeta = 1$  or  $\zeta = 0.01$ , then there is no dip in the transmission coefficient. However, the low resistance parameter, e.g.,  $\zeta = 0.001$ , shows the presence of zero transmission frequency and the destructive interference effect takes place, leading to standing waves in the centre region and HQ zone at frequencies  $f_1 = 967\text{Hz}$ ,  $f_2 = 1320\text{Hz}$ ,  $f_3 = 2097\text{Hz}$ .

Indeed, the core resistance in the HQ region should be as soft as possible so that the significant contribution of the two HQ branches can create destructive interference at the filter output. Otherwise, the hard core will prevail over the HQ branches, leading to energy transfer at the output.

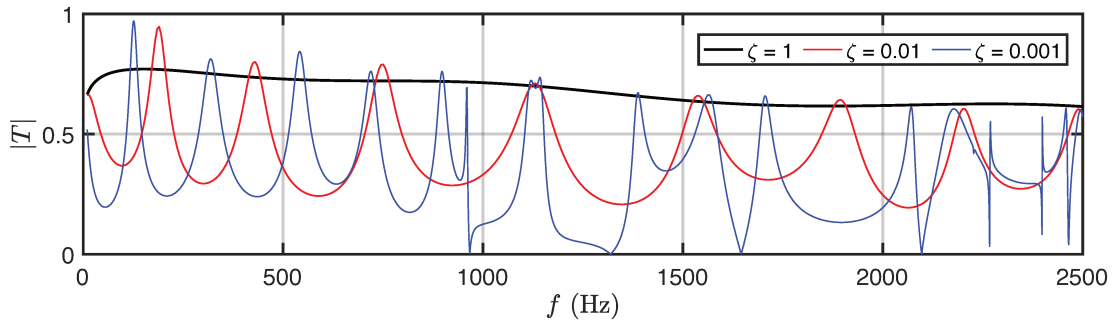


Fig. 4.14 Frequency dependence of the transmission coefficient at different coefficient  $\zeta$  determining the core resistance in the HQ zone. Displacement field for zero transmission frequency at  $\zeta = 0.001$  and  $n = 0$ .

#### 4.8 CONCLUSION

The results obtained in this chapter showed that the HQ concept can be easily integrated into the plate problem. The analysis of the problem with zero transmission frequencies revealed the same effect of the out-of-phase between the two HQ branches leading to standing waves and no energy transfer at the output of the plate, as in the beam problem.

It was obtained that the dominant mode at which destructive interference effects occur in HQ plate is the axisymmetric oscillations for  $n = 0$ . The energy flux analysis also confirmed this hypothesis. The Insertion Loss analysis then revealed an amplification problem in which the energy flux in the HQ plate becomes greater than in a uniform plate at certain frequencies. As a result, this problem is associated with an external force acting on the centre of coordinates, where the energy flux is directly related to how much energy has been injected.

In the last section, the HQ filter in the sandwich panel was considered. The analysis of the HQ sandwich panel showed that the filtering effect of the HQ filter can be achieved not only by the difference in thickness between the two HQ branches, but also by changing the characteristics of the elastic modulus or stiffness of one of the skins. Hence, the results showed that the small contrast in elastic moduli between the two branches leads to zero transmission frequency. The effect of the core in the HQ zone of the sandwich panel also revealed that its elastic modulus characteristic should be much lower than that of the two HQ branches in order to achieve zero transmission frequencies.

---

## SOPHISTICATED HQ FILTERS

---

In this chapter, we present various variations around the original HQ filter design, in order to extend the frequency band on which the transmission coefficient is reduced or to obtain additional zero transmission frequencies.

Following on from the Chapter 3, it is possible to modify the HQ filter by using a multi-branch or multi-cell configuration, whereby the beam is considered to consist of multiple regional elements and several separated paths, with the result that each travelling wave in each path will induce destructive interference at the output of the device. As the first examples for this analysis, serial, parallel and mixed arrangement in a Timoshenko beam are proposed.

Next, as a continuation of Chapter 2, the configuration of a periodic HQ filter chain for longitudinal waves will be considered to simulate the effects of the pass band and stop bands using Floquet theory.

## 5.1 MULTI-BRANCH CONFIGURATIONS

The branches of HQ filter can be arranged in many different ways. We propose to study a few simple arrangements described in Fig.5.1, ranging from 'serial' and 'parallel' to 'mixed' arrangements.

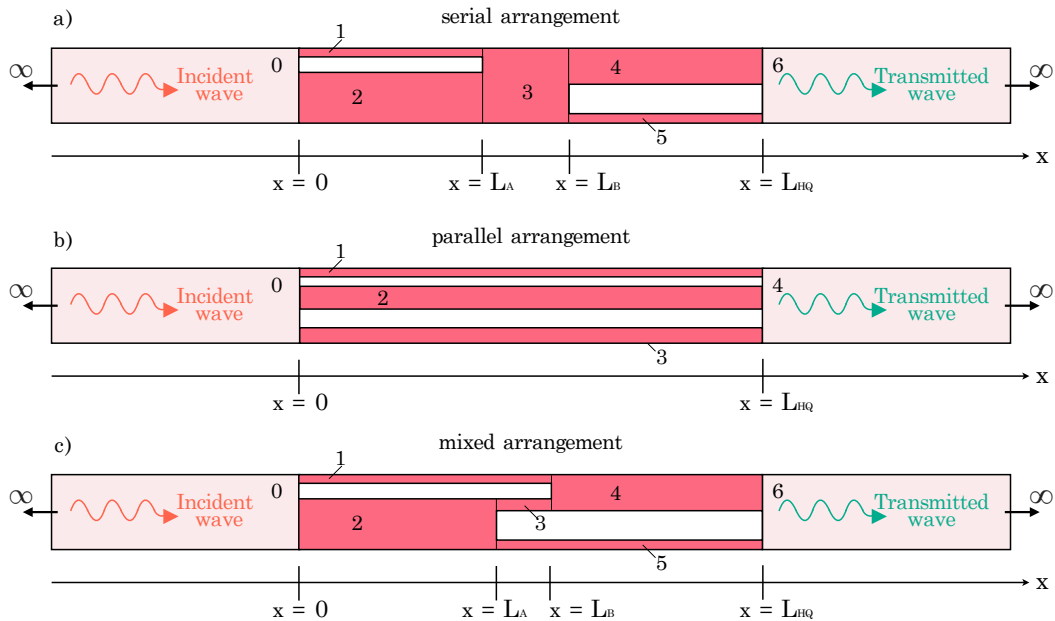


Fig. 5.1 a) Scheme of HQ filter with a) serial arrangement, where the distance between two HQ cells is adjusted by  $L_A$  and  $L_B$ ; b) parallel arrangement; c) mixed arrangement.

## 5.1.1 HQ filter with serial arrangement

The composite HQ filter with serial arrangement consists of an infinite split beam with two single HQ filters shown in Fig.5.1a. The distance between the two single HQ filters is controlled by the segment 3.

The analysis of such a 'multi-cell' configuration is similar to that of HQ filter with 2 branches in Chapter 3, except that the difference lies in the number of studied segments, which divide the HQ device into other extra subzones.

The material characteristics of aluminum and solution of the equation of motion 3.1.1 with time convention  $e^{-j\omega t}$  remain the same as for the HQ filter with two branches from Chapter 3. We use the Timoshenko beam theory with unit incoming amplitude  $A_0^+ = 1$  in segment 0. Then, considering the continuity and equilibrium

equations 3.1.5, 3.1.6 not taking into account longitudinal waves and the auxiliary continuity and equilibrium equations for extra segments 4, 5 and 6, we obtain by analogy with the equation 3.1.7, the homogeneous linear algebraic equations for the unknown wave amplitudes  $A_0^-, B_0^- \dots A_6^+, B_6^+$ . Substituting the wave amplitudes  $A_0^+, A_6^+$  into the equation 3.1.10 we can calculate the frequency dependence of the transmission coefficient for the serial arrangement. Note that a model based on the scattering matrix would also allow the estimation of the R and T coefficients.

In Fig.5.2, the frequency dependences of the transmission coefficient for the serial arrangement and for the 1st and 2nd single HQ filter at total thickness  $h_0 = 10\text{mm}$  and length of the segment 3,  $L_s = 100\text{mm}$ , are presented. The zero

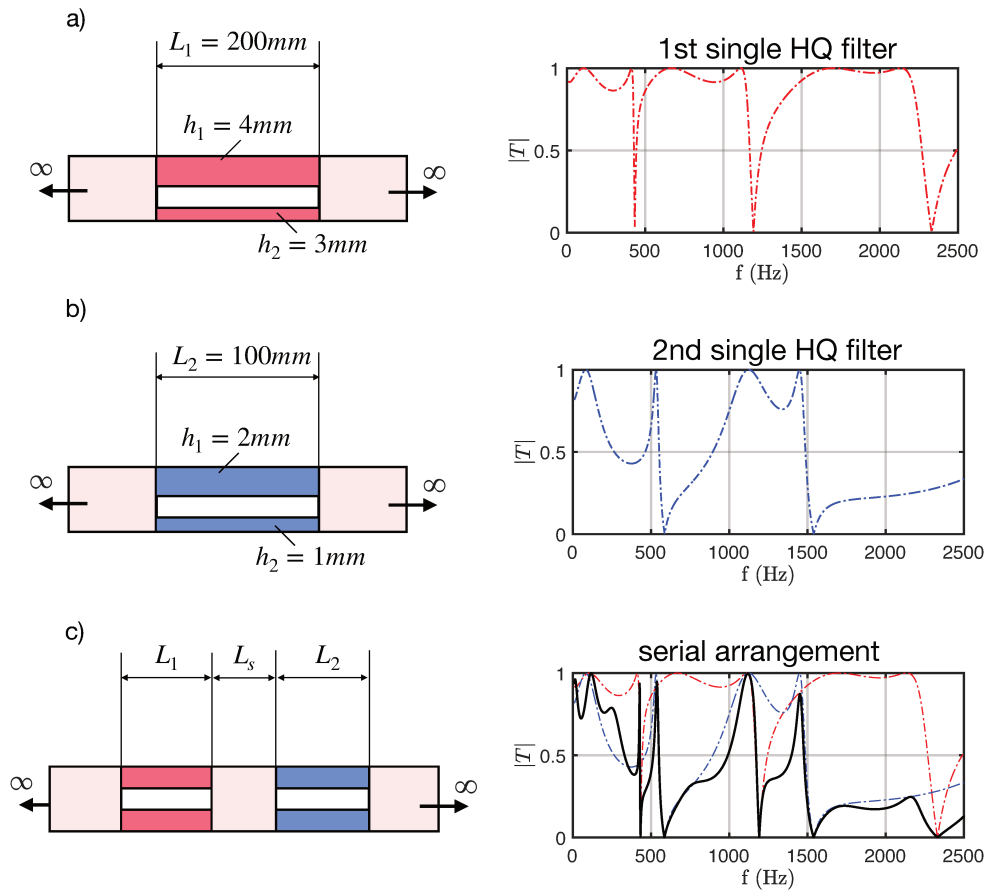


Fig. 5.2 a) Transmission coefficient of a) the 1st single HQ filter and b) the 2nd single HQ filter and their geometric characteristics. c) Transmission coefficient of the serial arrangement at the length of the central segment 3,  $L_s = 100\text{mm}$ .

transmission frequencies of the 1st and 2nd single HQ filter shown in Fig.5.2a,b strictly correspond to the zero transmission frequencies of the composite HQ filter

in Fig.5.2c. It implies that each subsequent single HQ filter with its inherent zero transmission frequencies will produce additional dips in the transmission coefficient for the serial arrangement at which destructive interference occur.

In addition, the low transmission coefficient of the mixed arrangement can be found such that the frequency of the dip in the T coefficient of the second single HQ filter coincides with the frequency of the first single HQ filter at which T coefficient is equal to one.

#### *Tunelling effect in serial arrangement of HQ filter*

The changing of the length of the segment 3, called  $L_s$ , can produce a tunneling effect in which the evanescent waves in segment 3 can transmit energy and, disturb the zero transmission frequencies. This effect is well-known in quantum mechanics. In acoustics, it has been studied in [87, 88]. Therefore, Table.5.1 shows the tunneling effect at the zero transmission frequency around 433Hz from Fig.5.2c when the length of segment 3 is changed. At small length of segment 3, the transmission coefficient close to zero, at large length, the transmission coefficient is strictly zero due to the vanishing of  $B_3^+$ .

$L_s$	0,5mm	5mm	100mm
$ T $	$8,5 \times 10^{-5}$	$1,5 \times 10^{-5}$	0

Table 5.1 Magnitude of the transmission coefficient  $|T|$  of the serial arrangement around the zero transmission frequency 433Hz for different lengths of the central segment 3,  $L_s$ .

#### 5.1.2 HQ filter with parallel arrangement

The basic HQ filter configuration can also be extended by increasing the number of branches in the split beam, as shown in Fig.5.1b. We consider an extended HQ configuration consisting of an infinite split beam with three HQ branches in the middle, where the dimensions of these branches are set as  $h_1 = 3\text{mm}$ ,  $h_2 = 2\text{mm}$  and the ancillary branch  $h_3 = 1\text{mm}$  with the same length  $L_{HQ} = 220\text{mm}$ , the total thickness of the split beam is  $h_0 = h_4 = 10\text{mm}$ .

The analysis of the HQ filter with parallel arrangement is similar to the analysis of the serial arrangement in the previous Section 5.1.1. We set a given amplitude of

the incoming wave  $A_0^+ = 1$  in segment 0. Hence, by analogy with Section 5.1.1, the system of linear equations 3.1.5, 3.1.6 (without considering the longitudinal wave components) can be used in conjunction with new boundary conditions for the ancillary branch through the ratio of displacements, rotations and forces between each subzone 0,1,2,3,4. The continuity equations at  $x = 0$  are then given by the form

$$\begin{cases} w_0(0) = w_1(0) = w_2(0) = w_3(0), \\ \theta_0(0) = \theta_1(0) = \theta_2(0) = \theta_3(0), \end{cases} \quad (5.1.1)$$

and equilibrium equations are

$$\begin{cases} M_0(0) = M_1(0) + M_2(0) + M_3(0), \\ F_0(0) = F_1(0) + F_2(0) + F_3(0), \end{cases} \quad (5.1.2)$$

By analogy, we can compose the same equations 5.1.1, 5.1.2 at  $x = L_{HQ}$

Combining the equations 5.1.1, 5.1.2 for all subzones 0,1,2,3,4 leads to the system of 16 linear algebraic equations for wave amplitudes  $A_0^-; B_0^- \dots A_4^+; B_4^+$

The transmission coefficient is now defined as the ratio of wave amplitudes  $A_0^+$  and  $A_4^+$

$$T = \frac{A_4^+}{A_0^+} \quad (5.1.3)$$

Fig.5.3a shows a comparison of the frequency dependence of the transmission coefficients of the basic configuration of HQ filter with 2 branches (see Fig.3.1) and the extended configuration with 3 branches, where the thicknesses of the two branches of the basic configuration in Fig.3.1 correspond to the first two thicknesses of HQ filter with 3 branches in Fig.5.1a as  $h_1 = 3\text{mm}$ ,  $h_2 = 2\text{mm}$ , and the other geometric and material parameters keep the same.

The extended configuration with 3 branches induces more dips in the  $T$  coefficient than the configuration with 2 branches in the studied frequency range, leading to an increase in the number of specific frequencies at which the destructive interference effect is observed, as shown in Fig.5.3a. For example, in the frequency range of 1950Hz to 2150Hz, a single zero transmission frequency occurs for a 2 branch configuration, whereas a 3 branch configuration generates double zero transmission frequencies in the same frequency range.

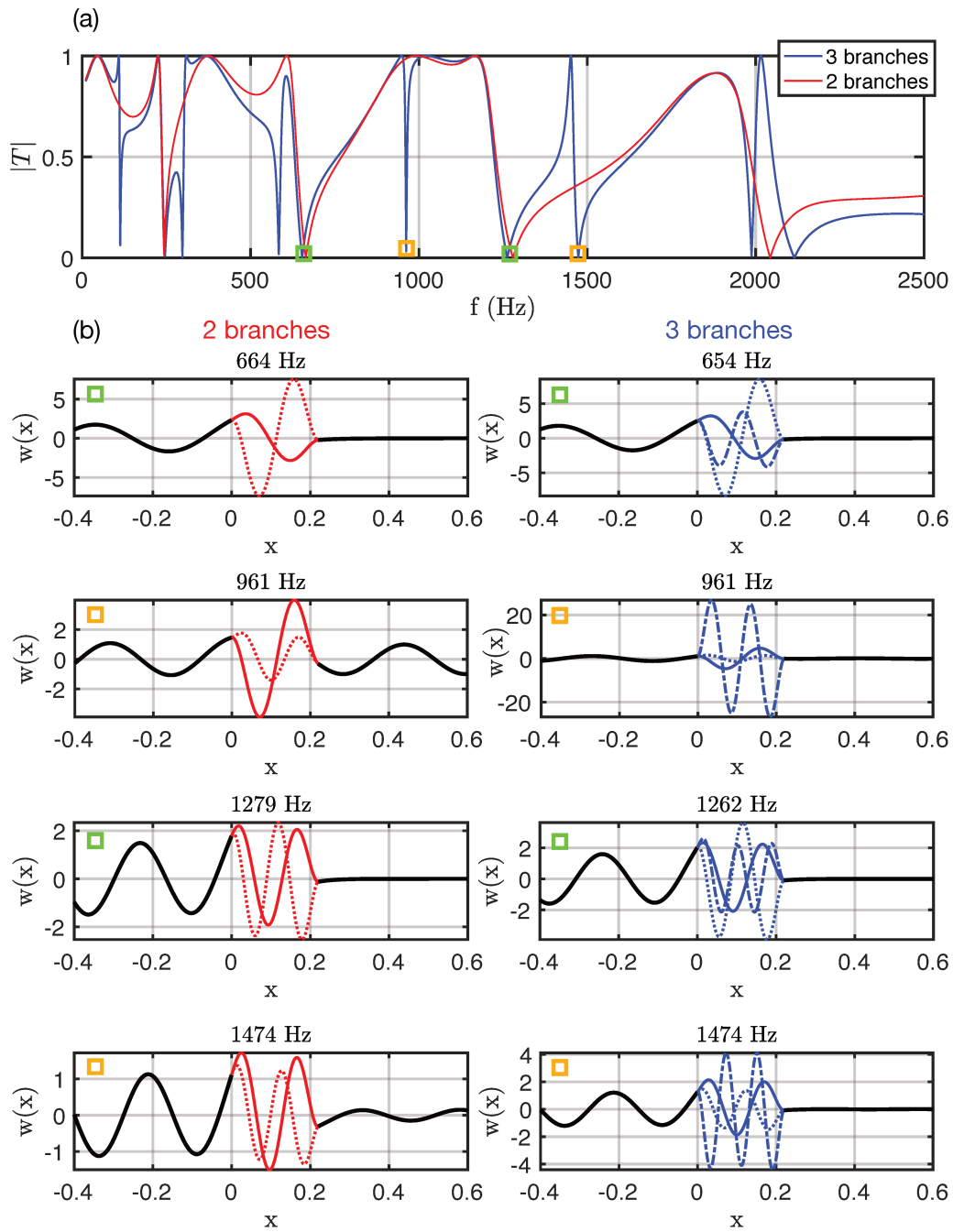


Fig. 5.3 a) Transmission coefficient for the HQ filter with 2 branches (red line) at  $h_1 = 3\text{mm}$ ,  $h_2 = 2\text{mm}$  and with 3 branches (blue line) at  $h_1 = 3\text{mm}$ ,  $h_2 = 2\text{mm}$ ,  $h_3 = 1\text{mm}$ . b) Deflection shapes for two different configurations at the selected frequencies (green and orange squares in the transmission coefficient).

At selected frequencies (green squares for matching between 3 and 2 branch configurations and orange squares for additional dips of the 3 branch configuration),

the operating deflection shapes for the two configurations are shown in Fig.5.3b, where the red areas denote the basic configuration with 2 branches and the blue areas denote the extended configuration with 3 branches. The operating deflection shapes at frequencies  $f = 664\text{Hz}$ ,  $f = 1279\text{Hz}$ , which are close to the frequencies of the HQ filter with 3 branches, e.g.,  $f = 654\text{Hz}$ ,  $f = 1262\text{Hz}$ , show that the destructive effect is caused by a basic configuration with 2 branches that work in out-of-phase and the presence of a third thin branch on the filtering performance is negligible. However, frequencies of the extended configuration, such as  $f = 1474\text{Hz}$ , show the opposite effect, a pair of waves propagating in the third thin branch  $h_3$  generates other standing waves that localize around the HQ filter and no transmitted energy take place. The vibration shape of the first two branches in the extended model remains the same as in the basic model. At frequency  $f = 961\text{Hz}$ , a dip is observed on the  $T$  diagram, the thin branch has a large deformation, as can be seen from the modal analysis.

Fig.5.4 depicts the absolute values of the amplitudes of the positive and negative-going bending wave in each segment of HQ configuration with 3 branches around selected zero transmission frequencies. From this figure, it follows that the am-

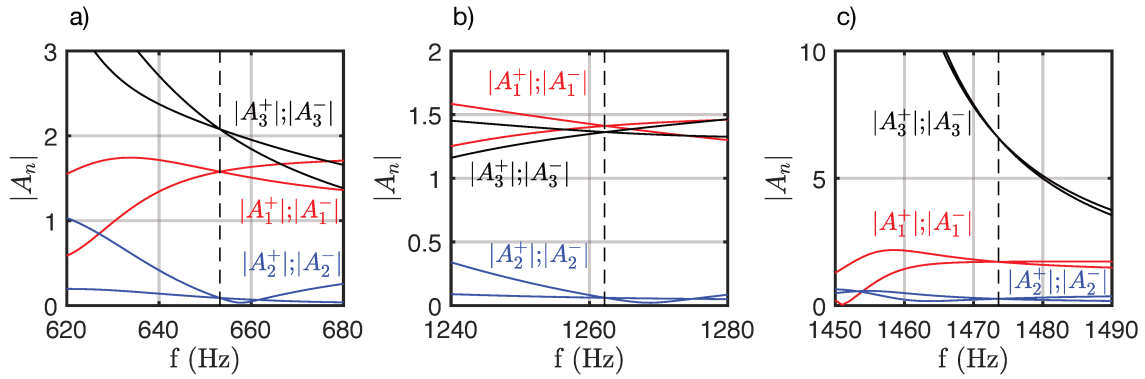


Fig. 5.4 Amplitudes of bending waves at zero transmission frequency (dashed vertical line) a)  $f = 654\text{Hz}$ ; b)  $f = 1262\text{Hz}$ ; c)  $f = 1474\text{Hz}$ .

plitudes of the two waves in each segment 1,2,3 are equal to each other at zero transmission frequency, e.g.,  $f = 654\text{Hz}$ ,  $f = 1262\text{Hz}$ ,  $f = 1474\text{Hz}$ , resulting in standing waves. The influence of the ancillary branch is shown in Fig.5.4a and 5.3b (deflection shape at  $f = 1474\text{Hz}$ ), namely the amplitude value of the ancillary branch is larger than the other two branches and as a result, a new zero transmission frequency is generated.

### 5.1.3 HQ filter with mixed arrangement

In this section, we propose an infinite HQ filter with mixed arrangement, where two single HQ filters are partially overlapped, making segment 3 an auxiliary thin branch, as shown in Fig.5.1c. This configuration can be viewed as a mixture of serial and parallel arrangements. The solution of the transmission coefficient for the mixed arrangement remains the same as in the previous Sections 5.1.1 and 5.1.2, except for the continuity and equilibrium equations for each subzone of the HQ filter.

The distance between the two single HQ filters is controlled by the coordinates  $x = L_A$  and  $x = L_B$ , as shown in Fig.5.1c and Fig.5.5. Accordingly, we can investigate the effect of single HQ filters on the transmission coefficient of this mixed arrangement: 1) when the two single HQ filters are overlapped by symmetrically tuning the coordinates  $x = L_A$  and  $x = L_B$  with respect to the center coordinate of the mixed configuration  $L_c$  and in this case, the difference between  $x = L_B$  and  $x = L_A$  is positive, 2) when two single HQ filters correspond to the serial arrangement in Section 5.1.1 and in this cases, the difference between  $x = L_B$  and  $x = L_A$  is negative. In the former case, the coordinate  $x = L_B$  will be shifted to the end of HQ filter coordinate  $x = L_{HQ}$ , and the coordinate  $x = L_A$  will be symmetrically shifted relative to center coordinate  $L_c$  to the origin of HQ filter coordinate  $x = 0$ . The length of segment 3 is increased along with the length of the two single HQ filters. In the second case, the coordinate  $x = L_A$  and  $x = L_B$  will be shifted in reverse, namely, the coordinate  $x = L_A$  will be shifted to the end of HQ filter coordinate  $x = L_{HQ}$ , and the coordinate  $x = L_B$  will be symmetrically shifted relative to center coordinate  $L_c$  to the origin of HQ filter coordinate  $x = 0$ .

To summarize, we can categorize the following cases:

- If  $L_B - L_A = -L_{HQ}$ , the configuration is a uniform beam, with no HQ filter.
- If  $-L_{HQ} < L_B - L_A < 0$ , the configuration corresponds to a serial arrangement with 2 single HQ filters (results of the red region in Fig.5.5).
- If  $0 < L_B - L_A < L_{HQ}$ , the configuration corresponds to a mixed arrangement (results of the black region in Fig.5.5).
- If  $L_B - L_A = L_{HQ}$ , the configuration corresponds to a parallel arrangement with 3 HQ branches.

Fig.5.5 shows the frequency dependences of the transmission coefficient for a symmetrically varying difference with respect to the center coordinate  $L_c$  of the distance between  $L_B$  and  $L_A$ , when  $L_B - L_A \geq 0$  and  $L_B - L_A \leq 0$  at thicknesses  $h_0 = 10\text{mm}$ ,  $h_1 = 3\text{mm}$ ,  $h_2 = 5\text{mm}$ ,  $h_3 = 2\text{mm}$ ,  $h_4 = 7\text{mm}$ ,  $h_5 = 1\text{mm}$  and length of HQ filter  $L_{HQ} = 200\text{mm}$ . From Fig.5.5, it follows that as the difference  $L_B - L_A$

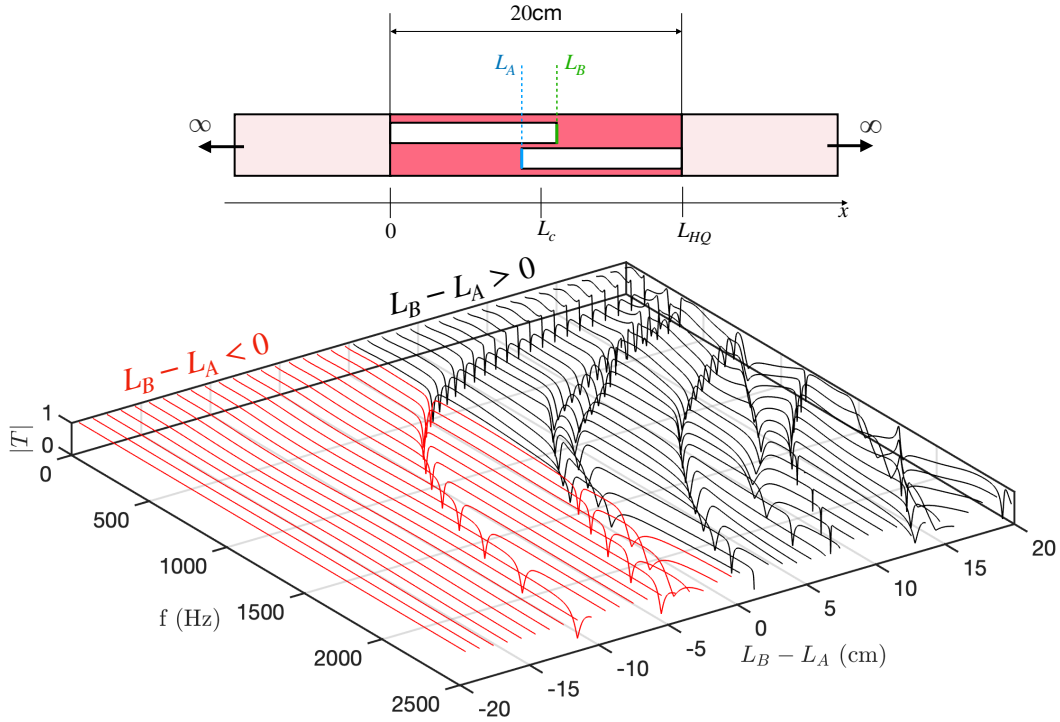


Fig. 5.5 Frequency dependences of the transmission coefficient for the mixed arrangement at different symmetrically changing distances between  $L_B$  and  $L_A$  with respect to the coordinate  $L_c$ . The transmission coefficient in the red zone corresponds to  $L_B - L_A < 0$  and the transmission coefficient in the black zone corresponds to  $L_B - L_A > 0$ .

becomes positive, the dips in the transmission coefficient, at which destructive interference occurs, shift toward low frequencies, and when the coordinate  $x = L_A$  comes to  $x = 0$  and  $x = L_B$  comes to  $x = L_{HQ}$ , i.e.,  $L_B - L_A = 20\text{cm}$ , then the zero transmission frequency strictly correspond to the zero transmission frequencies of the parallel arrangement, as shown in Fig.5.3. As the difference  $L_B - L_A$  is large and negative, e.g.,  $L_B - L_A = -18\text{cm}$ , there are no dips and the energy is transmitted in the beam. Therefore, the length of the single HQ filters in a mixed arrangement

must be large to ensure good filtering properties of the HQ device, and its size should also depend on the frequency range it is targeting.

#### 5.1.4 Experimental demonstration

This section presents the experimental study of the transmission coefficient in a beam of 2000mm length with HQ filter consisting of three branches. The aluminum beam with two through-holes with a length of 205mm is shown in Fig.5.6, the

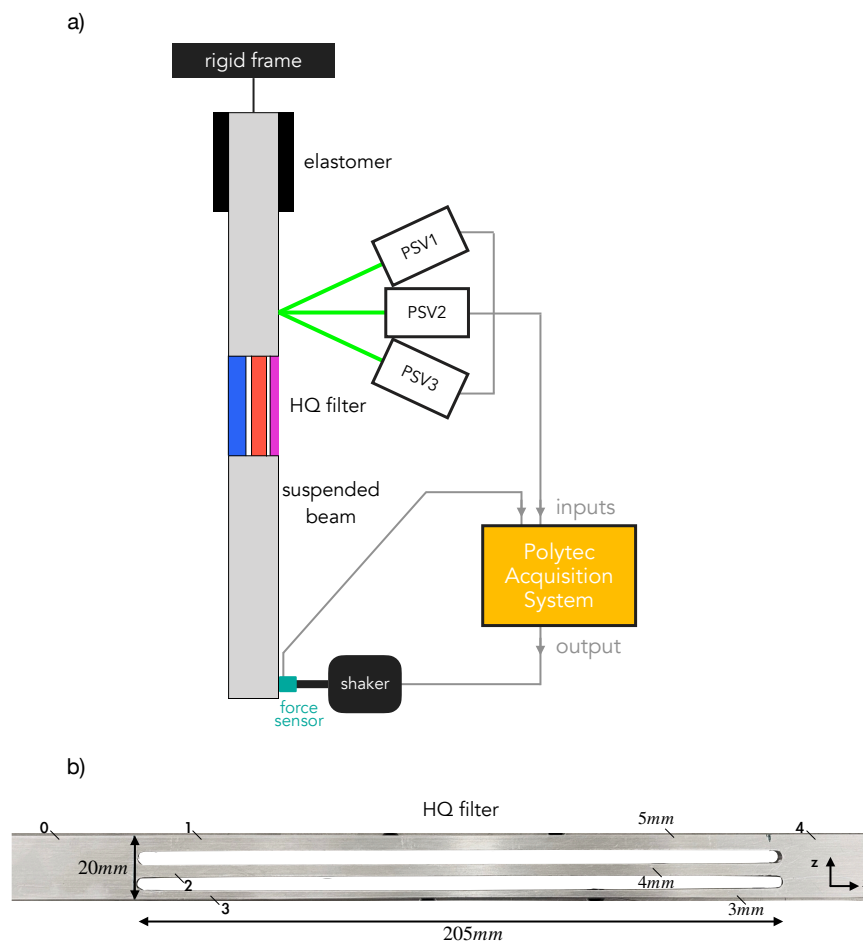


Fig. 5.6 a) Experimental set up of HQ filter with a damping layer at the end. b) Picture of HQ filter with 3 branches and its geometrical characteristics.

dimensions of the total thickness 20mm, the thickness of the first segment 5mm, the second segment 4mm and the third segment 3mm, and the width of the HQ filter specimen 10mm, respectively.

The beam was suspended vertically by strings to simulate free-free boundary conditions and excited by an electrodynamic shaker perpendicular to the x-axis and along the beam centerline to avoid beam torsion, similar to the 2-branch HQ filter measurement in Chapter 3. The vibration measurements were then performed using the 3Dvib experimental platform, as shown in Fig.3.8. Since only one plane subjected to bending motion is scanned, it is sufficient to use one scanning laser vibrometer head, which reduces the problem of experimental fitting.

The transmission coefficient 5.1.3 was estimated from the same pseudo-inverse of the matrix in 3.1.11 as in Section 3.4.2.

As was mentioned in the previous sections of Chapter 3, the frequency dependence of the transmission coefficient, defined by equation 3.1.10, becomes more complicated if there is a wave reflection effect at the beam end, i.e., the transmission coefficient is not between zero and one since several artefacts due to multiple origins are observed. Among the possible reasons, we can list the longitudinal waves resulting from the residual curvature of the beam, heterogeneity of the material due to the milling process, some errors in the exact locations of the measurement points, the existence of reflections at the final end of the beam, the fact that evanescent waves are not taken into account the computation of T (see Eq.3.1.10). Nevertheless, even if it has some limitations, the experimental technique is able to identify the o-transmission frequencies. To try to reduce the reflections at the end of the beam, we chose to introduce dissipative boundary conditions [89], [62], i.e., a damping material applied to the end of the beam to minimize the reflected wave from the boundaries on the measured signals. In practice, we use viscoelastic layer made of an elastomer that is attached to the end of the beam shown in 5.6a to ensure the absorption of the energy incident upon the boundaries.

Fig.5.7 shows the experimental identification of the transmission coefficient for a beam with damping (red line) and without damping (blue line) at the end. 1D model described by Timoshenko beam theory, the system of equations 5.1.1, 5.1.2, and the transmission coefficient, determined by equation 5.1.3, of this model has been compared with the experimental results, as shown in Fig.5.7 (black line).

The zero transmission frequencies in the experimental simulation with and without damping correspond to the frequencies of the 1D Timoshenko model (green circles) at  $f = 412\text{Hz}$ ,  $f = 557\text{Hz}$  and  $f = 1472\text{Hz}$ , as shown in Fig.5.7, but there is a discrepancy around  $f = 1060\text{Hz}$  due to the geometric curvature of the beam sample, the quality of the scanning vibrometer mesh and the effect of

longitudinal waves in the HQ filter. The zero transmission frequencies in Fig.5.7a are the same as in Fig.5.7b. It follows that the zero transmission frequencies are independent of the type of boundary conditions in the HQ filter, and the estimation of the transmission coefficient at which the destructive interference effect is captured can be done by equation 5.1.3. On the other hand, the choice of different dissipative boundary conditions can affect the amplification problem, which disturbs the estimation of the transmission coefficient, as shown, e.g., in Fig.5.7a. Namely, a beam without absorption at the end leads to an increase in the magnitude of the transmission coefficient beyond one, when the absorption is set, the magnitude of the transmission coefficient becomes low Fig.5.7b.

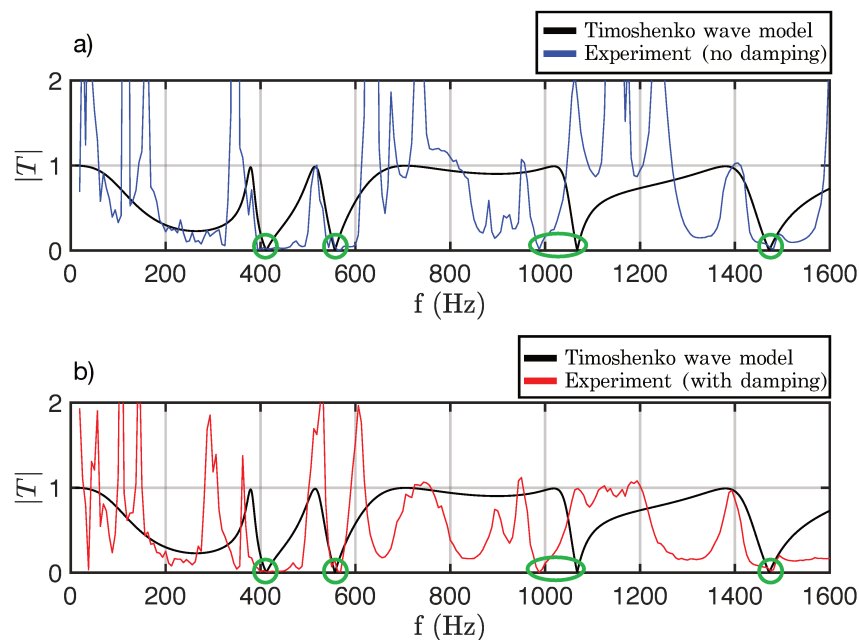


Fig. 5.7 Comparison of the transmission coefficient by Timoshenko wave model with a) experimental results without damping at the end, b) experimental results with damping at the end.

## 5.2 PERIODIC CHAIN OF HQ INSERTIONS FOR AXIAL WAVES

5.2.1 *Simple periodic chain configuration of HQ inserts for axial waves and its filtering performance*

The study of wave propagation in periodic structures has been extensively researched in acoustics [6, 56, 90–94]. This section deals mainly with longitudinal wave propagation in an infinite one-dimensional periodic model with a chain of HQ filters. The phenomenon of the destructive interference in such a periodic arrangement can be described by the Floquet theory, which predicts the existence of stop bands and the attenuation frequencies.

As was shown in previous chapters, HQ filtering effect is achievable in relatively narrow frequency ranges. On the other hand, the periodicity introduces stop bands, with their positions and widths determined by the impedance mismatch and traverse times ratio [56]. Therefore it is expedient to explore possible benefits of combining HQ and periodicity effects.

Fig.5.8 illustrates an example of periodic rods with multiple HQ filters.

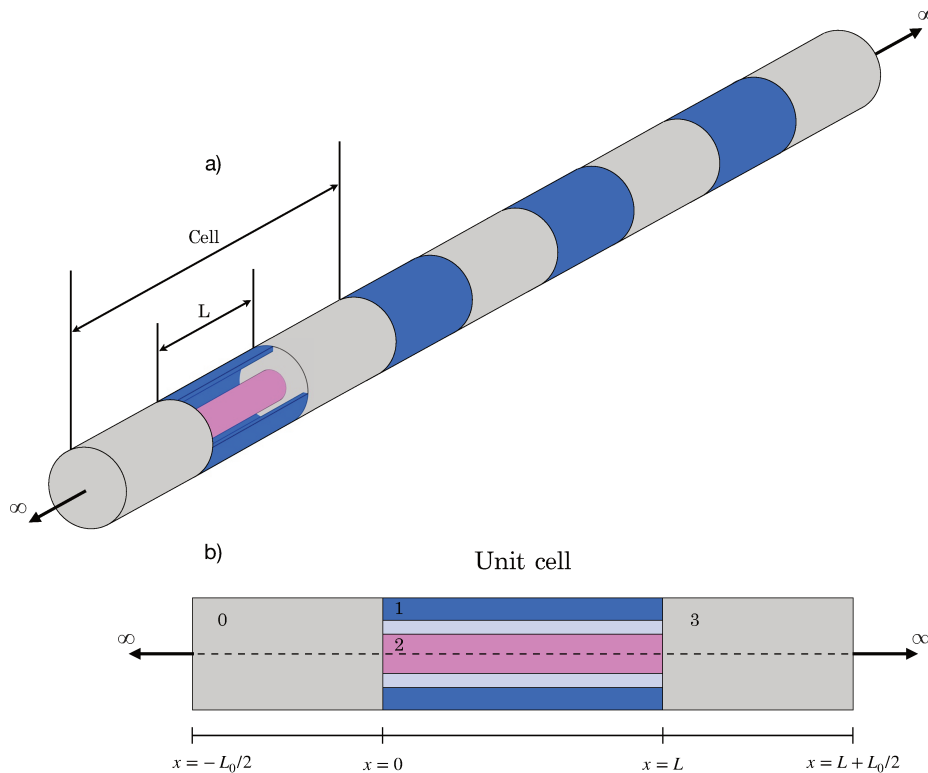


Fig. 5.8 a) Infinite periodic rod with HQ filters. b) Unit periodicity cell.

The whole rod can be regarded as an assembly of indential unit cells connected to each other. Each of these unit cells consists of several regional elements, which are made of different materials, similar to Fig.2.1.

To study wave propagation in an infinite periodic structure, it is sufficient to consider a unit periodicity cell. Its choice is not unique, but the most advantageous one is to consider a symmetric unit cell shown in Fig.5.8b.

In addition to the length  $L$  of a HQ insert, we introduce  $L_0$ , the distance between neighbouring inserts. Then a symmetric periodicity cell of the total length  $L_0 + L$  is located between  $x = -L_0/2$  and  $x = L + L_0/2$ .

### 5.2.2 Pass and stop bands in an infinite periodic structure

The solution ansatz remains defined as 2.2.1, and interfacial conditions are still formulated as 2.2.6, 2.2.7. Now we acknowledge existence of waves travelling in both directions in each segment, and set  $B_3 \neq 0$ . To complete the problem formulation, we introduce periodicity conditions as

$$u_0 \left( -\frac{L_0}{2} \right) = \Lambda u_3 \left( L + \frac{L_0}{2} \right), \quad (5.2.1a)$$

$$F_0 \left( -\frac{L_0}{2} \right) = \Lambda F_3 \left( L + \frac{L_0}{2} \right), \quad (5.2.1b)$$

where the propagation constant with the Bloch parameter  $K_B$  is

$$\Lambda = \exp(iK_B L), \quad (5.2.2)$$

Combining equation 5.2.1 with equations 2.2.6, 2.2.7, we obtain a system of eight homogeneous linear algebraic equations with respect to the wave amplitudes  $B_n, D_n, n = 0, 1, 2, 3$  (see Fig.2.1), it has a nontrivial solution when its determinant vanishes. This condition has a simple analytical form

$$\Lambda^2 + P\Lambda + 1 = 0, \quad (5.2.3)$$

where,

$$P = \frac{p_1}{\alpha_2 \beta_2 \sin(\alpha_1 \Omega L) + \alpha_1 \beta_1 \sin(\alpha_2 \Omega L)} \sin(2\Omega L_0) - \frac{p_2}{\alpha_2 \beta_2 \sin(\alpha_1 \Omega L) + \alpha_1 \beta_1 \sin(\alpha_2 \Omega L)} 2\cos(2\Omega L_0),$$

$$p_1 = -2\alpha_1\beta_1\alpha_2\beta_2 \left[ \cos(\alpha_2\Omega L)\cos(\alpha_1\Omega L) - 1 \right] + \left[ 1 + (\alpha_1\beta_1)^2 + (\alpha_2\beta_2)^2 \right] \sin(\alpha_2\Omega L)\sin(\alpha_1\Omega L),$$

$$p_2 = \alpha_2\beta_2\cos(\alpha_2\Omega L)\sin(\alpha_1\Omega L) + \alpha_1\beta_1\sin(\alpha_2\Omega L)\cos(\alpha_1\Omega L)$$

where the non-dimensional parameters are (see Chapter 2):

the frequency  $\Omega = \frac{\omega r_0}{c_0}$ ,

the ratio of sound velocities  $\alpha_n = \frac{c_0}{c_n}$ ,

the stiffness ratio  $\beta_n = \frac{E_n A_n}{E_0 A_0}$ ,

the scaled length  $L = \frac{L_{dim}}{r_0}$ .

Depending upon the sign of the discriminant  $P^2 - 4$ , roots of equation 5.2.3,  $\Lambda_{1,2}$ , are either purely real or complex conjugates. The former case defines stop bands, and the latter case, in which  $|\Lambda_1| = |\Lambda_2| = 1$ , defines pass bands. In pass bands, the Bloch parameter  $K_B$  is purely real. As expected, at the HQ zero transmission frequencies  $P \rightarrow \infty$  and an infinitely large attenuation is attained.

The resulting characteristic shown in Fig.5.9b displays module of the eigenvalues  $\Lambda$  as a function of the dimensionless frequency  $\Omega = \frac{\omega r_0}{c_0}$ . The dimensionless parameters were chosen as follows: the wave speed ratio between segments 0 and 1 as  $\alpha_1 = 3$ , and segments 0 and 2 as  $\alpha_2 = 0.3$ , the ratio of material characteristics  $\beta_1 = 0.5$  and  $\beta_2 = 1.5$ , scaled length of HQ insert  $L = 20$  and distance  $L + L_0/2 = 3L/4$ , respectively. This figure indicates that the periodic system with HQ filter has a pass band for  $|\Lambda| = 1$  and a stop band for  $|\Lambda| \neq 1$ . Accordingly, the wave is completely blocked within the stop band.

To ensure that the zero transmission frequencies at which destructive interference take place in HQ rod belong to the stop bands, the frequency dependence of the transmission coefficient of the forcing problem for a single HQ insert, described by equation 2.2.8, shown in Fig.5.9a. For  $0.075 < \Omega < 0.1$ , the zero transmission frequencies is within the stop bands and the wave decays rapidly due to the large value of  $|\Lambda|$ , as shown in 5.9b. In addition, the problem of narrowband attenuation is reduced to broadband attenuation as the periodicity effect captures other wide frequency ranges (stop bands).

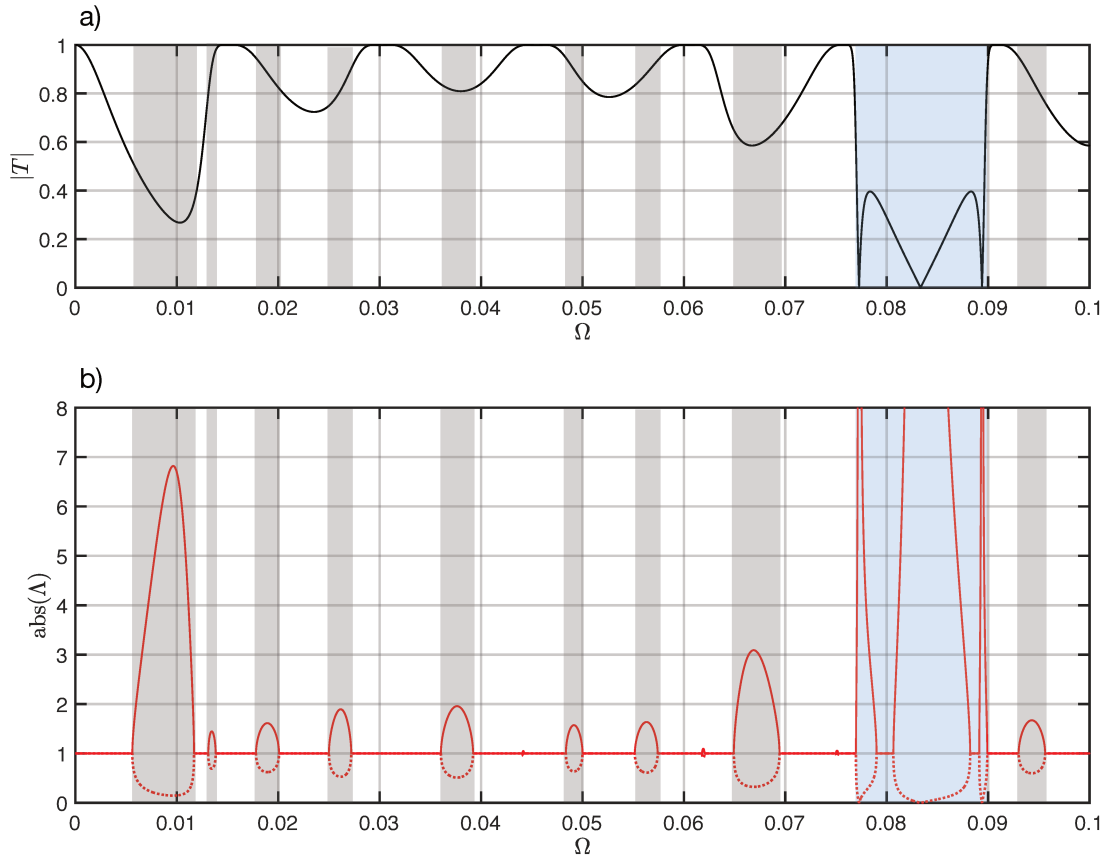


Fig. 5.9 a) Transmission coefficient of a single symmetric periodicity cell inserted into a uniform infinite structure at the wave speed ratio between segment 0 and 1  $\alpha_1 = 3$ , between segment 0 and 2  $\alpha_2 = 0.3$ , the ratio of material characteristics between segment 0 and 1  $\beta_1 = 0.5$ , between segment 0 and 2  $\beta_2 = 1.5$  and HQ length  $L_{HQ} = 20$ . b) Pass and stop bands (grey and blue stripes) of an infinite elastic periodic rod with HQ unit cell parameters  $L = 20$  and  $L_0 = L/2$ .

It should be observed that the transmission coefficient is calculated for a single HQ insert. Adding HQ inserts decreases the transmission coefficient in all stop band and keeps its magnitude virtually not affected in pass band.

### 5.2.3 Eigenfrequencies of a periodicity cell and stop-band boundaries

The relationship between the eigenfrequencies and the positions of the pass and stop bands of the periodic structure was demonstrated by D. Mead [95, 96]. In conventional periodic structures, the boundary between pass and stop bands coincide with eigenfrequencies of symmetric unit periodicity cells with class-consistent

boundary conditions [97, 98]. This property is used to check the accuracy of the solution of the Floquet equation 5.2.3.

The solution procedure for the eigenfrequency problem is similar to the one outlined in Section 5.2.2. For the cell shown in Fig.5.8 these two set of conditions are

$$\text{Class A: } u_0 \left( -\frac{L_0}{2} \right) = 0, \quad u_3 \left( L + \frac{L_0}{2} \right) = 0 \quad (5.2.4a)$$

$$\text{Class B: } F_0 \left( -\frac{L_0}{2} \right) = 0, \quad F_3 \left( L + \frac{L_0}{2} \right) = 0 \quad (5.2.4b)$$

When Class A boundary conditions replace periodicity conditions, and the determinant of the system of eight homogeneous linear algebraic equation 2.2.6, 2.2.7, 5.2.4a with respect to the wave amplitudes  $B_n, D_n, n=0, 1, 2, 3$  is equaled to zero, the eigenfrequency equation becomes

$$\begin{aligned} & 2\alpha_1\beta_1\alpha_2\beta_2 \left[ \cos(\alpha_2\Omega L) \cos(\alpha_1\Omega L) - 1 \right] \sin^2(\Omega L_0) \\ & + \sin(\alpha_2\Omega L) \sin(\alpha_1\Omega L) \left[ \cos^2(\Omega L_0) - \left( (\alpha_1\beta_1)^2 + (\alpha_2\beta_2)^2 \right) \sin^2(\Omega L_0) \right] \\ & + \left[ \alpha_2\beta_2 \cos(\alpha_2 L \Omega) \sin(\alpha_1 L \Omega) + \alpha_1\beta_1 \cos(\alpha_1 L \Omega) \sin(\alpha_2 L \Omega) \right] \sin(2L_0\Omega) = 0 \end{aligned} \quad (5.2.5a)$$

For the Class B boundary conditions, the eigenfrequencies equation is

$$\begin{aligned} & \cos^2(L_0\Omega) \left[ -2\alpha_1\beta_1\alpha_2\beta_2 \left( \cos(\alpha_2\Omega L) \cos(\alpha_1\Omega L) - 1 \right) \right. \\ & + \left. \left( \alpha_1^2\beta_1^2 + \alpha_2^2\beta_2^2 \right) \sin(\alpha_2\Omega L) \sin(\alpha_1\Omega L) \right] + \alpha_1\beta_1 \cos(\alpha_1\Omega L) \sin(\alpha_2\Omega L) \sin(2\Omega L_0) \\ & + \sin(\alpha_1\Omega L) \left[ -\sin(\alpha_2\Omega L) \sin^2(\Omega L_0) + \alpha_2\beta_2 \cos(\alpha_2\Omega L) \sin(2\Omega L_0) \right] = 0 \end{aligned} \quad (5.2.5b)$$

The eigenfrequencies  $\Omega_n$  of Class A and Class B in the range  $0.076 < \Omega < 0.1$  are presented in the Table.5.2. These eigenfrequencies coincide with the borders between the pass and stop bands in Fig.5.9. Therefore, the solution of the Floquet equation 5.2.3 predicts the same frequencies at the borders between pass and stop bands as the eigenfrequencies described by the equations 5.2.5.

	$\Omega_n$			
<b>Class A</b>	0.077	0.088	0.089	0.096
<b>Class B</b>	0.079	0.08	0.09	0.093

Table 5.2 Eigenfrequencies of a symmetric unit cell at the wave speed ratio between segments 0 and 1  $\alpha_1 = 3$ , between segments 0 and 2  $\alpha_2 = 0.3$ , the ratio of material characteristic between segments 0 and 1  $\beta_1 = 0.5$ , between segments 0 and 2  $\beta_2 = 1.5$ , the scaled length  $L = 20$  and for the frequency range  $0.076 < \Omega < 0.1$ .

Fig.5.10a shows the eigenfrequencies of a symmetric unit cell dependence on the wave speed ratio between segments 0 and 1,  $\alpha_1$ , when the wave speed ratio between segments 0 and 2 is  $\alpha_2 = 1$ , and the difference in material parameters between each segment can be set as  $\beta_1 = 1.5$ ,  $\beta_2 = 0.2$ , the length  $L = 20$  and distance  $L + L_0/2 = 3L/4$ . The eigenfrequency problem of Class A and Class B is solved by using frequency sweep. The 'grey fill' in Fig.5.10a,b and the red dots of Class A and Class B in Fig. 5.10b depict the location of the stop bands. The zero transmission frequencies, which is defined by the equation 2.2.15 from Chapter 2, are also shown in Fig.5.10a,b (green line), in order to demonstrate their link with the stop bands.

As  $\alpha_1$  increases, the stop band shifts toward low frequencies and the size of the width of the stop band also changes. The zero transmission frequencies lie within the stop band around  $\Omega = 0.025$ ,  $\Omega = 0.05$ ,  $\Omega = 0.075$ ,  $\Omega = 0.01$  and by analogy with Fig.2.5 we can find that for any integer values of  $\alpha_1 = 1, 2, 3, \dots$  at  $\alpha_2 = 1$ , the zero transmission frequency can be defined as  $\sin(\alpha\Omega L) = 0$  (see Chapter 2).

The values of  $|\Lambda|$ , described by the Floquet equation 5.2.3, or pass and stop bands for different values of sound velocity between segments 0 and 1,  $\alpha_1$ , are presented in Fig.5.10c. At  $\alpha = 2.6$  the stop bands which is associated with the zero transmission frequencies is clearly defined. For any integer values  $\alpha_1 = 1, 2, 3, \dots$  there are isolated frequencies at which the stop band has zero width, which corresponds to the black dashed line in 5.10c (see Fig.5.10b green dot of Class A and Class B), which is consistent with the case of the trapped mode as discussed in Chapter 2.

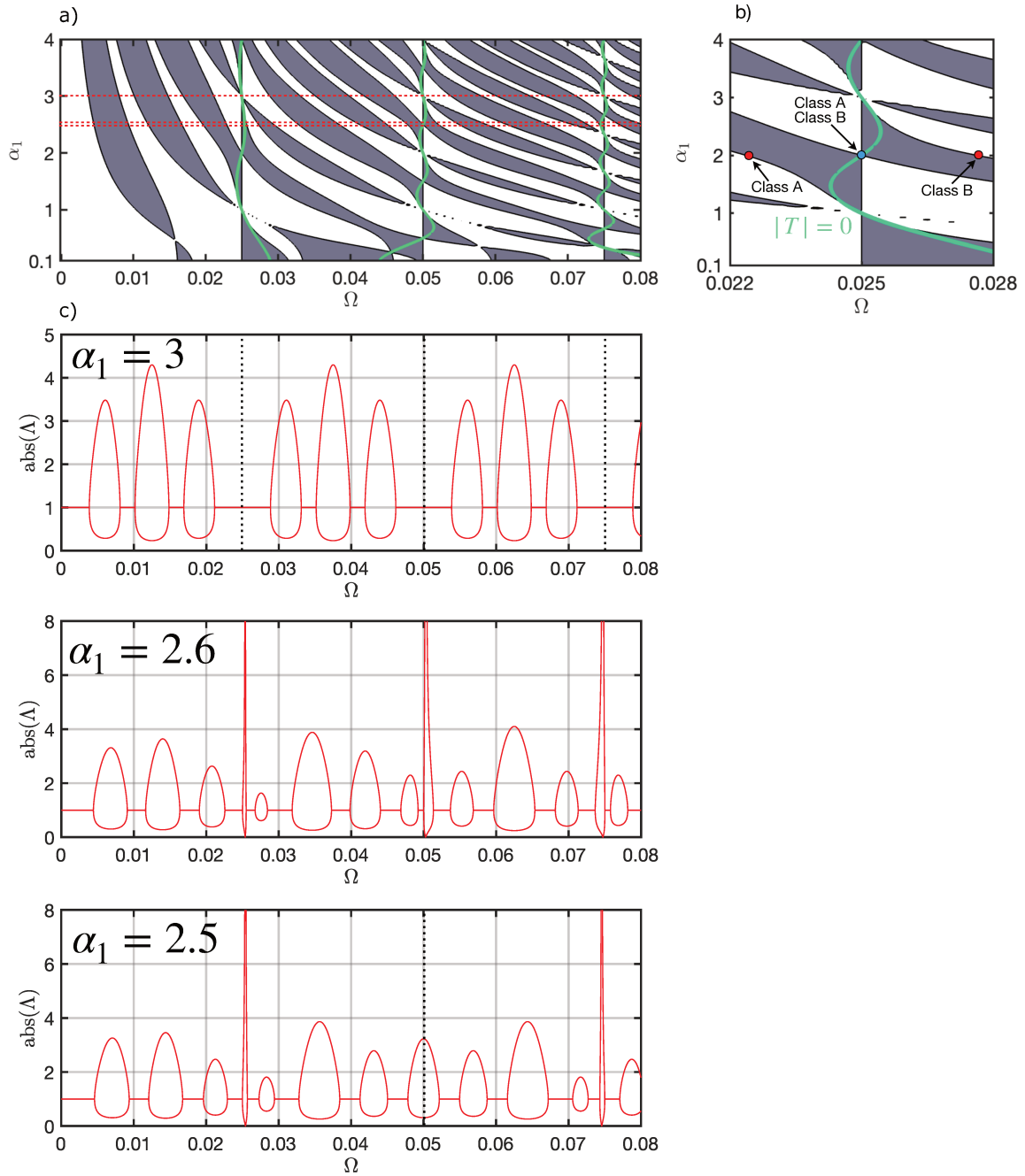


Fig. 5.10 a) Eigenfrequencies of a symmetric unit cell (black outline of the grey area) dependence on the wave speed ratio between segments 0 and 1  $\alpha_1$  with zero transmission frequencies (green line) at the wave speed ratio between segments 0 and 2  $\alpha_2 = 1$ , the ratio of material characteristics between segments 0 and 1  $\beta_1 = 1.5$ , between segments 0 and 2  $\beta_2 = 0.2$ , and scaled length of the unit HQ filter  $L = 20$ . b) Zoomed-in view of stop band borders (points of boundaries of Class A and Class B) at  $\alpha_1 = 2$  for  $0.022 < \Omega < 0.028$  c) Pass and stop bands of an elastic periodic rod with HQ filter for  $\alpha_1 = 3$ ,  $\alpha_1 = 2.6$ ,  $\alpha_1 = 2.5$ .

## 5.3 CONCLUSION

Different HQ configurations have been considered in order to improve its efficiency. For the bending waves, serial, parallel, and mixed arrangements were proposed. Indeed, all these configurations offer benefits in enhancing the vibroacoustic properties of the HQ filter. The results showed that increasing the number of branches or the number of single HQ filters can lead to an increased number of dips in the transmission coefficient due to the effect of the auxiliary branches. For the serial arrangement, the tunneling effect was observed in which evanescent waves can disturb the zero transmission frequency.

The experimental demonstration of the parallel arrangement has shown that at certain frequencies there is an effect of destructive interference at which there is no energy transfer at the end of the beam as in the Timoshenko wave model. However, at some frequencies there is a discrepancy with the Timoshenko wave model, which is due to the accuracy of the experiment and the effect of the longitudinal waves.

The periodic chain for axial waves in rods showed that the periodic effect can be enhanced by using an HQ filter. Namely, the zero transmission frequencies of the single HQ insert coincides with the stop band boundaries of the periodic rod. The periodic configuration with the HQ filter can transform the problem of narrowband frequency vibration attenuation of the HQ filter into broadband frequency vibration attenuation.

---

## CONCLUSIONS AND PERSPECTIVES

---

The main objective of this thesis was to investigate the HQ filter for the attenuation of elastic bending waves in mechanical structures such as rods, beams, and plates. The first examples of the adaptation of such a device were applied in acoustic ducts, where vibration mitigation occurs due to the difference in path length between two tubes, causing destructive interference at particular frequencies. In this thesis, by analogy with the acoustic counterpart, we have used the same destructive interference effect in beams and plates, where the energy canceling effect at the output of HQ device can be obtained by the difference in thickness of two parallel HQ branches.

The thesis has been written in order to analyze in detail the application of HQ filter for solid elastic structures, namely starting from simple cases based on the consideration of axial waves in rods, where three typical formulations of HQ filter analysis are proposed, to more complex cases, when bending and longitudinal waves occur simultaneously in the HQ device. The general conclusion of this thesis will be presented below.

### 6.1 CONCLUSIONS

#### *HQ filter for non-dispersive elastic waves*

In this thesis, we have firstly formulated three problems to calculate the filtering properties of HQ filter: unit amplitude incoming wave problem, forced problem and zero transmission frequency problem. All these problems agree well and give the same frequencies at which the destructive interference effect of HQ filter occurs.

We have derived a straightforward equation for the zero transmission frequencies of axial waves in HQ rods, solely based on the wave velocity and the stiffness

of the segments. This equation applies universally to any HQ waveguide system involving elastic longitudinal or torsional waves, where differences in velocities and stiffnesses between segments dictate transmission characteristics. Unlike methods relying on force equations or continuity conditions, this approach simplifies the analysis. Furthermore, our investigation of zero transmission frequencies extends beyond longitudinal waves to include bending waves. This broader perspective enhances our understanding and application of wave propagation phenomena in diverse structural configurations.

#### *HQ filter for flexural waves*

The HQ filter has been studied for its application to bending waves in beams and plates. At specific frequencies, the difference in bending wave speeds between the two HQ branches can create a zero transmission effect. This phenomenon arises from the destructive interference of these waves at the interfaces between components of HQ device. Computations of the reflection coefficient  $R$  and transmission coefficient  $T$  of the bending waves in beams and plate have been done semi-analytically (using a wave model based on Timoshenko theory for beams and Kirchhoff-Love theory for plate), numerically (using the finite element code in Comsol software package), and experimentally (using a 3D scanning laser vibrometer).

In analyzing the energy flow, we have demonstrated the coexistence of two modes of wave motion. In certain frequency ranges, it is unidirectional in both segments, while in other ranges energy fluxes are in opposite directions with the net flux always remaining non-negative. The frequencies, which separate these ranges, are the zero transmission frequencies. They define the formation of a standing wave in the whole beam.

We have considered a link between the zero transmission frequency problem and eigenfrequencies. The zero transmission frequencies are close to the real part of the eigenfrequencies of the HQ modes for which the two HQ branches move in out-of-phase.

Parametric variations have been carried out to show how the zero transmission frequencies and hence the performance of the HQ filter can be controlled.

This dissertation also demonstrated the effectiveness of HQ filter in plates. The analysis of the problem with zero transmission frequencies revealed the same effect of the out-of-phase between the two HQ branches leading to standing waves as in the beam problem. It was obtained that the dominant mode at which destructive

interference effects occur in HQ plate is the axisymmetric oscillations for  $n = 0$ . The energy flux analysis also confirmed this hypothesis. The Insertion Loss analysis then revealed an amplification problem in which the energy flux in the HQ plate becomes greater than in a uniform plate at certain frequencies. As a result, this problem is associated with an external force acting on the centre of coordinates, where the energy flux is directly related to how much energy has been injected. The analysis of the HQ sandwich panel showed that the filtering effect of the HQ can be achieved not only by the difference in thickness between the two HQ branches, but also by changing the characteristics of the elastic modulus or stiffness of one of the skins. Hence, the results showed that the small contrast in elastic moduli between the two branches leads to zero transmission frequency. The effect of the core in the HQ zone of the sandwich panel also revealed that its elastic modulus characteristic should be much lower than that of the two HQ branches in order to achieve zero transmission frequencies.

Various configurations of the HQ filter have been proposed to enhance its efficiency, including serial, parallel, and mixed arrangements. Increasing the number of branches or single HQ filters within these configurations can increase the number of dips observed in the transmission coefficient, attributed to the influence of auxiliary branches. Moreover, employing an HQ filter in a periodic chain configuration for axial waves in rods enhances periodic effects. Specifically, the zero transmission frequency of a single HQ insert lies at the stop band boundaries, effectively transforming narrowband frequency vibration attenuation into broadband frequency attenuation.

## 6.2 PERSPECTIVES

This thesis addresses the problem of vibration mitigation using an HQ filter. However, a limitation arises due to the attenuation in the narrow frequency band of the HQ filter, potentially constraining its effectiveness. To enhance the vibration properties of HQ filters, various methods can be proposed. For instance, microstructures with periodic architectures can complement HQ filters. Additionally, as discussed in this thesis, configuring HQ filters with a greater number of branches can introduce more transmission dips, thereby improving isolation over a broader bandwidth, provided that the dimensions of the branches are carefully adjusted.

An illustrative design procedure is depicted in Fig.6.1, [99]. Utilizing a hollow beam with numerous slender branches on the sides seems promising due to its favorable strength-to-weight ratio and structural efficiency in achieving effective filtering properties with HQ devices. Notably, opting for a higher number of thin branches in a hollow beam can significantly influence the transmission coefficient by utilizing resonance effects of each branch to create destructive interference effect at certain frequencies.

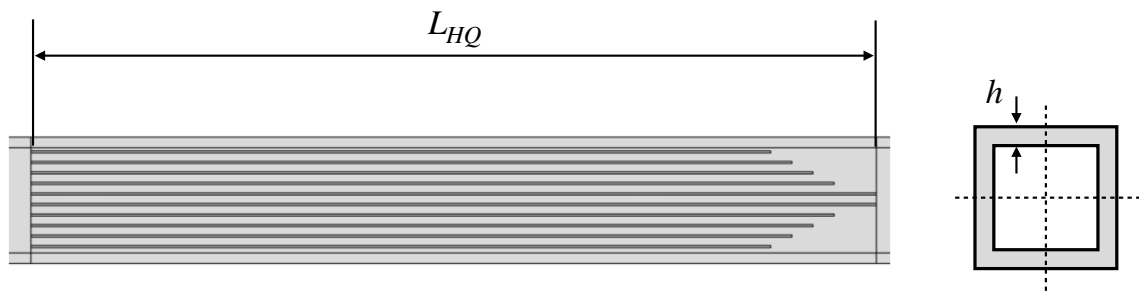


Fig. 6.1 Profile of the hollow HQ beam [99].

Optimization of the parallel configuration can also be extended and continued, for example, branches with variable heights ('arch') can be modeled and then its size tuned to specific frequency regions.

Further advances in this work can be based on the analysis of a sandwich panel with a honeycomb core and an embedded HQ filter. Due to their light weight and high stiffness, sandwich structures are widely used in practice. However, they can have poor acoustic properties, making HQ filters an interesting solution for the vibration problem of sandwich panels. This optimization requires a good understanding of the analysis of sandwich structures. The first step may involve the use and implementation of the Mindlin plate theory, which takes into account the effect of shear deformation. Additionally, the bending stiffness parameter of the sandwich panel, which can be strongly frequency dependent, should be considered in detail [100–104]. The obtained results of the HQ filter in a sandwich plate should demonstrate the same effect of destructive interference at a certain frequency, as in the Kirchhoff-Love plate analysis. An important aspect in the analysis of 2D plates can also be the study of the radiation of plates with HQ filter.

---

## REFERENCES

---

- [1] I.L. Vér and L.L. Beranek, editors. *Noise and vibration control engineering: principles and applications*. Wiley, Hoboken, N.J, 2nd ed edition, 2006.
- [2] D.A. Bies, C.H. Hansen, and C.Q. Howard. *Engineering noise control*. CRC Press, Taylor & Francis Group, Boca Raton, fifth edition edition, 2018.
- [3] L. L. Beranek and T. J. Mellow. *Acoustics: sound fields, transducers and vibration*. Academic Press, London [England], second edition edition, 2019.
- [4] D.J. Inman. *Engineering vibration*. Pearson, Boston, fourth edition edition, 2014.
- [5] M. L. Munjal. *Noise and vibration control*. Number volume 3 in IISc lecture notes series. World Scientific, New Jersey, 2013.
- [6] A. Baz. *Active and passive vibration damping*. Wiley, Hoboken, NJ, 2019.
- [7] P. Hagedorn, editor. *Active and passive vibration control of structures*. Number 558 in Courses and lectures / International Centre for Mechanical Sciences. Springer, Wien, 2014.
- [8] A. Nashif, D. Jones, and J. Henderson. *Vibration damping*. New York: Wiley., 1985.
- [9] C. Vemula, A.N. Norris, and G.D. Cody. Attenuation of waves in plates and bars using a graded impedance interface at edges. *Journal of Sound and Vibration*, 196(1):107–127, September 1996.
- [10] J. Leng. Controlling flexural waves using subwavelength perfect absorbers: Application to acoustic black holes. *These de doctorat, Le Mans*, 2019.
- [11] G. Raybaud, A. Pelat, M. Ouisse, and F. Gautier. Zero reflections by a 1D Acoustic Black Hole termination using thermally controlled damping. *Journal of Sound and Vibration*, 510:116282, October 2021.
- [12] O. Aklouche. Réduction des niveaux vibratoires d'un panneau au moyen de trous noirs acoustiques structurés en réseau périodique : conception d'une méta-plaque. *These de doctorat, Le Mans*, 2017.
- [13] H. Frahm. Device for damping vibrations of bodies. *US Patent 989,958*, April 18 1911.
- [14] C. Liang and C.A. Rogers. Design of Shape Memory Alloy Springs With Applications in Vibration Control. *Journal of Vibration and Acoustics*.
- [15] V. Birman. Review of Mechanics of Shape Memory Alloy Structures. *Applied Mechanics Reviews*, 50(11):629–645, November 1997.

- [16] S. Saadat, J. Salichs, M. Noori, Z. Hou, H. Davoodi, I. Bar-on, Y. Suzuki, and A. Masuda. An overview of vibration and seismic applications of NiTi shape memory alloy. *Smart Materials and Structures*, 11(2):218–229, April 2002.
- [17] H. Sheng, M.-X. He, J. Zhao, C.T. Kam, Q. Ding, and H.P. Lee. The ABH-based lattice structure for load bearing and vibration suppression. *International Journal of Mechanical Sciences*, 252, August 2023.
- [18] J. Guo, Y. Xiao, H. Ren, H. Chen, D. Yu, and J. Wen. Broadband low-frequency sound insulation of double-panel metastructures with a perforated lattice truss-core sandwich plate. *Mechanical Systems and Signal Processing*, 200:110634, October 2023.
- [19] H. Wadley. Fabrication and structural performance of periodic cellular metal sandwich structures. *Composites Science and Technology*, 63(16):2331–2343, December 2003.
- [20] A.G. Evans, J.W. Hutchinson, N.A. Fleck, M.F. Ashby, and H.N.G. Wadley. The topological design of multifunctional cellular metals. *Progress in Materials Science*, 46(3-4):309–327, January 2001.
- [21] V.S. Deshpande, N.A. Fleck, and M.F. Ashby. Effective properties of the octet-truss lattice material. *J. Mech. Phys. Solids*, 2001.
- [22] R.V. Craster and S. Guenneau, editors. *Acoustic Metamaterials: Negative Refraction, Imaging, Lensing and Cloaking*, volume 166 of *Springer Series in Materials Science*. Springer Netherlands, Dordrecht, 2013.
- [23] J.F.W. Herschel. LXIII. *On the absorption of light by coloured media, viewed in connexion with the undulatory theory*. *The London, Edinburgh, and Dublin Philosophical Magazine and Journal of Science*, 3(18):401–412, December 1833.
- [24] G. Quincke. Ueber interferenzapparate fur schallwellen. *Applied Acoustics*, 128:177–192, 1866.
- [25] G.W. Stewart. The Theory of the Herschel-Quincke Tube. *Physical Review*, 31(4):696–698, 1928.
- [26] G.W. Stewart. The Theory of the Herschel-Quincke Tube. *The Journal of the Acoustical Society of America*, 17(2):107, 1945.
- [27] A. Selamet, N. S. Dickey, and J. M. Novak. The Herschel–Quincke tube: A theoretical, computational, and experimental investigation. *The Journal of the Acoustical Society of America*, 96(5):3177–3185, November 1994.
- [28] A. Selamet and V. Easwaran. Modified Herschel–Quincke tube: Attenuation and resonance for n-duct configuration. *The Journal of the Acoustical Society of America*, 102(1):164–169, July 1997.
- [29] J.M. Desantes, A.J. Torregrosa, H. Climent, and D. Moya. Acoustic performance of a Herschel–Quincke tube modified with an interconnecting pipe. *Journal of Sound and Vibration*, 284(1-2):283–298, June 2005.

- [30] A.J. Torregrosa, A. Broatch, H. Climent, and D. Moreno. Acoustic performance of Herschel-Quincke tubes with gradually variable cross-section ducts. *Noise Control Engineering Journal*, 57(1):16, 2009.
- [31] A.J. Torregrosa, A. Broatch, and R. Payri. A study of the influence of mean flow on the acoustic performance of Herschel-Quincke tubes. *The Journal of the Acoustical Society of America*, 107(4):1874–1879, April 2000.
- [32] M. Karlsson, R. Glav, and M. Åbom. The Herschel-Quincke tube: The attenuation conditions and their sensitivity to mean flow. *The Journal of the Acoustical Society of America*, 124(2):723–732, August 2008.
- [33] Z. Zhichi, Li Song, T. Rui, G. Rui, D. Genhua, and Li Peizi. Application of Quincke tubes to flow ducts as a sound attenuation device. *Noise Control Engineering Journal*, 46(6):245, 1998.
- [34] S.N. Panigrahi and M.L. Munjal. Plane wave propagation in generalized multiply connected acoustic filters. *The Journal of the Acoustical Society of America*, 118(5):2860–2868, November 2005.
- [35] J.S. Alonso, R.A. Burdisso, D. Ivers, and Hwa W. Kwan. Adaptive Concepts for Herschel-Quincke Waveguides. *Journal of Vibration and Acoustics*, 135(3):031016, June 2013.
- [36] S. Griffin, S. Huybrechts, and S.A. Lane. An adaptive Herschel-Quincke tube. *Journal of Intelligent Material Systems and Structures*, 1999.
- [37] R.F. Hallez. Investigation of the Herschel-Quincke Tube Concept as a Noise Control Device for Turbofan Engines. *PhD thesis, Virginia Tech*, 2001.
- [38] R.A. Burdisso and F.Ng Wing. Fan Noise Control Using Herschel-Quincke Resonators. *Prepared under Grant NAG3-2694*, 2003.
- [39] J.P. Smith and R.A. Burdisso. Experimental Investigation of the Herschel-Quincke Tube Concept on the Honeywell TFE731-60. *Langley Research center under Grant NAG1-2137*, 2002.
- [40] D.H. de la Riva. Modeling of herschel/quincke-liner systems for the control of aft fan radiation in turbofan engines. *PhD thesis, Virginia Tech*, 2006.
- [41] L. Brady. Application of the Herschel-Quincke Tube Concept to Higher-Order Acoustic Modes in Two-Dimensional Ducts.
- [42] B. Poirier, C. Maury, and J.-M. Ville. The use of Herschel-Quincke tubes to improve the efficiency of lined ducts. *Applied Acoustics*, 72(2-3):78–88, February 2011.
- [43] B. Poirier, J.-M. Ville, C. Maury, and D. Kateb. Bicylindrical model of Herschel-Quincke tube-duct system: Theory and comparison with experiment and finite element method. *The Journal of the Acoustical Society of America*, 126(3):1151–1162, September 2009.

- [44] Z.B. Wang, Y.K. Chiang, Y.S. Choy, C.Q. Wang, and Q. Xi. Noise control for a dipole sound source using micro-perforated panel housing integrated with a Herschel–Quincke tube. *Applied Acoustics*, 148:202–211, May 2019.
- [45] R. Haworth, R. McLean, and Z. Vanderveen, K.and Xia. (76) Inventors: Paul Desmond Daly, Troy, MI (US);.
- [46] T. Lato. Passive Damping Mechanism of Herschel-Quincke Tubes for Pressure Pulsations in Piping Systems. *PhD thesis, Ontario Tech University*, 2018.
- [47] T. Lato and A. Mohany. Passive damping of pressure pulsations in pipelines using Herschel-Quincke tubes. *Journal of Sound and Vibration*, 448:160–177, May 2019.
- [48] Da-Y. Kim, J.-G. Ih, and M. Åbom. Virtual Herschel-Quincke tube using the multiple small resonators and acoustic metamaterials. *Journal of Sound and Vibration*, 466:115045, February 2020.
- [49] T. K. Papathanasiou, E. Tsolakis, V. Spitas, and A. B. Movchan. The Herschel-Quincke tube with modulated branches. *Philosophical Transactions of the Royal Society A: Mathematical, Physical and Engineering Sciences*, 380(2237), November 2022.
- [50] D. Mead. *Passive Vibration Control*. John Wiley & Sons.
- [51] E. Shoavi. Reduction of Vibration transmission by destructive interference. *Ph.D. thesis, The University of Auckland*.
- [52] Y.-H. Kim. *Sound propagation: an impedance based approach*. Wiley, Singapore ; Hoboken, NJ, 2010.
- [53] F. W. J. Olver, D. W. Lozier, R. F. Boisvert, and C. W. Clark. *NIST handbook of mathematical functions*. Cambridge University Press, Cambridge New York Melbourne, 2010.
- [54] V. Pagneux. Trapped Modes and Edge Resonances in Acoustics and Elasticity.
- [55] J.D. Kaplunov and S.V. Sorokin. A simple example of a trapped mode in an unbounded waveguide. *The Journal of the Acoustical Society of America*, 97(6):3898–3899, June 1995.
- [56] R.B. Nielsen and S.V. Sorokin. Periodicity effects of axial waves in elastic compound rods. *Journal of Sound and Vibration*, 353:135–149, September 2015.
- [57] C. Mei and B.R. Mace. Wave Reflection and Transmission in Timoshenko Beams and Wave Analysis of Timoshenko Beam Structures. *Journal of Vibration and Acoustics*, 127(4):382–394, August 2005.
- [58] S.V. Sorokin. Wave propagation in solids and structures. *Lecture Notes for Day 2, Department of Mechanical and Manufacturing Engineering, Aalborg University*.

- [59] B.R. Mace. Wave reflection and transmission in beams. *Journal of Sound and Vibration*, 97(2):237–246, November 1984.
- [60] C.L. Dym and I.H. Shames. *Solid Mechanics: A Variational Approach, Augmented Edition*. Springer New York, New York, NY, 2013.
- [61] F. Fahy and P. Gardonio. *Sound and structural vibration: radiation, transmission and response*. Elsevier/Academic, Amsterdam ; Boston, 2nd ed edition, 2007.
- [62] M.-H. Moulet J.-C. Pascal Gautier, F. Reflection, Transmission and Coupling of Longitudinal and Flexural Waves at Beam Junctions. Part I: Measurement Methods. *Acta Acustic United with Acustica*, 92, 2006.
- [63] L. Cremer, M. Heckl, and B. A. T. Petersson. *Structure-borne sound: structural vibrations and sound radiation at audio frequencies*. Springer, Berlin ; New York, 3rd ed edition, 2005.
- [64] S.S. Rao. *Vibration of continuous systems*. Wiley, Hoboken, NJ, 2007.
- [65] B. Yang. *Stress, strain, and structural dynamics: an interactive handbook of formulas, solutions, and MATLAB toolboxes*. Elsevier Academic Press, Amsterdam Boston, Mass, 2005.
- [66] A.W. Leissa. *Vibration of plates*. Office of Technology Utilization National Aeronautics and Space Administration, Ohio State University, Columbus, Ohio, 1969.
- [67] J.-L. Guyader. *Vibration in continuous media*. ISTE, Newport Beach, CA, 2006.
- [68] M. Geradin. *Mechanical Vibrations*.
- [69] N.W. McLachlan. *Bessel Functions for Engineers*. Oxford Engineering science series, Oxford University, London, 1934.
- [70] B.G. Korenev. *Bessel Functions and their Applications*. An International Series of Monographs in Mathematics, 2002.
- [71] W. Soedel. *Vibrations of Shells and Plates*. A Series of textbooks and References Books, Purdue University, Indiana, 2005.
- [72] S. Woinowsky-Krieger S. Timoshenko. *Theory of Plate and Shells*. Engineering Societies monographs, 1989.
- [73] E. Ventsel and T. Krauthammer. *Thin plates and shells: theory, analysis, and applications*. Dekker, New York Basel, 2001.
- [74] V. Birman. *Plate Structures*, volume 178 of *Solid Mechanics and Its Applications*. Springer Netherlands, Dordrecht, 2011.
- [75] F. Fahy. *Foundations of engineering acoustics*. Academic, San Diego, Calif. ; London, 2001.

- [76] S. Giani and H. Hakula. Free vibration of perforated cylindrical shells of revolution: Asymptotics and effective material parameters. *Computer Methods in Applied Mechanics and Engineering*, 403:115700, January 2023.
- [77] T. Slot and W. J. O'Donnell. Effective Elastic Constants for Thick Perforated Plates With Square and Triangular Penetration Patterns. *Journal of Engineering for Industry*, 93(4):935–942, November 1971.
- [78] J. P. Duncan and R. W. Upfold. Equivalent Elastic Properties of Perforated Bars and Plates. *Journal of Mechanical Engineering Science*, 5(1):53–65, March 1963.
- [79] W.J. O'Donnell and B.F. Langer. Design of Perforated Plates. *Journal of Engineering for Industry*, 84(3):307–319, August 1962.
- [80] M. Forskitt, J.R. Moon, and P.A. Brook. Elastic properties of plates perforated by cusp-shaped holes. *Applied Mathematical Modelling*, 15(4):191–199, April 1991.
- [81] M. Forskitt, J.R. Moon, and P.A. Brook. Elastic properties of plates perforated by elliptical holes. *Applied Mathematical Modelling*, 15(4):182–190, April 1991.
- [82] K.A. Burgemeister and C.H. Hansen. Calculating Resonance Frequencies of Perforated Panels.
- [83] P.Meijers. Doubly-periodic stress distributions in perforated plates. 1967.
- [84] H. Li, P. O'Donoghue, F. Masson, A. Pelat, F. Gautier, and C. Touzé. Broad-band shock vibration absorber based on vibro-impacts and acoustic black hole effect. *International Journal of Non-Linear Mechanics*, 159:104620, March 2024.
- [85] M. Rebillat and X. Boutillon. Identification of honeycomb sandwich properties by high-resolution modal analysis. *EPJ Web of Conferences*, 6:41005, 2010.
- [86] S.A. Hambric. Structural Acoustics Tutorial—Part 1: Vibrations in Structures. *Acoustics Today*, 2(4):21, 2006.
- [87] A. Hvatov and S. Sorokin. A simple example of the tunnelling effect in periodic elastic structures. *European Journal of Mechanics - A/Solids*, 100:104807, July 2023.
- [88] R.B. Nielsen and N. Peake. Tunnelling effects for acoustic waves in slowly varying axisymmetric flow ducts. *Journal of Sound and Vibration*, 380:180–191, October 2016.
- [89] M.-H. Moulet. Les jonctions en mécanique vibratoire: représentation par matrice de diffusion et caractérisation expérimentale pour des poutres assemblées. *Thèse de doctorat, L'Université du Maine*, 2003.
- [90] D.J. Mead. Free wave propagation in periodically supported, infinite beams. *Journal of Sound and Vibration*, 11(2):181–197, February 1970.

- [91] D.M. Mead. Wave Propagation in continuous periodic structures: research contributions from Southampton, 1964–1995. *Journal of Sound and Vibration*, 190(3):495–524, February 1996.
- [92] A. Hvatov and S. Sorokin. Free vibrations of finite periodic structures in pass- and stop-bands of the counterpart infinite waveguides. *Journal of Sound and Vibration*, 347:200–217, July 2015.
- [93] A. Hvatov and S. Sorokin. Assessment of reduced-order models in analysis of Floquet modes in an infinite periodic elastic layer. *Journal of Sound and Vibration*, 440:332–345, February 2019.
- [94] L. Brillouin. Wave Propagation in Periodic Structures. *second ed. Dover Publications, New York*, 1946.
- [95] D.J. Mead. Wave propagation and natural modes in periodic systems: II. Multi-coupled systems, with and without damping. *Journal of Sound and Vibration*, 40(1):19–39, May 1975.
- [96] D.J. Mead. Wave propagation and natural modes in periodic systems: I. Mono-coupled systems. *Journal of Sound and Vibration*, 40(1):1–18, May 1975.
- [97] L.S. Ledet and S.V. Sorokin. On the application of bi-orthogonality relations for analysis of linear dynamic systems. *Journal of Sound and Vibration*, 465:115020, January 2020.
- [98] S.V. Sorokin, F. Gautier, and A. Pelat. A hierarchy of models of axisymmetric wave propagation in a fluid-filled periodic cylindrical shell composed of high-contrast cells. *Mechanical Systems and Signal Processing*, 136:106487, February 2020.
- [99] D. Franchi, A. Pelat, F. Gautier, and S. Avetisov. Herschel quincke filter in hollow beams - research and correlation with simple beams. *Master's thesis, Le Mans*, 2024.
- [100] M.N. Ichchou, O. Bareille, and J. Berthaut. Identification of effective sandwich structural properties via an inverse wave approach. *Engineering Structures*, 30(10):2591–2604, October 2008.
- [101] S.V. Sorokin and N. Peake. Vibrations of sandwich plates with concentrated masses and spring-like inclusions. *Journal of Sound and Vibration*, 237(2):203–222, October 2000.
- [102] A.C. Nilsson and B. Liu. Prediction of some vibro-acoustic properties of sandwich plates with honeycomb and foam cores. *The Journal of the Acoustical Society of America*, 144(3):1600–1614, September 2018.
- [103] E. Nilsson and A.C. Nilsson. Prediction and measurement of some dynamic properties of sandwich structures with honeycomb and foam cores. *Journal of Sound and Vibration*, 251(3):409–430, March 2002.
- [104] A. Nilsson, S. Baro, and E.A. Piana. Vibro-acoustic properties of sandwich structures. *Applied Acoustics*, 139:259–266, October 2018.

# A

---

## A.1 DYNAMIC MATRIX SIMULATION

The continuity and equilibrium equations can be written in the matrix form  $\Phi = \mathbf{M}\Lambda$  where  $\Phi$  and  $\Lambda$  are defined by Eqs.3.1.8 and 3.1.9, and where  $\mathbf{M}$  is detailed as follows :

$$\mathbf{M} = \begin{bmatrix} M_1 & M_2 & M_3 & M_4 & M_5 & M_6 \\ M_7 & M_8 & M_9 & M_{10} & M_{11} & M_{12} \\ M_{13} & M_{14} & M_{15} & M_{16} & M_{17} & M_{18} \end{bmatrix},$$

with

$$\mathbf{M}_1 = \begin{bmatrix} -1 & -1 & 1 \\ -1 & -1 & 0 \\ -N_{12} & -N_{14} & N_{21} \\ -N_{12} & -N_{14} & 0 \\ -EI_1N_{12}k_{12} & -EI_1N_{14}k_{14} & EI_2N_{21}k_{21} \\ -\kappa GS_1(k_{12} - N_{12}) & -\kappa GS_1(k_{14} - N_{14}) & \kappa GS_2(k_{21} - N_{21}) \end{bmatrix},$$

$$\mathbf{M}_2 = \begin{bmatrix} 1 & 1 & 1 \\ 0 & 0 & 0 \\ N_{22} & N_{23} & N_{24} \\ 0 & 0 & 0 \\ EI_2N_{22}k_{22} & EI_2N_{23}k_{23} & EI_2N_{24}k_{24} \\ \kappa GS_2(k_{22} - N_{22}) & \kappa GS_2(k_{23} - N_{23}) & \kappa GS_2(k_{24} - N_{24}) \end{bmatrix},$$

$$\mathbf{M}_3 = \begin{bmatrix} 0 & 0 & 0 \\ 1 & 1 & 1 \\ 0 & 0 & 0 \\ N_{31} & N_{32} & N_{33} \\ EI_3 N_{31} k_{31} & EI_3 N_{32} k_{32} & EI_3 N_{33} k_{33} \\ \kappa GS_3(k_{31} - N_{31}) & \kappa GS_3(k_{32} - N_{32}) & \kappa GS_3(k_{33} - N_{33}) \end{bmatrix}, \quad \mathbf{M}_4 = \begin{bmatrix} 0 & 0 & 0 \\ 1 & 0 & 0 \\ 0 & 0 & 0 \\ N_{34} & 0 & 0 \\ EI_3 N_{34} k_{34} & 0 & 0 \\ \kappa GS_3(k_{34} - N_{34}) & 0 & 0 \end{bmatrix},$$

$$\mathbf{M}_5 = \begin{bmatrix} 0 & 0 & 0 \\ 0 & 0 & 0 \\ 0 & 0 & 0 \\ 0 & 0 & 0 \\ 0 & t_1 ES_2 k_{25} & t_1 ES_2 k_{26} \\ 0 & 0 & 0 \end{bmatrix}, \quad \mathbf{M}_6 = \begin{bmatrix} 0 & 0 & 0 \\ 0 & 0 & 0 \\ 0 & 0 & 0 \\ 0 & 0 & 0 \\ -t_2 ES_3 k_{35} & -t_2 ES_3 k_{36} & 0 \\ 0 & 0 & 0 \end{bmatrix},$$

$$\mathbf{M}_7 = \begin{bmatrix} 0 & 0 & e^{k_{21}LHQ} \\ 0 & 0 & 0 \\ 0 & 0 & N_{21} e^{k_{21}LHQ} \\ 0 & 0 & 0 \\ 0 & 0 & EI_2 N_{21} k_{21} e^{k_{21}LHQ} \\ 0 & 0 & \kappa GS_2(k_{21} - N_{21}) e^{k_{21}LHQ} \end{bmatrix},$$

$$\mathbf{M}_8 = \begin{bmatrix} e^{k_{22}LHQ} & e^{k_{23}LHQ} & e^{k_{24}LHQ} \\ 0 & 0 & 0 \\ N_{22} e^{k_{22}LHQ} & N_{23} e^{k_{23}LHQ} & N_{24} e^{k_{24}LHQ} \\ 0 & 0 & 0 \\ EI_2 N_{22} k_{22} e^{k_{22}LHQ} & EI_2 N_{23} k_{23} e^{k_{23}LHQ} & EI_2 N_{24} k_{24} e^{k_{24}LHQ} \\ \kappa GS_2(k_{22} - N_{22}) e^{k_{22}LHQ} & \kappa GS_2(k_{23} - N_{23}) e^{k_{23}LHQ} & \kappa GS_2(k_{24} - N_{24}) e^{k_{24}LHQ} \end{bmatrix},$$

$$\mathbf{M}_9 = \begin{bmatrix} 0 & 0 & 0 \\ e^{k_{31}LHQ} & e^{k_{32}LHQ} & e^{k_{33}LHQ} \\ 0 & 0 & 0 \\ N_{31} e^{k_{31}LHQ} & N_{32} e^{k_{32}LHQ} & N_{33} e^{k_{33}LHQ} \\ EI_3 N_{31} k_{31} e^{k_{31}LHQ} & EI_3 N_{32} k_{32} e^{k_{32}LHQ} & EI_3 N_{33} k_{33} e^{k_{33}LHQ} \\ \kappa GS_3(k_{31} - N_{31}) e^{k_{31}LHQ} & \kappa GS_3(k_{32} - N_{32}) e^{k_{32}LHQ} & \kappa GS_3(k_{33} - N_{33}) e^{k_{33}LHQ} \end{bmatrix},$$

$$\mathbf{M}_{10} = \begin{bmatrix} 0 & -e^{k_{41}LHQ} & -e^{k_{43}LHQ} \\ e^{k_{34}LHQ} & -e^{k_{41}LHQ} & -e^{k_{43}LHQ} \\ 0 & -N_{41}e^{k_{41}LHQ} & -N_{43}e^{k_{43}LHQ} \\ N_{34}e^{k_{34}LHQ} & -N_{41}e^{k_{41}LHQ} & -N_{43}e^{k_{43}LHQ} \\ EI_3N_{34}k_{34}e^{k_{34}LHQ} & -EI_4N_{41}k_{41}e^{k_{41}LHQ} & -EI_4N_{43}k_{43}e^{k_{43}LHQ} \\ \kappa GS_3(k_{34} - N_{34})e^{k_{34}LHQ} & -\kappa GS_4(k_{41} - N_{41})e^{k_{41}LHQ} & -\kappa GS_4(k_{43} - N_{43})e^{k_{43}LHQ} \end{bmatrix},$$

$$\mathbf{M}_{11} = \begin{bmatrix} 0 & 0 & 0 \\ 0 & 0 & 0 \\ 0 & 0 & 0 \\ 0 & 0 & 0 \\ 0 & t_1ES_2k_{25}e^{k_{25}LHQ} & t_1ES_2k_{26}e^{k_{26}LHQ} \\ 0 & 0 & 0 \end{bmatrix}, \quad \mathbf{M}_{12} = \begin{bmatrix} 0 & 0 & 0 \\ 0 & 0 & 0 \\ 0 & 0 & 0 \\ 0 & 0 & 0 \\ -t_2ES_3k_{35}e^{k_{35}LHQ} & -t_2ES_3k_{36}e^{k_{36}LHQ} & 0 \\ 0 & 0 & 0 \end{bmatrix},$$

$$\mathbf{M}_{13} = \begin{bmatrix} 0 & 0 & t_1N_{21} \\ 0 & 0 & 0 \\ 0 & 0 & 0 \\ 0 & 0 & t_1N_{21}e^{k_{21}LHQ} \\ 0 & 0 & 0 \\ 0 & 0 & 0 \end{bmatrix}, \quad \mathbf{M}_{14} = \begin{bmatrix} t_1N_{22} & t_1N_{23} & t_1N_{24} \\ 0 & 0 & 0 \\ 0 & 0 & 0 \\ t_1N_{22}e^{k_{22}LHQ} & t_1N_{23}e^{k_{23}LHQ} & t_1N_{24}e^{k_{24}LHQ} \\ 0 & 0 & 0 \\ 0 & 0 & 0 \end{bmatrix},$$

$$\mathbf{M}_{15} = \begin{bmatrix} 0 & 0 & 0 \\ -t_2N_{31} & -t_2N_{32} & -t_2N_{33} \\ 0 & 0 & 0 \\ 0 & 0 & 0 \\ -t_2N_{31}e^{k_{31}LHQ} & -t_2N_{32}e^{k_{32}LHQ} & -t_2N_{33}e^{k_{33}LHQ} \\ 0 & 0 & 0 \end{bmatrix}, \quad \mathbf{M}_{16} = \begin{bmatrix} 0 & 0 & 0 \\ -t_2N_{34} & 0 & 0 \\ 0 & 0 & 0 \\ 0 & 0 & 0 \\ -t_2N_{34}e^{k_{34}LHQ} & 0 & 0 \\ 0 & 0 & 0 \end{bmatrix},$$

$$\mathbf{M}_{17} = \begin{bmatrix} 1 & -1 & -1 \\ 1 & 0 & 0 \\ -ES_1k_{16} & ES_2k_{25} & ES_2k_{26} \\ 0 & -e^{k_{25}LHQ} & -e^{k_{26}LHQ} \\ 0 & 0 & 0 \\ 0 & ES_2k_{25}e^{k_{25}LHQ} & ES_2k_{26}e^{k_{26}LHQ} \end{bmatrix},$$

$$\mathbf{M}_{18} = \begin{bmatrix} 0 & 0 & 0 \\ -1 & -1 & 0 \\ ES_3k_{35} & ES_3k_{36} & 0 \\ 0 & 0 & e^{k_{45}L_{HQ}} \\ -e^{k_{35}L_{HQ}} & -e^{k_{36}L_{HQ}} & e^{k_{45}L_{HQ}} \\ ES_3k_{35}e^{k_{35}L_{HQ}} & ES_3k_{36}e^{k_{36}L_{HQ}} & -ES_4k_{45}e^{k_{45}L_{HQ}} \end{bmatrix}$$

A.2 ANALYSIS OF THE EQUIVALENT CHARACTERISTIC FOR A PERFORATED PLATE

In this appendix, we study the effective material properties of the perforated plate [76–83], which are necessary for the vibration isolation properties of the two branches in the HQ filter, as presented in Chapter 4. In Chapter 4, we focused only on the characterization of the effective Young’s modulus for the two branches in the HQ filter, without considering the real and practical simulation of the penetration patterns in the perforated plate. Therefore, the analysis of the choice of penetration patterns will be presented here.

The perforated plates are proposed by performing several finite element analyses in COMSOL, taking into account different ligament efficiencies  $\eta = \frac{h}{p}$ . The location and diameter of the holes are determined based on these ligament efficiencies, as shown in Fig.A.1. Using the effective properties, the perforated plate is simulated as solid plate with plane strain condition, e.g., axial stress is  $\sigma = 10MPa$ , at the right end and its modal characteristics are investigated.

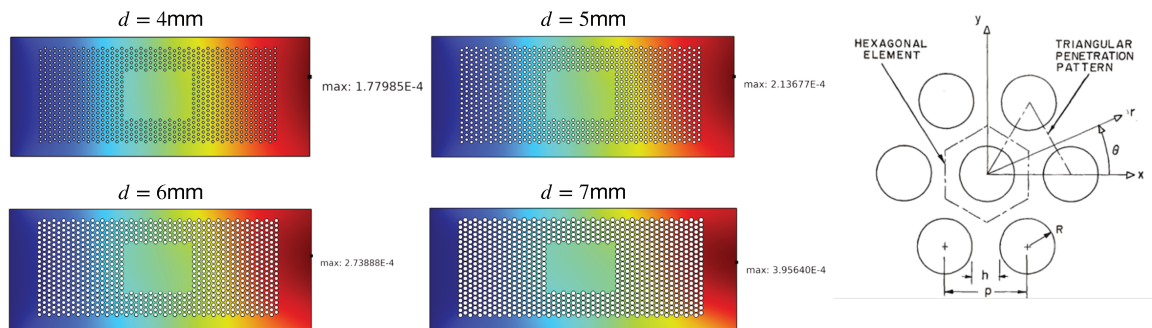


Fig. A.1 Perforated plates with different triangular penetration patterns and their sizes.

The procedure for determining equivalent material constants, such as effective elastic modulus  $E^*$  and effective Poisson's ratio  $\nu^*$ , can be represented as follows: 1) modeling a flat perforated plate and its equivalent solid plate, 2) determining the same material, axial load and boundary conditions, 3) determining the difference in deformation between the perforated and the equivalent plate 4) registering the effective elastic modulus  $E^*$  and effective Poisson's ratio  $\nu^*$  for different ligament efficiencies, then comparing them with the Young's modulus  $E$  and Poisson's ratio  $\nu$  of the equivalent plate.

In Fig.A.2 shows the equivalent material constants, namely the effective elastic modulus  $E^*$ , Fig.A.2a, and effective Poisson's ratio  $\nu^*$ , Fig.A.2b, depending on the ligament efficiency  $\eta$ . As can be seen, the size and location of the holes in the perforated plates can affect the selection of appropriate equivalent material constants for the plate. Therefore, the choice of design of a real perforated plate with an HQ filter can be realized using this methodology.

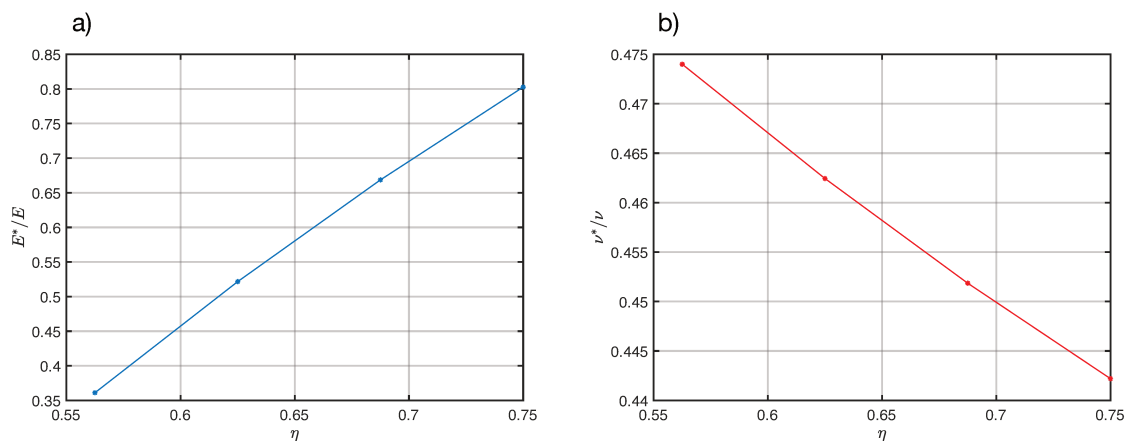


Fig. A.2 Equivalent elastic constants: a) Effective elastic modulus b) Effective Poisson's ratio at different ligament efficiencies  $\eta$ .



---

**Titre :** Filtres Herschel-Quincke pour l'atténuation passive des vibrations

**Mots clés :** Filtrage vibratoire passif, structures fractionnées en parallèle, principe de Herschel- Quincke, modèle ondulatoires, mise en évidence expérimentale

**Résumé :** Les vibrations et les bruits de structure sont généralement des phénomènes indésirables pour des raisons de fiabilité et de confort. De nombreuses approches du contrôle des vibrations ont été étudiées au fil des ans, en utilisant diverses conceptions géométriques, des matériaux d'amortissement ou des stratégies de contrôle actif. En outre, l'allègement des structures mécaniques est un défi majeur en termes de consommation d'énergie, en particulier pour les applications de transport. Dans ces contextes combinés, l'objectif de cette thèse est de développer de nouveaux concepts de contrôle des vibrations en adaptant le principe des filtres de Herschel-Quincke (HQ), traditionnellement appliqué aux ondes acoustiques planes dans les tubes, au domaine des ondes élastiques dans les poutres et les plaques. En acoustique, les filtres HQ exploitent le principe de la différence de marche entre deux tubes parallèles de longueurs variables créés à partir d'un tube primaire, ce qui entraîne une interférence destructive et donc une transmission nulle à certaines fréquences. Cette étude étend ce principe aux ondes de flexion en divisant une poutre mince en deux segments de longueur égale mais d'épaisseur différente. La différence de rigidité de flexion qui en résulte induit la différence de phase requise, ce qui conduit au filtrage des ondes. Cette approche fait des filtres HQ une solution prometteuse pour les applications de contrôle des vibrations et du bruit sans augmenter la masse de la structure considérée.

---

**Title :** Herschel-Quincke filters for passive vibration mitigation

**Keywords :** Passive vibration filtering, parallel split structures, Herschel-Quincke principle, wave based models, experimental evidence.

**Abstract :** Vibration and structure borne noise are generally undesirable phenomena for both the reliability and comfort issues. Many approaches to vibration control have been studied over the years, using various geometrical designs, damping materials, or active control strategies. In addition, lightening mechanical structures is a major challenge in terms of energy consumption, particularly for transport applications. In these combined contexts, the aim of this thesis is to develop new vibration control concepts by adapting the principle of Herschel-Quincke (HQ) filters, traditionally applied to plane acoustic waves in tubes, to the realm of elastic waves in beams and plates. In acoustics, HQ filters exploit the principle of a phase shift between two parallel tubes of varying lengths created from a primary tube, resulting in destructive interference and hence zero transmission at certain frequencies. The attractiveness of HQ filters lies in their capacity to provide multiple transmission loss peaks, presenting a viable alternative to traditional resonance-based approaches. This study extends this principle to bending waves by partitioning a thin beam into two segments of equal length but different thicknesses. The resulting disparity in bending stiffness induces the requisite phase difference, leading to wave filtering. This approach positions HQ filters as a promising solution for vibration and noise control applications without increasing the mass of the considered structure.